UiT The Arctic University of Norway

Faculty or science and technology, Department of geoscience

Climate and sea-ice development between 890 and 1660 CE in SW Greenland revealed by marine diatom studies

Eira Triguero Enguídanos

Master's thesis in Geology GEO-3900 November 2022

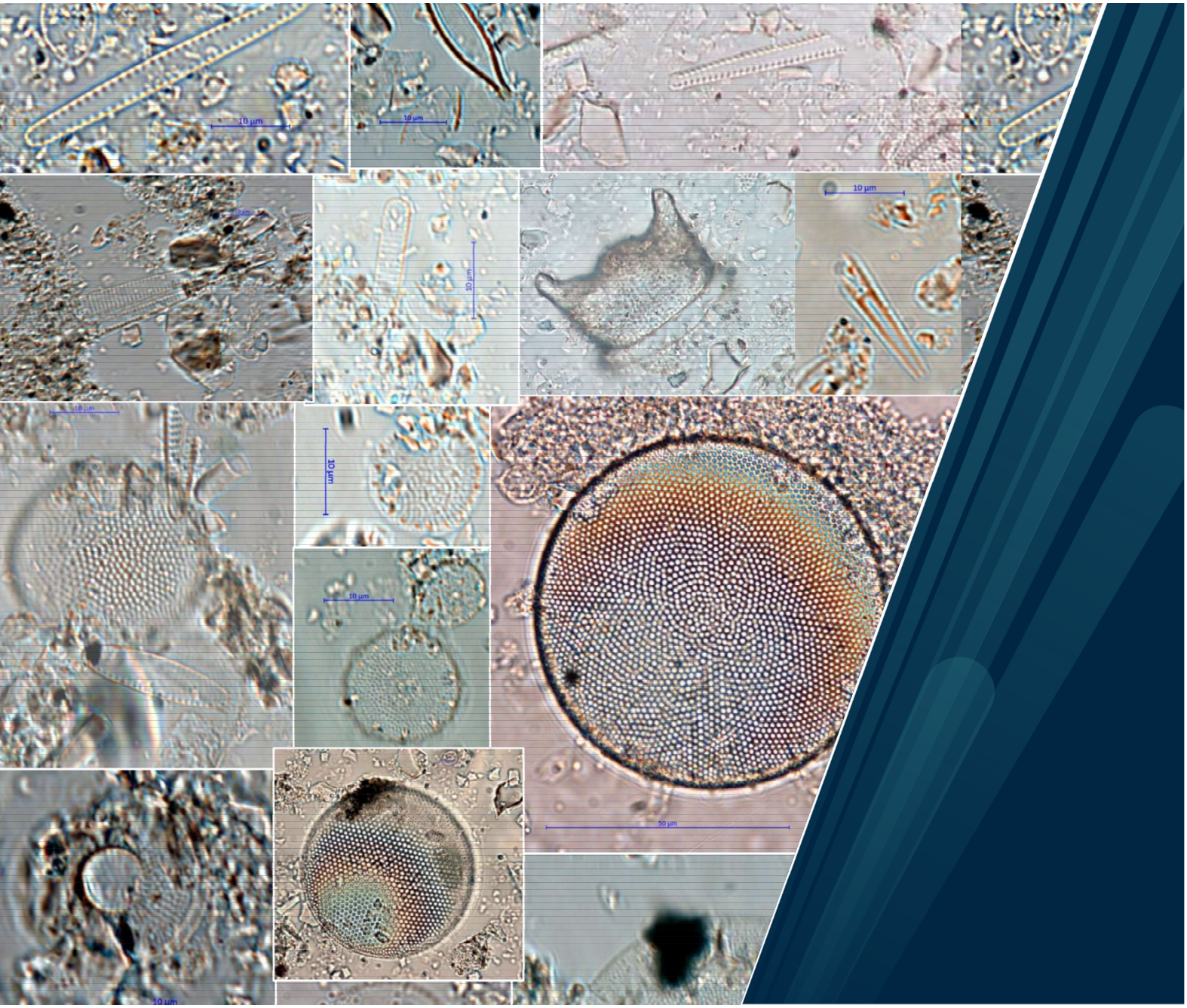

Abstract

This thesis presents the results of august Sea Surface Temperature reconstructions from marine diatom assemblages in samples from core Ga3-2 retrieved from Narsaq Sound, inside the Ikersuad fjord, South Greenland. The diatom samples provide a high-resolution (~30-year) reconstruction dating between 890 and 1660 CE (common era). The results show variable conditions with warm periods between 960 and 1010 CE and from 1370 to 1590 CE and cold periods from 890 to 960 CE and from 1010 to 1190 CE. This means cold summer Sea Surface temperatures during the Medieval Climate anomaly and warm temperatures during the Little Ice age. These results are compared to other records from the area, including diatom assemblages from other cores and temperature reconstructions from ice cores, as well as other sea temperature proxies like foraminiferal assemblages or alkenones from haptophyte algae. The comparisons show a complex relation between different proxies and indicate an opposite summer temperature trend between the Northeast Atlantic and South Greenland, probably linked to heat transport by the North Atlantic Current and its two branches, the Northwest Atlantic Current and the Irminger Current.

Acknowledgements

I would like to thank all the people who have helped me complete this work.

I am deeply indebted to my supervisors, Tine Lander Rasmussen and Arto Miettinen, who have been key to my work, answering my many questions and guiding me throughout. I would specially like to thank Tine for believing in me and being encouraging, kind and supportive. Thank you for your help in every stage. I would like to thank Arto for introducing me to the world of diatoms and providing with such an interesting and exciting topic. I am also grateful to Niels Nørgaard-Pedersen for providing the field pictures at a personal request of Arto Miettinen. Thanks should also go to Trine Merete Dahl and the rest of the lab staff for the aassistance with the practical matters.

I would like to express my sincere gratitude to Line and André, from the Studentrådgiving, this master would not have been completed without you. Thank you for being there when I most needed you. I would like to thank Line for helping me with the «paperwork». And I would like to say thank you to André for offering me coffee every morning. Still do not like it though. Thank you for making sure I did not give up. And I would like to acknowledge Astrid, for the talks we had together.

I would be remiss not mentioning my parents, who have encouraged me towards science since I was little; and my brother, who has been there when I have needed him.

And finally, thanks go to Paul, without whom any of this would not have been possible. Like you once said, thank you for sailing by my side in good winds and helping me stay on course in stormy weather.

Contents

Abstract 1

Acknowledgements 3

Introduction 8

Objectives 8

Background 10

Study area. Oceanographic and environmental settings 11

Diatoms as a proxy 14

Structure of diatoms: 16

Life cycle 18

About this study 19

Material and methods 21

Sediment core Ga3-2 21

Magnetic susceptibility 24

Dating and age model 24

Sample preparation 25

Slide preparation 25

Sample counting 27

Transfer functions 28

$\delta^{18}O$ and temperature 28

Sea ice 29

Results....30
Sediment core Ga3-2....30
Diatom analyses, species distribution and SST....35
Sea surface temperature....36
Sea ice....39
Discussion....41
Interpretation....41
Description of sediment cores MD-2322 and Rapid 21-COM....47
Description of MD99-2322....47
Description of Rapid21-COM....49
Comparison between Ga3-2 and the other sediment cores....50
Description of the ice cores GISP 2, DYE-3 and Renland....54
Description of DYE-3....54
Description of GISP 2....55
Description of Renland....56
Comparison between Ga3-2 and ice cores....57
Comparison to other records....59
Conlusions....65
References....67
Figures....73
Tables....78
Appendix 1: Diatom taxa from Ga3-2 samples from....79

Appendix 2 Diatom abundances in Ga 3-2 (%).....83

Appendix 3: Main diatom abundances. Figure 15 – page 3.....89

Introduction

With the undeniable global climate warming happening nowadays (Chen et al., 2017; Hughes et al., 2019; Park and Latif, 2019; Plass, 1959), there is an increasing concern about the future of the biosphere, and a higher demand for more and better quantifications of the trends in ocean and atmospheric temperatures, ocean pH, sea-ice quantities and distributions, etc. in order to better understand the changes that are already occurring and also to predict more accurately what will occur in the future. It is useful and fundamental to investigate the past beyond the instrumental records of the last c. 150 years.

The climate of the Earth has been variable since its origin, and natural climate variability occur due to the orbital changes, as well as feedback loops (Gildor and Tziperman, 2000). In the Quaternary, there have been several glacial and interglacial periods in the last 2.6 Ma (Flesche Kleiven et al., 2002) as cited in PAGES (2016) with large fluctuations in global temperatures and size of the ice caps.

Due to this necessity, the climate has been recorded more thoroughly in the last years around the globe. However, the Arctic region is difficult to access and the existing records are few and discontinuous (Backman et al., 2004; Vermassen et al., 2021).

Objectives

In this study, a sediment core from the the Ikersuaq Fjord, in southern Greenland is presented. The main purpose of the work is to reconstruct august Sea Surface Temperature (SST) from the marine sediment core Ga3-2 during the recent past on species identification and distribution of diatoms and absolute SST based on transfer functions.

The obtained results of the SST reconstruction are compared with the temperature records for sediment core MD99-2322 taken from the east Greenland shelf, just south of the Greenland-Scotland Ridge and from the sediment core Rapid 21-COM from the Reykjanes Ridge, south

of Iceland, central North Atlantic Ocean. They are also compared to ice cores GISP 2 in the northern part of Greenland from the central inland ice divide; Dye-3, which is also inland, but further south; and Renland, which is an ice core position at the Eastern coast of Greenland (all cores plotted in Figure 1).

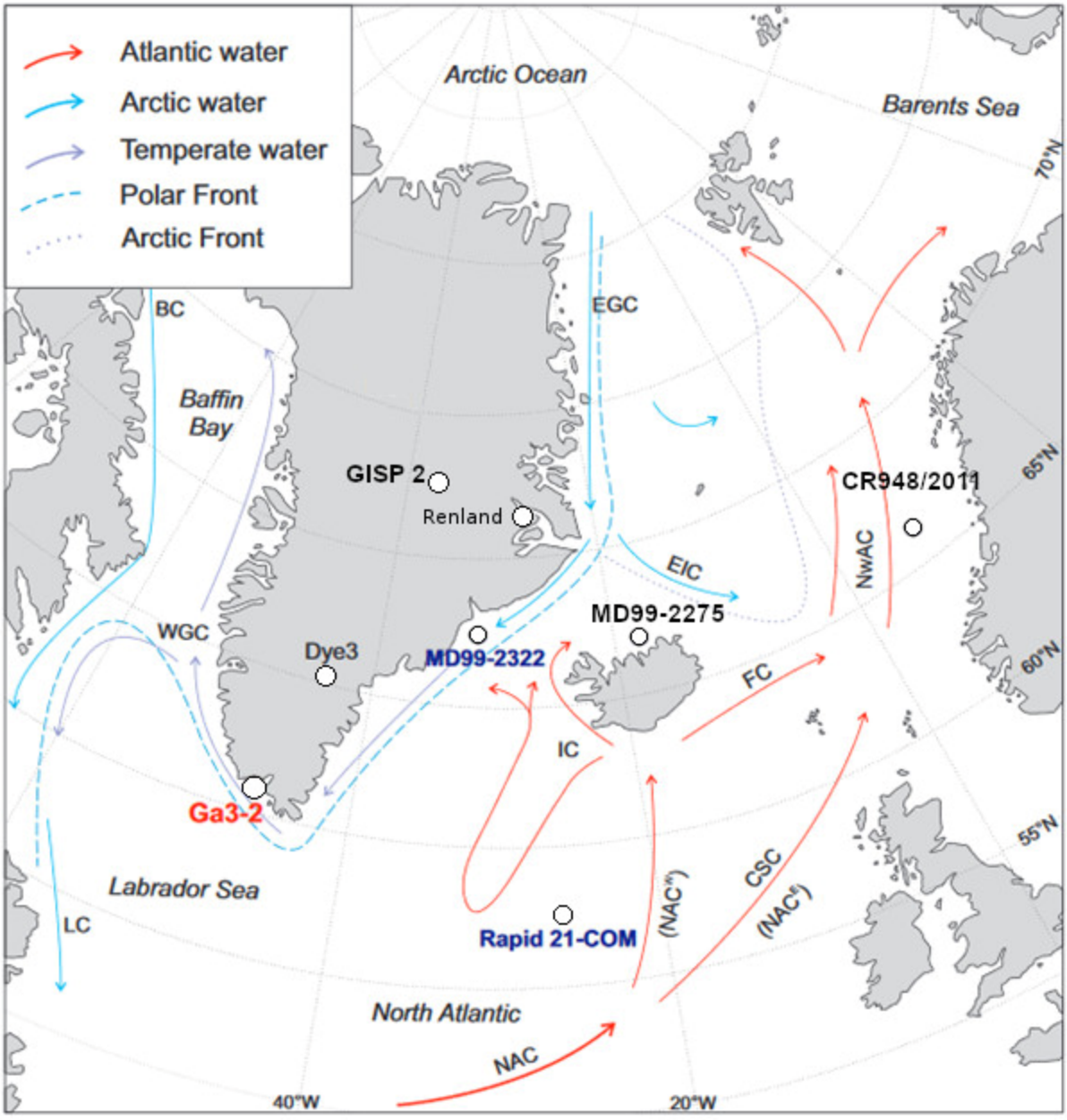

Figure 1 Map with marine core Ga3-2 and other cores referred to in this study. The main ocean currents in the area are also represented: Baffin Current (BC), Continental Slope Current (CSC), East Greenland Current (EGC), East Irminger Current (EIC), Faroe Current (FC), Irminger Current (IC), Labrador Current (LC), North Atlantic current (NAC) with both east and west ramifications (NAC^E and NAC^W respectively), Northwestern Atlantic Current (NwAC) and West Greenland Current (WGC). Modified from Miettinen et al. (2012).

Background

During the last years there has been a growing concern for the present climate change, and more focus has been put on past climate. Many studies have identified different climatic events in recent history, like the Medieval Climate Anomaly (MCA, also known as Medieval Warm Period) from around 950 CE (common era) to 1250 CE (Hughes and Diaz, 1994; Lamb, 1965; Mann et al., 2009). The MCA displays warm conditions in northern Europe (Goosse et al., 2012; Guiot et al., 2010). However, PAGES 2k Consortium (2013) finds no global warm trend, but rather regional climate variabilities.

The so-called Little ice age (LIA) is marked between 1500 CE and 1700 CE (Lamb, 1965) (Matthes (1939) as cited in Matthews and Briffa (2005)). It manifests as a period of lower temperature in many regions around the world, even though it is not considered a global-scale cooling (Grove, 2012; PAGES 2k Consortium, 2013; Schleussner et al., 2015).

Recent studies link the warmings in the last time period to the inflow of Atlantic water towards the Arctic (Spielhagen et al., 2011; Zamelczyk et al., 2020). This variation related to the North Atlantic Oscillation (NAO) is being studied (Mann et al., 2009; Trouet et al., 2009). The NAO is characterised by a movement of air masses over the North Atlantic due to a different air pressure between the Azores High and the Iceland low. The NAO index indicates how strong this air mass movement is (Hurrel et al., 2003; Wanner et al., 2001).

The relation between NAO and the Atlantic Meridional Overturning Circulation (AMOC) is shown in Bellucci et al. (2008). While the NAO redistributes the atmospheric air masses and energy therein, the AMOC transports the heat through water masses, and it is thought to have a significant role in the climate of the Northern Hemisphere (Bjerknes, 1964; Landerer et al., 2015). It is thought that a positive NAO is associated with a strong North Atlantic Current (NAC) and AMOC (Trouet et al., 2012; Vellinga and Wood, 2002). The short scale AMOC

changes are driven by atmospheric processes, and the ocean is responsible for longer term variability (Bjerknes, 1964; Knight et al., 2005; Marshall et al., 2001).

Study area. Oceanographic and environmental settings

The core studied in this work, Ga3-2 was retrieved in the Narsaq sound, inside Ikersuaq fjord, at the southwestern coast of Greenland (Figure 3) during the Danish Galathea-3 cruise in summer 2006. This area is influenced by two main currents, the Irminger Current, carrying warm and salty water from the North Atlantic Ocean, and the East Greenland Current which carries Arctic water from the Arctic Ocean into the North Atlantic (Jennings et al., 2011; Knutz et al., 2011). This polar water mass is cold and of low salinity.

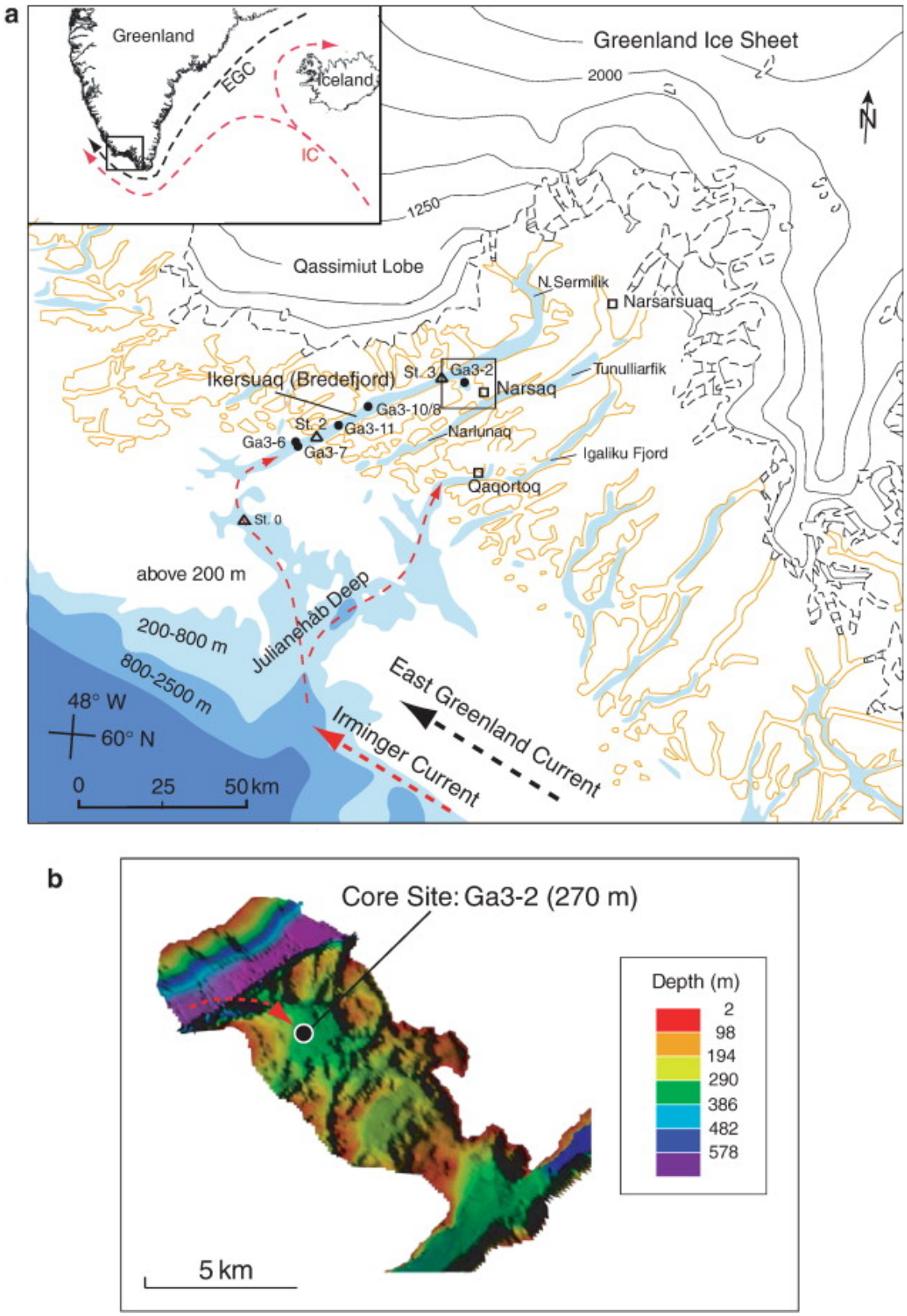

Figure 2 a) Map for the core site Ga3-2. Left upper corner shows the zoomed out map of the area corresponding to the south of Greenland. The black dashed arrow represents the East Greenland current (EGC) and the red dashed arrow represents the Irminger current (IC). b) Multibeam bathymetric map of Narsaq Sound, with the black dot to mark the Ga3-2 core site. The CTD (see Figure 4) points are also plotted as St. 0, St. 2 and St.3 (Nørgaard-Pedersen and Mikkelsen, 2009)

The Narsaq sound connects the Ikersuaq Fjord to the Tunulliarfik-Narlunaq fjord (Figure 2). It is 12 km long and 5 km wide, and has a maximum depth of 275 m, near the connection to Ikersuaq. Towards Tunulliarfik-Narlunaq, the sea floor rises to only 55 m of depth at the shallowest point. The sediment source for the Narsaq sound is mainly the Narsaq ice stream draining the Narsaq Mountain Glacier situated 10 km away (Nørgaard-Pedersen and Mikkelsen, 2009).

The area usually receives drift ice from the East Greenland Current and the ice stays from late winter until the summer (Nørgaard-Pedersen and Mikkelsen, 2009).

Figure 3 Picture from the Narsaq sound during the Galathea 3 cruise (picture from Niels Nørgaard-Pedersen)

These two water masses can and do mix, and in the study area, the modified East Greenland Current water can be found in the upper 200 m of the water column with lower temperatures

and lower salinities, while the Irminger Current is denser even when warmer, and follows the subsurface, between 200 and 700 m water depth, a CTD of the area can be seen in Figure 4 below.

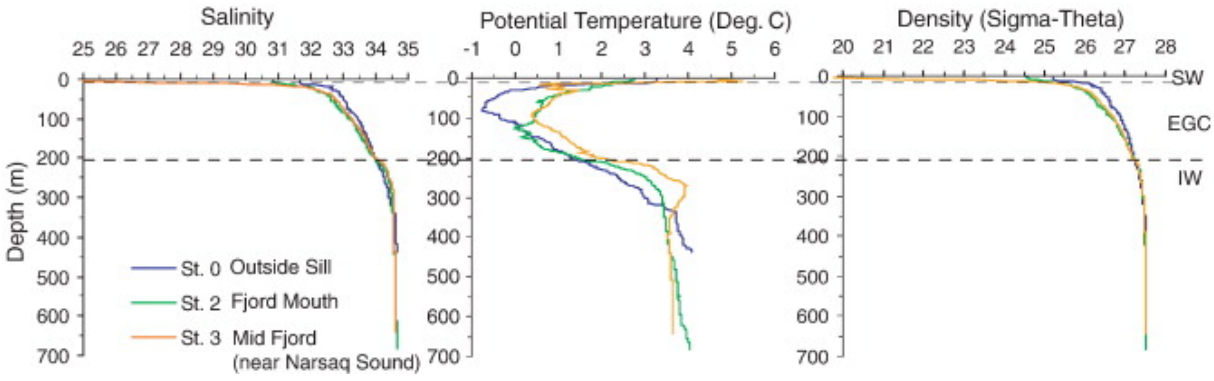

Figure 4 Hydrographic profiles of temperature, salinity, and density from the shelf area (St. 0, outside the Ikersuaq Fjord Sill, the outer Ikersuaq Fjord (St. 2), and mid fjord area near Narsaq Sound (St. 3). Data recorded by the Danish Meteorological

Diatoms as a proxy

Diatoms are unicellular, microscopic siliceous algae with a size of ~2 to 1000 µm and usually between 10 and 200 µm (Hasle et al., 1996; Miettinen, 2018). They are algae surrounded by an opaline silica wall. They are eukaryotic organisms that belong to the Bacillariophyceae class. They can live almost in any moist environment, including but not limited to warm and cold oceans, lakes, rivers, ice surfaces and even puddles and forests. Since they are photosynthetic organisms, diatoms require light, water and nutrients, and silica is the main limiting factor.

With the many diverse environments they can live in, there are many different species adapted to the various conditions. They are thought to be the group of algae with the highest diversity (number of species), they include more than 200 genera and as much as 100,000 species (Miettinen, 2014a, 2018).

They are the main group of phytoplankton in the oceans and play an important role in the carbon cycle, the silica cycle, and the cycles of other nutrients: they contribute with up to 40% of the

yearly organic carbon production and make up to more than 70% of suspended silica in the water column. Once they die, they can sink to the seafloor and contribute to the down flux of carbon and the export of CO_2 from the atmosphere to the deep-sea sediments (Hopkinson et al., 2011).

In everyday life, we use diatoms for multiple and diverse products, their silica walls are abrasive, and are therefore used in toothpaste, skin creams and soaps, as well as to polish metals and other harder materials. Since their walls are not smooth but can be perforated and have many small structures that can trap small particles, they are used as filters for hot tubs and swimming pools, but also for the manufacture of syrups and medicines. Even as an insecticide, the smallness of the diatoms is useful against invertebrate pests by damaging their exoskeleton and dehydrating them.

They are also prevalent as a proxy in science, where they are used in paleoenvironmental studies. The extensive number of different species with each their sensitivity to different factors like temperature, salinity, pH or nutrient availability make them ideal as indicators for those variables along the sediment cores and are thus useful for paleoclimatic research. When diatoms appeared for the first time is debated, with studies affirming the existence of diatoms during Proterozoic and Early Paleozoic (Sieminska, 2000; Sieminska and Kwiecinska, 2000) and studies that disprove it and insist on a probable common ancestor no earlier than 250 Ma ago based on molecular analysis (Sorhannus, 2007). The first accepted diatoms come from Wütrtemberg from the early Jurassic (c. 190 Ma) (Rothpletz, 1896, 1900). Modern taxa are found already during the Tertiary and remain largely unchanged until today (Katz et al., 2004; Rothpletz, 1896; Sieminska, 2000; Sieminska and Kwiecinska, 2000). However, it is worth noticing that diatom species do not have a stable nomenclature and many synonyms for various species exist (Bidgood et al., 1999), and identification criteria are being revised regularly (Bidgood et al., 1999; Jahn and Kusber, 2009; Weckström et al., 2020).

Structure of diatoms:

Diatoms have silica walls forming a skeleton with two valves that interlock with each other like a box, named frustules.

As mentioned earlier, there are many identified species of diatoms, their taxonomy is based on their appearance, e.g. specific characters of the frustules. The valves can have diverse shapes, sizes, and different ornamentations. In Figure 5, there are some examples of species with different ornamentation including grooves, pores, spines, hooks, ribs, ridges, raphes, and striae. As for the shape, we distinguish between pennate and centric diatoms. Pennate diatoms are elongated and bilaterally symmetric (for example, Figure 5 A, B, C, D, E and G), while centric diatoms are circular and radially symmetric (as in Figure 5 F, I, J, K, L, M, N, O and P).

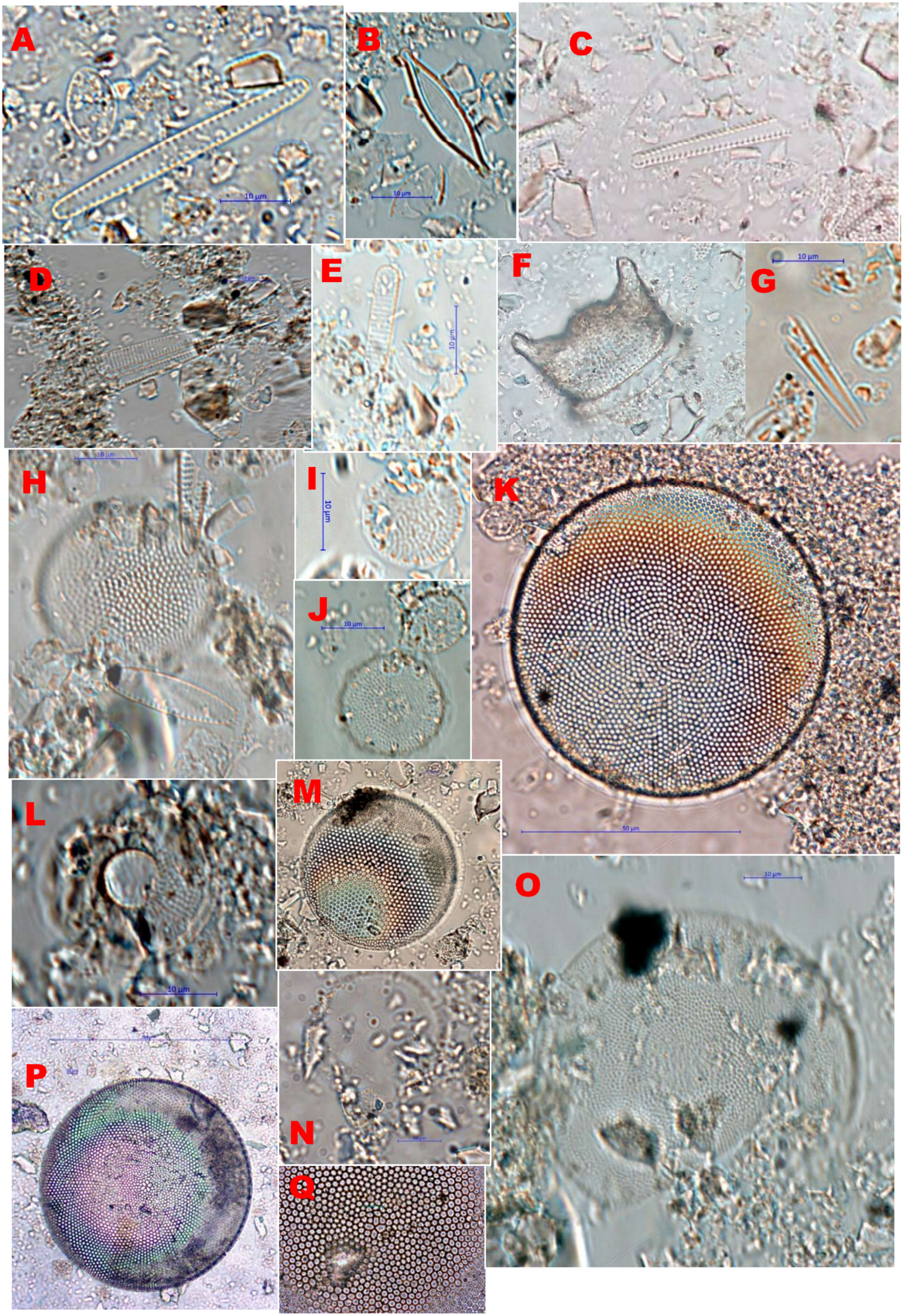
A
10 µm
B
10 µm
C
D
E
10 µm
F
G
10 µm
H
10 µm
I
10 µm
J
10 µm
K
50 µm
L
10 µm
M
N
O
10 µm
P
Q

Figure 5 Diatom images of specimens from this study taken with Axiocam 105 color and processed with ZEN (blue edition). A: Fragilariopsis reginae-jahniae; B: Nitzschia bicapitata; C: Thalassiotrix 18ikipedia18; D: Nitzschia angularis; E: Fragilariopsis cylindrus; F: Odontella aurita; G: Rhizosolenia hebata f. *hebata; H: T. 18ikipedia18 on the top, Thalassiosira antarctica* var. *borealis in the middle and Fragilariopsis oceanica down; I: Thalassiosira gravida; J: Thalassiosira nordenskioldii; K: Actinocyclus curvatulus; L: Bacterosira bathyomphala; M: Thalassiosira trifulta; N: Thalassiosira hyalina; O: Porosira glacialis; P: Coscinodiscus asteromphalus; Q: detail of the centre of a C. asteromphalus.*

Life cycle

Diatoms mainly reproduce asexually, by binary fission, from which both resulting halves receive one of the frustules and produce a new one that is slightly smaller, fitting inside the parent frustule, as shown in Figure 6. Since the newly produced frustule is always smaller than the received during cell division, the average cell size reduces with every division (every division creates a cell of the same size as the parent cell and one slightly smaller). After some generations, the size is too small to reproduce asexually and sexual reproduction occurs by gametogenesis, generating larger cells again.

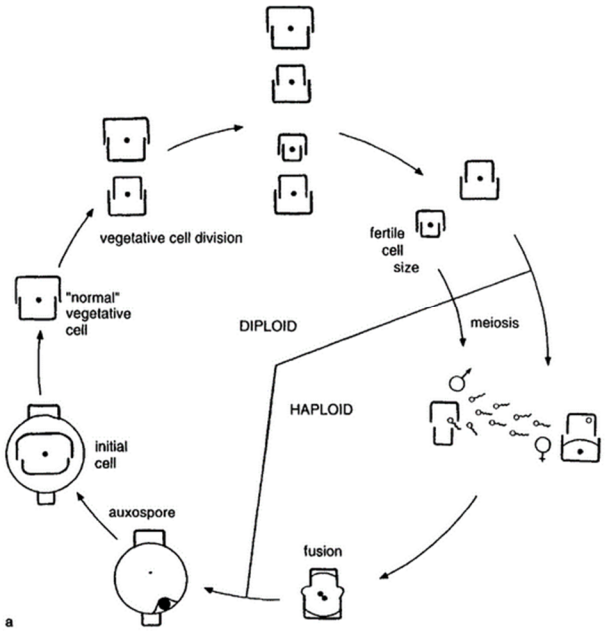

Figure 6 Life cycle of diatoms (Tomas, 1997)

About this study

This study uses marine diatoms as a proxy for temperature. Marine diatoms can be found in all seas ranging from the polar ice to the tropics, with highest abundance from high latitudes to temperate zones. Diatoms are especially useful in climate reconstruction from higher latitudes because the carbonates from other microfossils that could be used are frequently not as well preserved. This often makes diatoms a better choice in some cases for biostratigraphic and paleoclimatic reconstructions, although they too can be eroded and eliminated from the record by dissolution.

In this study, sediments from gravity core Ga3-2 are used to obtain and analyse diatom samples, and the results are run through transfer functions to obtain the sea surface temperature. The results are then compared with the SST of two published sediment cores Rapid 21-COM (Miettinen et al., 2012) and MD99-2322 (Stoner et al., 2007) and the $\delta^{18}O$ of ice core Dye3, the temperature of ice core GISP 2 and the $\delta^{18}O$ of ice core Renland. In addition, other published data is used to compare and interpret the results. In the following table is an overview of the cores used (Table 1):

Name	**Method**	**Depth of collection (m)**	**Core length (cm)**	**Latitude**	**Longitude**
Ga 3-2	Gravity corer	270	557	60º56.2′N	46º09.3′W
MD-2322	Piston corer	668	2635	67º08.18′N	30º49.67′W
Rapid 21-COM	Box corer Kasten corer	2630	54.3 372.5	57°27.09′N	27°54.53′W
Renland	Dry hole drilling	-	32435	71°16′N	24°44′W

Name	Method	Depth of collection (m)	Core length (cm)	Latitude	Longitude
Dye-3	Thermal drill	-	203763	65°10′N	43°49′W
GISP 2	Dry hole drilling	-	305300	72°36′N	38°30′W

Table 1 Information of the sediment cores compared in this study.

Material and methods

Sediment core Ga3-2

The main method to obtain undisturbed sediment samples in a chronologically ordered way is through sediment coring. This is done by using a tube that penetrates on the sediment and pulls it out. There are different types of corers that serve different purposes and have different characteristics.

Sediment core Ga3-2 was obtained using a gravity corer (Figure 7A). The gravity corer is a method that uses a long cylindrical PVC tube inserted into a metallic tube. On top of that tube there are several weights (yellow in the figure) that help the corer push into the soft sediments by gravity. On the bottom of the metal tube, there is a metallic piece called an 'orange-peel' core catcher (Figure 8) that acts as a one-way trap and allows the sediment to get into the tube as it penetrates the bottom of the sea, but prevents that same sediment from running out when the corer is pulled back into the boat. The corer is lowered by a cable and suspended a few meters over the sediment to stabilize it, and then is rapidly dropped to puncture the sediment. The cable is then pulled up again and the PVC pipe is recovered. The length of the column depends greatly on the characteristics of the sediments. It also depends on the dropping speed.

Similar methods include the Kasten corer (Figure 7 B), used to obtain the sediments forRapid21-COM. This is a modification of the gravity corer, it has a square cross-section and has no inner liner.

The Box corer (Figure 7 D) is a metallic structure with a square cross section container with a grab-like structure that is triggered when the corer hits the sea floor and closes the sediment inside. It is useful to obtain undisturbed surface sediments, and it usually obtains the first 40-80 cm layer of sediments, while gravity corers are penetrating a few meters inside the sediment, but often have disturbed the surface sediments.

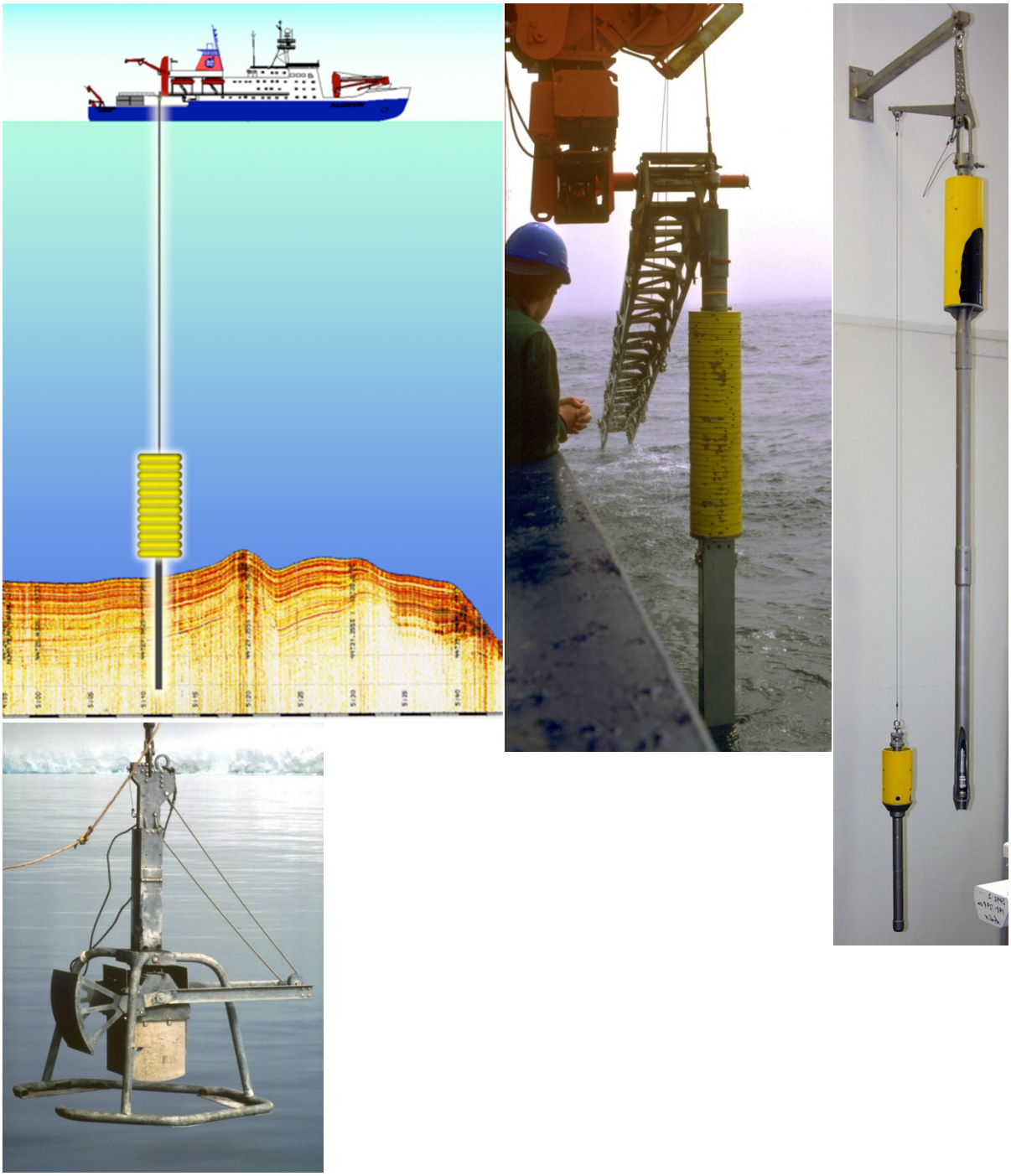

Figure 7 Images of the different types of corers used for the sediment cores. A (Upper left): Sketch of a Gravity Corer penetrating the sediment (https://commons.wikimedia.org/wiki/File:Gravity-corer_hg.png) Hannes Grobe/AWI 2009. B (Upper middle): Kasten Corer (https://commons.wikimedia.org/wiki/File:Gravity_corer-ps_hg.jpg) Hannes Grobe/ AWI 2006. C (Upper right): Piston corer (https://commons.wikimedia.org/wiki/File:Piston-corer_model_hg.jpg) Hannes Grobe, AWI 2008. D(Down): Box corer (https://commons.wikimedia.org/wiki/File:Giant-box-corer_hg.jpg) Hannes Grobe 2006.

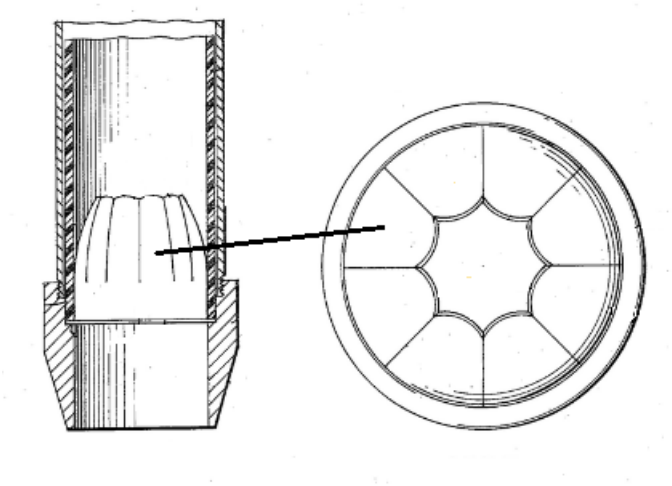

Figure 8 Sketch of a section of a corer with a catcher (left) and view of a catcher from top (right). Modified from (Duperon, 1974).

Finally, among the main sediment cores used for comparison in this work, MD99-2322 uses a piston corer (Figure 7 C), which is not unlike the gravity corer, in that it uses a long cylindrical tube with weight and retrieves a column of sediment. In this case, however, the artifact has a trigger that drops the main corer in free fall for a few meters, and inside the tube there is a piston that facilitates the collection of a longer sediment column by creating a suction force as the core penetrates the sediments.

The sediment core Ga 3-2 was taken from Narsaq Sund in Southern Greenland at 270 m depth (Figure 1). It was collected with a gravity corer that retrieved a 557cm column of sediment, and the upper 61 cm were used for the present study. Magnetic susceptibility on the split core was measured using a Bartington MS2E1 probe (area of response: 3.8 mm × 10.5 mm) (Nørgaard-Pedersen and Mikkelsen, 2009). A log of the core was catalogued, and pictures of the core were taken.

Previously published AMS-14C dates are used in this study (Nørgaard-Pedersen and Mikkelsen, 2009). Mixed benthic foraminifera were sent to the Leibiz-Laboratory for Radiometric Dating and Isotope Research in Kiel (Germany) for AMS-^{14}C dates. They were reservoir corrected by subtracting 400 years ($\Delta R=0$) (Nørgaard-Pedersen and Mikkelsen, 2009).

Magnetic susceptibility

Magnetic susceptibility (MS) measures the capacity of the material to be magnetic when an external magnetic field is applied on it (Czervionke et al., 1988). The value of magnetic susceptibility is higher when the sediments have higher concentrations of ferromagnetic minerals. In marine sediments, ferromagnetic sediments are often sourced on land and there is often a correlation between climate and the composition –grain size and mineralogy, and therefore with MS (Kent, 1982; Robinson et al., 1995; Sager and Hall, 1990).

Dating and age model

^{14}C is a radioactive isotope of carbon. It can be found in biological materials and when compared to the more common stable isotope (^{12}C) can be used to date the material. The time frame that this dating method can be used for is samples up to 50,000 years before present (BP) (Trumbore, 2000). Before present is stablished as the year 1950 common era (CE) (Goh, 1991).

For core Ga3-2, the age model from Nørgaard-Pedersen and Mikkelsen (2009) is used. They used ^{14}C from benthic foraminifera samples. Their age model assumes constant sedimentation rate between sample points and the first 14 cm are extrapolated. The calendar ages were calibrated with a reservoir correction of 400 years (see Table 2).

Table 2 AMS-14C dates on benthic foraminifera in core Ga3-2. Modified from Nørgaard-Pedersen and Mikkelsen (2009)

Lab. No.	**Depth (cm)**	**Conventional ^{14}C age (yr BP)**	**Cal. Age range (1σ) (yr BP)**	**Mean cal. Age (yr BP)**
KIA33122	14	795 ± 25	420–474	447
KIA 31753	56	1455 ± 40	950–1046	998
KIA33123	134	2535 ± 40	2154–2275	2215

Sample preparation

The method used is described by (Koç et al., 1993).

The core was sampled continuously every 2 cm in 1 cm slices to examine for diatoms. The samples were subsequently arranged for slide preparation. To do that, a sample of 0.5-1g of sediment was dried over night at 60°C and then cooled down in a desiccator to prevent rehydration. Next, it was weighted and covered with benzene to eliminate any possible mud clumps.

Since diatoms have a silica wall, it is possible to get a cleaner sample by eliminating the carbonates and the organic matter. For this reason, after evaporating the benzene, every sample was treated with muriatic acid (HCl) at 35% to dissolve all the carbonates, and hydrogen peroxide (H_2O_2) to eliminate the organic matter. After that, the samples were boiled until they became yellow (it takes about 15 to 20 minutes). The sample was then centrifuged for 3 minutes at 2000 rpm. The supernatant was decanted carefully to prevent loss of diatoms while the pellet was preserved, as it contains the diatoms. This process was repeated up to 7 times to eliminate the acid and H_2O_2; and most of the clay. The pellet was finally transferred to a glass vial for storage, and 2 drops of formaldehyde (CH_2O) were added to avoid algal or fungi growth (Koç et al., 1993).

Slide preparation

The samples were prepared for counting by preparing slides. The sample was poured over slide covers to have all diatoms on a similar depth when looking through the microscope, and to facilitate the diatoms sticking on the slide cover, a mixture of household gelatine and Fotoflow was first applied on them. For security, two duplicates were prepared for each sample, so that in case of mounting errors or other unfortunate events, there would be an extra slide. The two prepared slide covers were placed on a petri dish with the pretreated side up and with a small

drop of water under them to help them sticking and preventing them from moving during the process of pouring the samples over.

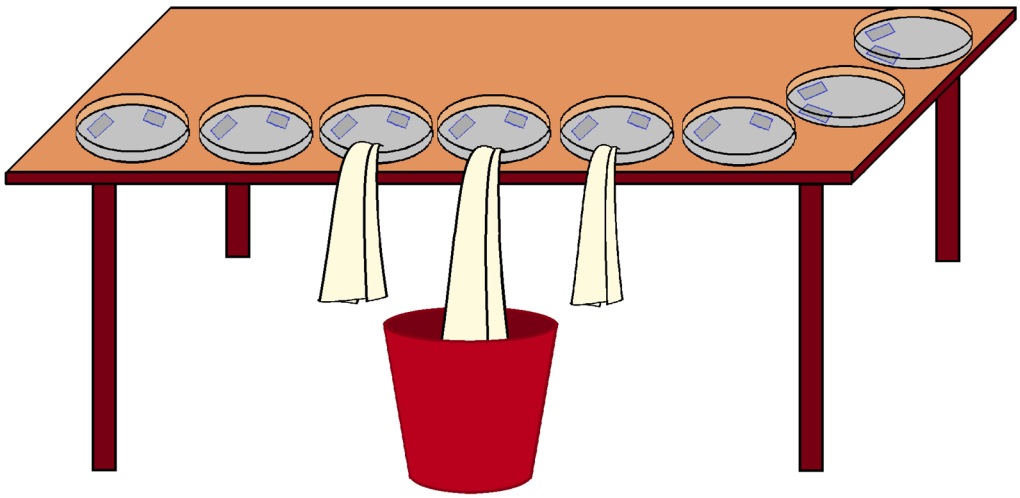

Figure 9 Sketch of the sample preparation.

The prepared sample was homogenized, and a known amount of sample was mixed –typically between 200 and 400 µL– with around 30 mL of distilled water. The petri dish was placed with the covers near the edge of the table and the mixture of water and sample was poured into the petri dish, so that the whole petri dish was completely covered by the mixture. The set-up was left to stand completely still for at least 2.5 hours to ensure a uniform coverage of the slide covers. After this time, a long piece of napkin was used to empty the water by placing one end on the empty space of the petri dish and the other hanging on the side of the table, which extracts the water by capillarity, as shown in Figure 9. After about 5 minutes most of the water was gone. Thereafter the petri dishes and samples were left to completely dry out, which took around 45 minutes. Once the samples were dry, they were heated up on a heating plate to around 110°C to ensure once more that they were dry. A line of Mountex fluid was added on glass slides and the slide covers with the samples were placed on top of it, with the sample facing down, as

shown in Figure 10. To fixate the samples, the slides were placed on the heating place until they started to bubble slowly, then they were taken out and cooled down.

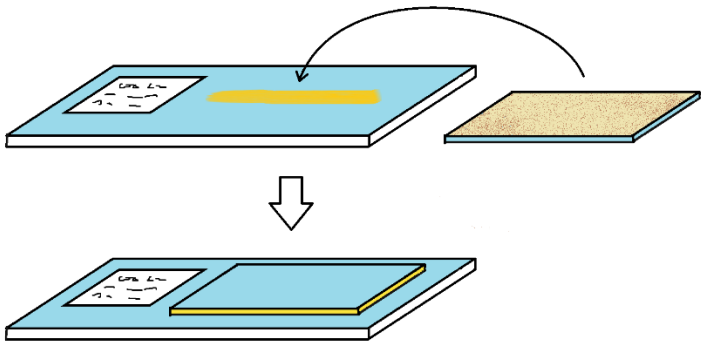

Figure 10 Sketch of slide preparation. A line of Mountex fluid (orange) was extended over the slide. Then the slide cover (right) was placed with the sample side facing down on the slide.

Sample counting

Once the slides were prepared, they were examined under the microscope. We used an optic microscope equipped with a x100 objective lens and a x10 eye lens, giving a magnification of x1000. Microscope immersion oil with refraction index n=1.5 was used to increase the resolving power of the microscope as it is indicated for this lens (x100). Since each sample had two replicas, the best looking one –in terms of homogeneity and eventual mounting errors – was chosen. At least 200 frustules of diatoms were counted and identified, excluding *Chaetoceros* spp. from the analysis. These forms are too abundant and would dilute any other findings. *Chaetoceros* spp. also show little to no relation to SST (Koc Karpuz and Schrader, 1990). Pennate diatoms were counted as 1 if they were whole and 0.5 if only one apex was present. They were not included in the counting spreadsheet if the terminal areas were missing. For radial diatoms, they were noted as 1 if more than 50% of the frustule was present and 0 if there was under 50%. Present diatoms of the 52 species included in the transfer function were identified. In case of a frustule not being identified, it would be noted in the spreadsheet as

"unidentified". Other frustules identified that do not belong to any of the 52 species were noted in the spreadsheet under "others". The countings were then processed into percentages of individuals of each species.

Transfer functions

The results were analysed through transfer functions at the Norwegian Polar Institute (NPI) using the Weighted averaging partial least squares regression (WA-PLS) transfer function (ter Braak and Juggins, 1993) with a modern calibration data set consisting of 184 surface sediment samples from the North Atlantic, the Labrador Sea, the Nordic Seas, and Baffin Bay (Miettinen et al., 2015).

This method consists of a combination of both weighted averaging regression (WA) and partial least squares regression (PLS) for a lower prediction error. It is commonly used for SST reconstructions because it shows a good statistical fit between observed and estimated SST through the temperature range of modern calibration data (Miettinen, 2018). This method has a root mean square error (RMSE) of 1.14ºC, a coefficient of determination between observed and inferred values (r^2) of 0.96 and a maximum bias of 0.60ºC (Miettinen et al., 2012).

The WA method assumes that the species distribution in the environment follow an unimodal or Gaussian response to the studied variable (ter Braak and Juggins, 1993).

The reconstructions indicate august Sea Surface Temperatures (aSST), as it gives the best match for diatoms (Berner et al., 2008).

$\delta^{18}O$ and temperature

Delta-O-18 or $\delta^{18}O$ is the ratio between the oxygen isotopes ^{16}O and ^{18}O. In nature, ^{16}O is the dominant isotope, and ^{18}O, with two more neutrons, is less abundant. The $\delta^{18}O$ value often reflects the temperature at the time of precipitation (Grootes et al., 1993; Johnsen et al., 1992).

$H_2{}^{18}O$ condenses more easily than $H_2{}^{16}O$, and therefore precipitation depletes the air of ^{18}O water vapor. Since air at higher temperatures can withhold higher amounts of water, as the air mass travels towards higher latitudes there are lower relative abundances of $H_2{}^{18}O$ at higher latitudes and cooler conditions (Aldaz and Deutsch, 1967; Dansgaard et al., 1975).

Sea ice

The results on sea ice from Ga3-2 in this study were obtained by adding the percentages of species related to sea ice (Andersen et al., 2004; Koc Karpuz and Schrader, 1990; Miettinen, 2018).The obtained data gives qualitative information on the amount of ice.

Results

Sediment core Ga3-2

The sediment column retrieved from Narsaq Sund measures 557cm. The open core shows uniform, massive, fine grained, bioturbated mud with some IRD clasts (Figure 11). The colour of the sediments is dark olive. There is no evidence of mass flow deposition or strong current winnowing in this core. The sediment column was opened and described by Nørgaard-Pedersen and Mikkelsen (2009), and an extended description of the lithology can be found in that article. Figure 11 shows the open core with sections 5 and 6 corresponding to the first centimetres of core.

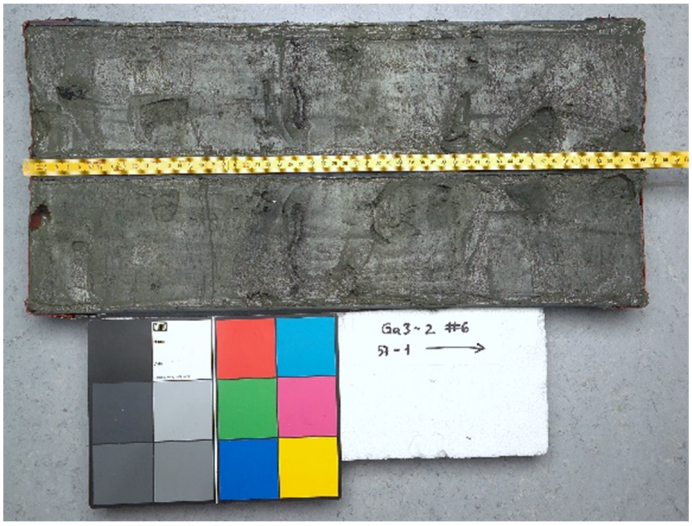

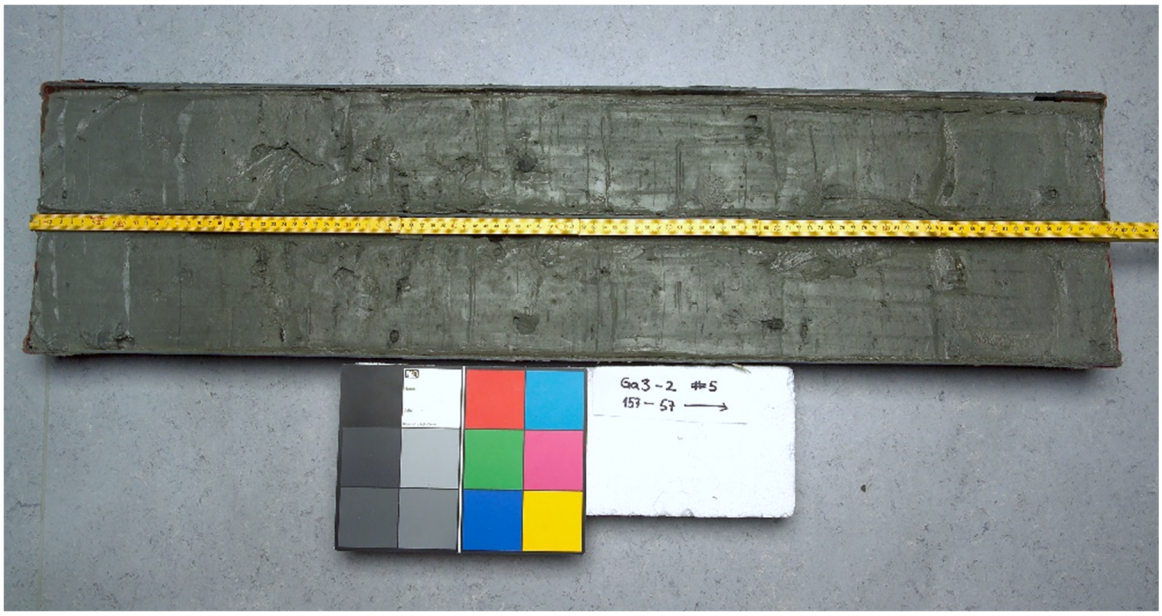

Figure 11 Core Ga3-2 open in half. Above from 1 to 57 cm, bellow from 57 to 157cm. Figures from Nørgaard-Pedersen and Mikkelsen (2009)

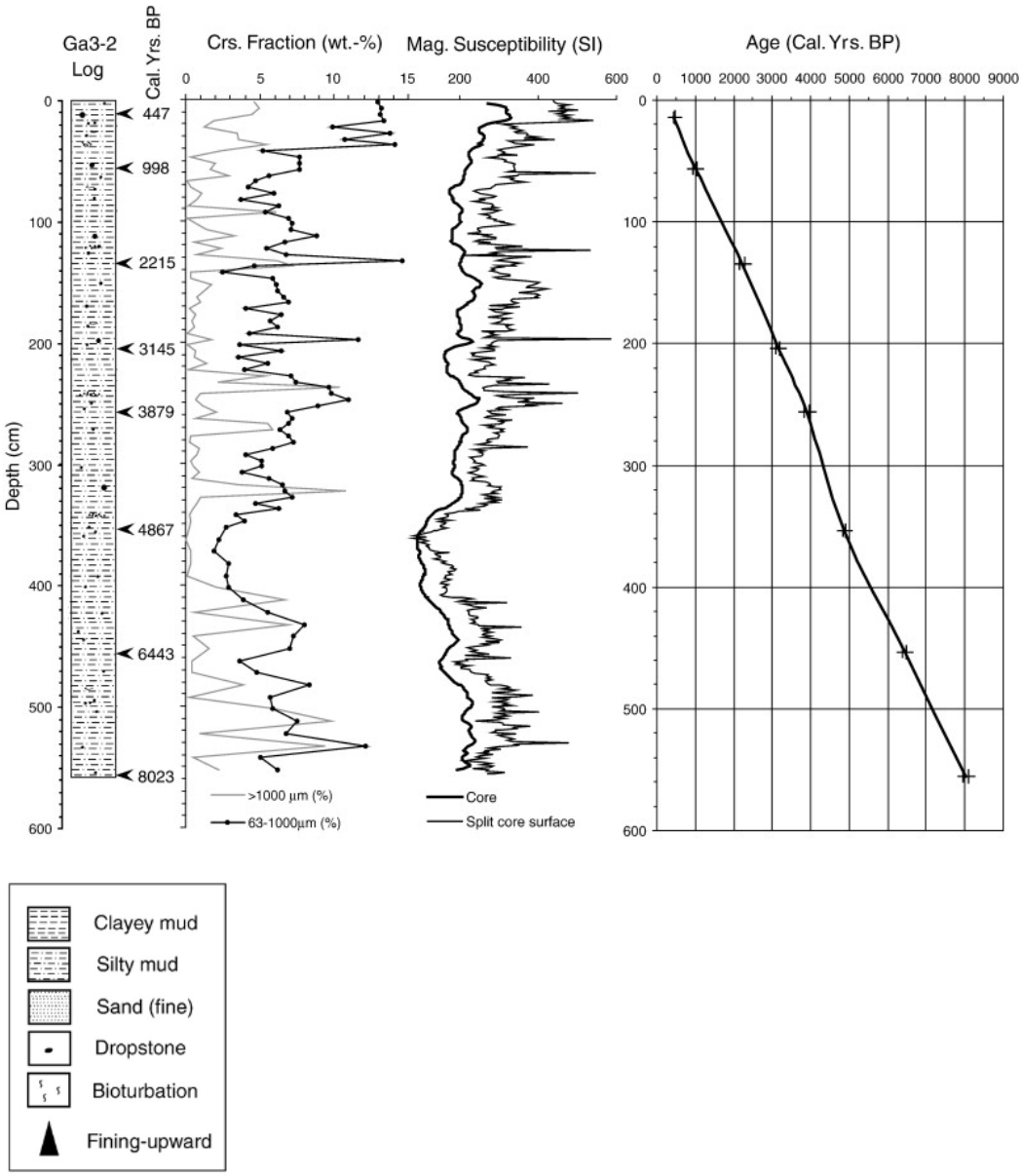

Figure 12 Lithological log, AMS- ^{14}C, coarse fraction content (63-1000 µm (%), >1000µm (%)) and age model of Ga 3-2 modified from (Nørgaard-Pedersen and Mikkelsen, 2009)

Figure 12 shows the lithological log for the whole core, the arrows on the right of the log show where the first samples for dating were taken, the numbers show the calibrated years BP. On the middle, a graphic shows both the coarse fraction content and the magnetic susceptibility. On the right, the age model is represented, showing the sedimentation rate. Note that the dates are shown are in years BP as shown in the original figure of the article (Nørgaard-Pedersen and Mikkelsen, 2009). Below, Figure 13, shows the sedimentation rate of the top of the core, using

the first 3 dated samples, with dates in years CE. The sedimentation rate is quite uniform and of high rates, taking on average 14 years to deposit 1 cm of sediment, or a sedimentation rate of around 70.4 cm/ka (Figure 13).

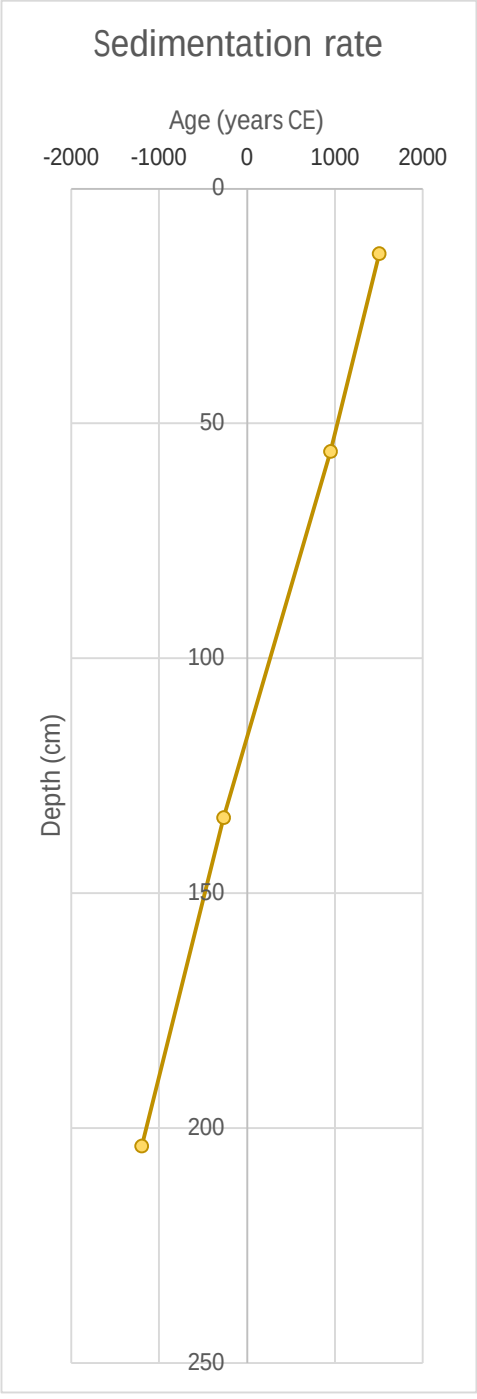

Figure 13 Sedimentation rate of the first 214 cm for the core Ga 3-2

In Figure 14, data from Ga3-2 presented in Nørgaard-Pedersen and Mikkelsen (2009) is put together with the SST reconstruction from this study. The data includes Magnetic susceptibility which varies between 300-500 $*10^{-6}$ SI units, as well as IRD grains, weight percent of particles in the size fraction 63-1000 µm and > 1000 µm, sortable silt mean, and quantity of benthic foraminifera. In the article, Nørgaard-Pedersen and Mikkelsen (2009) point out the close correlation between the high resolution magnetic susceptibility and grain size.

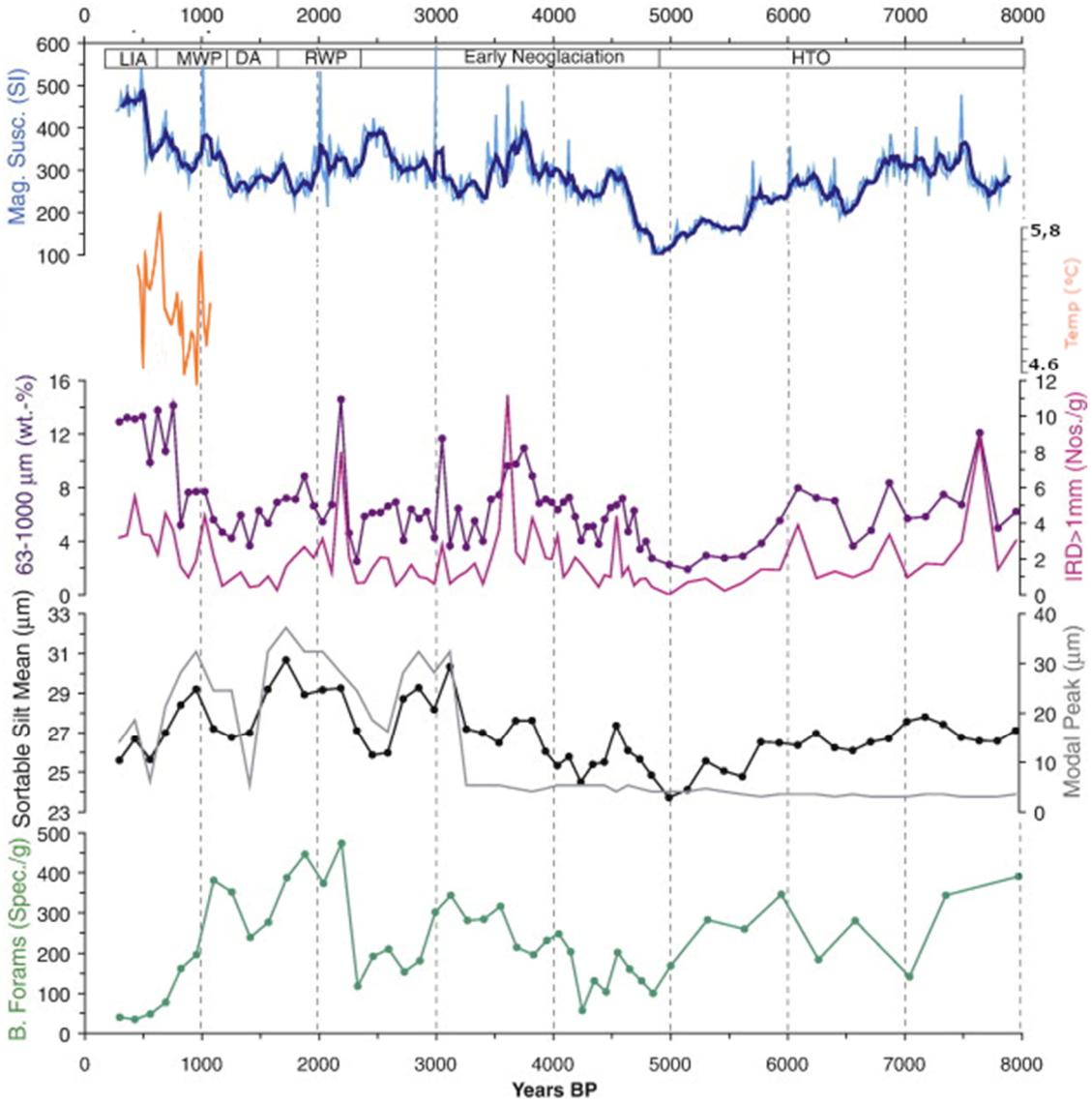

Figure 14 Basic data of core Ga3-2 and temperature record plotted versus age: Magnetic susceptibility (MS) with a 5 pt. running average overlay, 63–1000 µm (wt.%), nos. of IRD grains > 1000 µm/g, sortable silt weighted mean, modal grain size distribution peak values, and nos. of calcareous benthic foraminifera (> 125 µm)/g. LIA: 'Little Ice Age', MWP: 'Medieval Warm Period' (aka. Medieval Climate Anomaly (MCA), DA: 'Dark Ages', RWP : 'Roman Warm Period' HTO: 'Holocene Thermal Optimum'. The orange line indicates the timespan analysed in this study (Modified from Nørgaard-Pedersen and Mikkelsen, 2009) (Same as Figure 21).

Diatom analyses, species distribution and SST

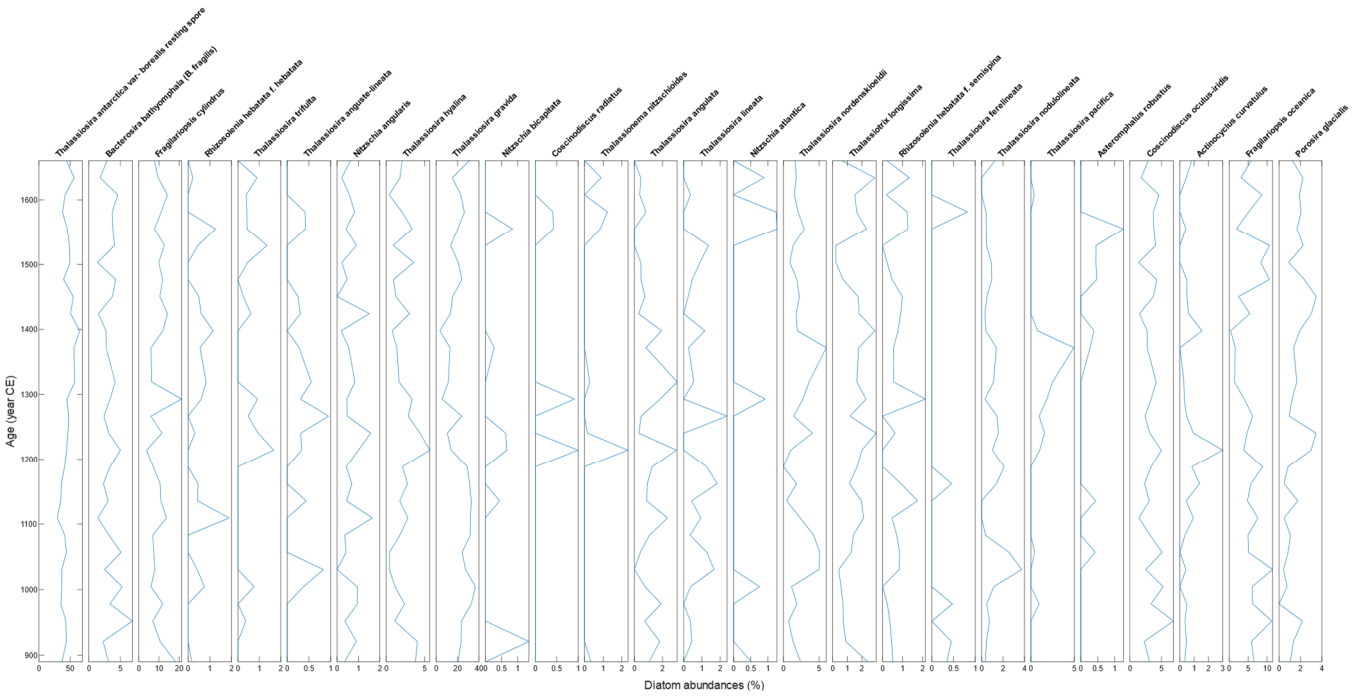

Figure 15 Relative abundances of main diatom species present in the record from Ga3-2. Species with <1% abundance in all samples were omitted. See the enlarged figure in Appendix 2

The total number of taxa in the samples includes 34 species. The most abundant species is *Thalassiosira antarctica* v. *borealis* spore with relative abundances ranging from around 30% in a few samples and up to 57%. *Thalassiosira gravida* is another species that is found in all samples, with relative abundances from 3 to 33%, *Fragillaropsis cylindrus* from 4% to 21%, *Fragillaropsis oceanica* from <1 to 11% and *Bacterosira bathyomphala* with relative abundances ranging from 1 to 7%. Frustules that were unidentified, either due to poor preservation or diagenetic alterations, constituted a maximum of 3% in any sample.

T. antartica var. *borealis* has a peak abundance at 1162 CE.

Figure 15 shows a graph with all diatom species identified with over 1% of abundance in at least one sample.

Sea surface temperature

The reconstruction of aSST from the diatom data for the first 61cm of the core is presented in Table 3.

Depth in core (cm)	Year cal BP	Year CE	Sea Surface Temperature ºC	
59-61	1060	890	5.2	
57-59	1029	921	4.9	
55-57	998	952	5.1	
53-55	972	978	5.5	
51-53	946	1004	5.5	
49-51	**919**	**1031**	**4.6**	**Coldest**
47-49	893	1057	5.0	
45-47	867	1083	5.0	
43-45	841	1109	4.9	
41-43	814	1136	4.8	
39-41	788	1162	4.7	
37-39	762	1188	5.2	
35-37	736	1214	5.0	
33-35	709	1241	5.3	
31-33	683	1267	5.1	
29-31	657	1293	5.1	
27-29	631	1319	5.1	
23-25	578	1372	5.1	
21-23	552	1398	5.6	
19-21	**526**	**1424**	**5.8**	**Warmest**
17-19	499	1451	5.6	
15-17	473	1477	5.5	
13-15	447	1503	5.4	

Depth in core (cm)	Year cal BP	Year CE	Sea Surface Temperature ºC	
11-13	421	1529	5.2	
9-11	395	1555	5.3	
7-9	368	1582	5.5	
5-7	342	1608	4.8	
3-5	316	1634	5.3	
1-3	290	1660	5.4	
			5.2	Mean temperature of the record

Table 3 Temperature record for Ga 3-2. Blue represents colder than the mean temperature and Red represents warmer than the mean temperature. In light yellow the temperatures that are similar to the mean. The coldest and warmest temperatures are marked with bold letters.

The record shows temperatures ranging from 4.6 to 5.8ºC and has a mean temperature of 5.2ºC. The data has an approximate 30-years temporal resolution between samples, and each sample corresponds to 1 cm of sediments covering c. 14 years. The most recent period is warm, from 1398 CE to 1660 CE, following a colder period from the oldest sample to 1372 CE. There is however a sample with colder temperature than the mean at 1608 CE and a few warmer than the mean at years 1241, 1004 and 978 CE.

The coldest temperature corresponds to 1031 CE, which contrast the warm temperature measurement shown in the sample before that corresponds to 1004 CE. The highest temperature peak in the record is the 5.8 ºC in 1424.

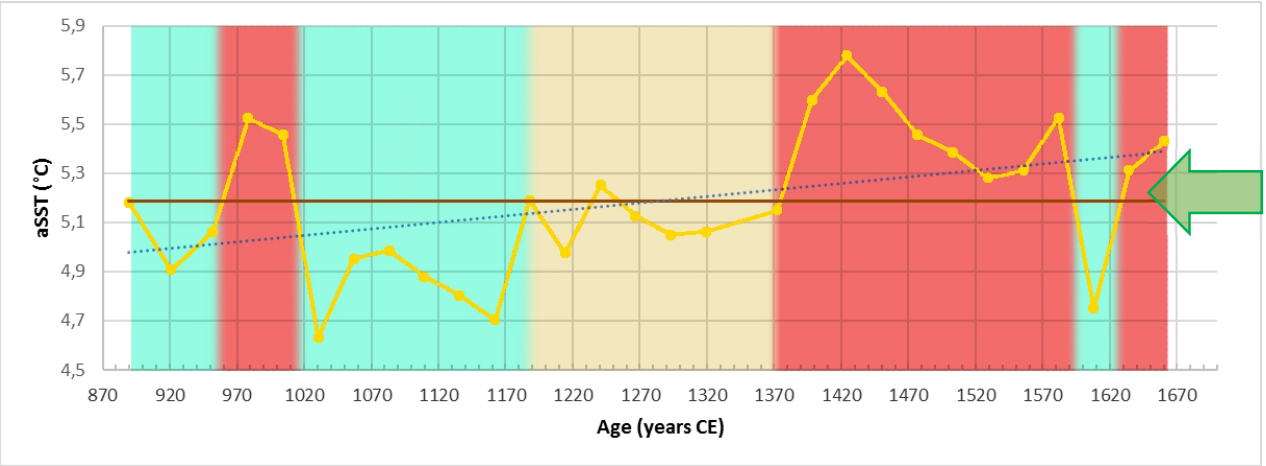

Figure 16 August Sea Surface Temperature reconstruction for Ga3-2 (yellow). The dark horizontal line represents the mean temperature for the record and the dashed line represents the linear trend. Colder periods are presented with a blue background, a temperate period has a beige color and warm periods have a red background. The green arrow presents the current temperature.

Figure 16 plots the temperature for the core Ga3-2 from Table 3. There is a cool period between 890 and 960 CE, followed by a warm period between 960 and 1010, followed by a rapid fall in temperatures of 0.8 ºC that keeps cold until 1180 CE where it continues to be slightly cool and the temperatures start rising from 1372 CE, when an abrupt warm up brings the temperature to its maximum for this record in 1424 CE and continues to be warm until another sudden cooling on 1608 CE.

There is also a trend of temperature increase through the record, the trendline shows an inclination corresponding to a warming of 0.05ºC per 100 years or an increase of 0.4 ºC during the almost 800 years represented in the study. The current Sea Surface Temperature is of approximately 5.2 ºC, as recorded by the CTD published in (Nørgaard-Pedersen and Mikkelsen, 2009), which is similar to the mean of the presented data.

Sea ice

A qualitative estimate for sea ice for Ga 3-2 is plotted in Figure 17Figure 17 Qualitative Sea ice cover reconstruction from ice diatom assemblage for Ga3-2 by adding together the percentages of the species *Fragilaropsis oceanica*, *Porosira glacialis*, *Actinocyclus curvatulus* and *Coscinodiscus occulus-iridis* (Andersen et al., 2004; Koc Karpuz and Schrader, 1990; Miettinen, 2018). There is a low in 1057 and a peak in 1319, in addition there is another peak in 1608. The ice is relatively stable except for those peaks and low, with smaller increases and decreases. The next figure (Figure 18) shows the relation between the sea ice and the sea surface temperature of the core. The results show a good inverse correlation between temperature and sea ice, meaning that when the SST is high, the ice is low, and vice versa. However, between c. 950 and 1050 the sea ice remains relatively stable while the temperature rises.

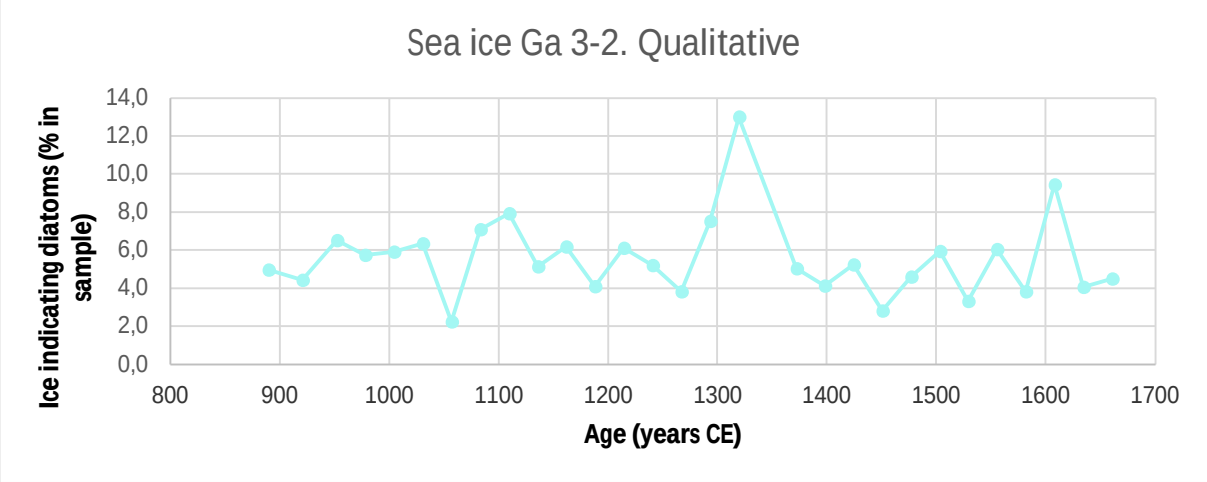

Figure 17 Qualitative Sea ice cover reconstruction from ice diatom assemblage for Ga3-2

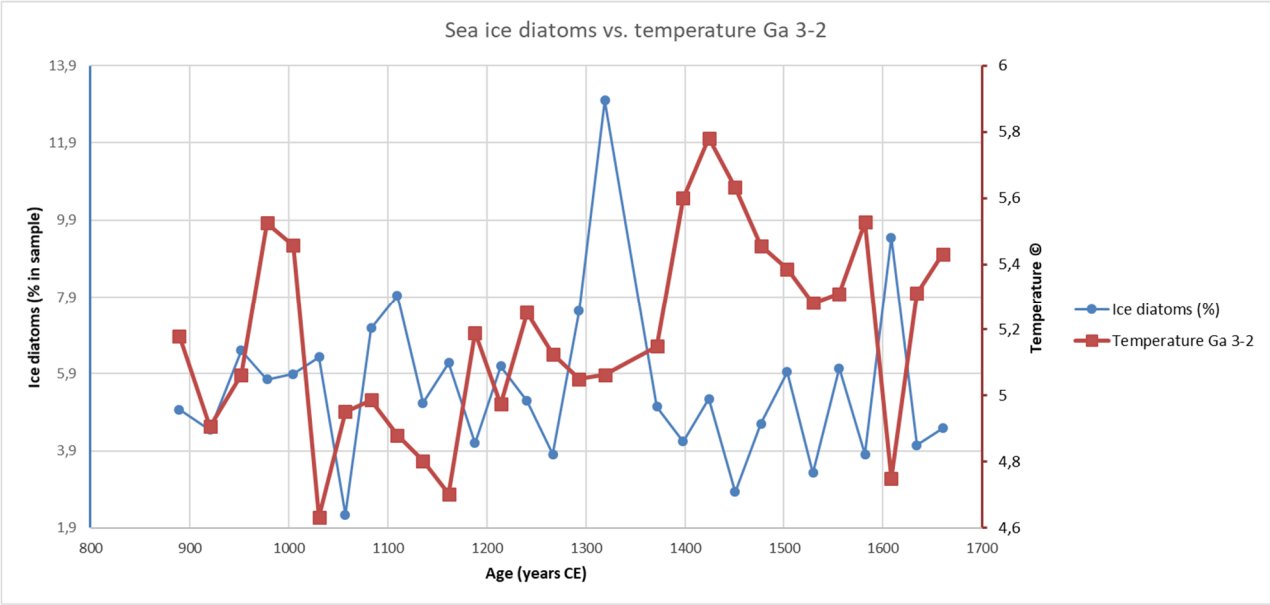

Figure 18 Relation between sea ice (blue) and SST (red) in core Ga3-2

Discussion

Interpretation

The diatom relative abundances are, as explained in the introduction, related to the surrounding environments, as different species are adapted to different ecosystems. Oksman et al. (2019) published an extensive study of diatom species from the data base for the transfer functions for diatoms showing significant ecological responses to april Sea-Ice Cover and august Sea Surface Temperatures. The summary is presented in Table 4.

Species	SST optimum	min. SST	max. SST	Response to SIC	Response model type	
					SST	SIC
Actinocyclus curvatulus	4.7	0	15.2	Yes	V	II
Bacterosira bathyomphala spore	4.6	1	13.2	No	IV	I
Coscinodiscus marginatus	7.1	1.6	15.7	No	IV	I
Coscinodiscus oculus-iridis	6.1	1.7	14.4	Yes	IV	VII
Coscinodiscus radiatus	10.0	1.6	19.7	Yes	IV	II
Fragilariopsis cylindrus	4.4	0	13.2	No	IV	I
Fragilariopsis oceanica	3.6	0	13.1	Yes	II	V
Porosira glacialis	4.3	0	13.4	Yes	V	V
Rhizosolenia hebetata f. *hebetata*	5.1	1.3	15.2	No	IV	I
Rhizosolenia hebetata f. *semispina*	8.5	1.3	18.9	Yes	IV	II
Shionodiscus oestrupii	13.4	2.8	19.7	Yes	III	II
Shionodiscus trifultus	4.4	2.5	15.2	No	V	I
Thalassionema nitzschioides	11.1	1.3	19.7	Yes	V	II
Thalassiosira angulata	9.1	2.0	15.5	Yes	IV	VII
Thalassiosira anguste-lineata	4.0	0	15.5	Yes	V	V
Thalassiosira antarctica var. *borealis* spore	4.9	0	19.7	No	IV	I
Thalassiosira gravida	7.1	0	18.9	Yes	IV	II
Thalassiosira hyalina	4.7	0	11.9	Yes	IV	VII
Thalassiosira nordenskioeldii	7.1	1	13.2	Yes	V	II
Thalassiosira pacifica	9.0	2.4	13.2	Yes	IV	II
Thalassiothrix longissima	8.6	1	19.7	Yes	IV	II

Table 4 Sea diatom taxa and their ecological response to temperature and ice. (SST= August sea surface temperature, SIC=April sea ice cover). The models (I) no relationship (II) through monotone sigmoid, (III) monotone sigmoid with plateau, (IV) unimodal symmetric, (V) unimodal skewed, (VI) bimodal with equal peaks and (VII) bimodal with unequal peaks to aSST (°C) and April sea ice for the 21 studied diatom taxa. (Oksman et al., 2019)

In the table, the ecological data from Oksman et al. (2019) is presented, and most diatom species are shown to have a unimodal symmetric response to sea surface temperature, which means that they have an optimum temperature and both colder and warmer temperatures affect them similarly. There are also some species with unimodal skewed relationship, meaning that they

have an optimum temperature, but can survive better in either warmer or colder than the optimum.

With that information, diatoms found in colder environments and diatoms found in warmer environments are plotted in Figure 19 together with the SST reconstruction. In the graph, the SST reconstruction follows the temperature, although it is not a perfect fit. In this plot, all species are given the same weight for the magnitude of response towards temperature, while on the SST reconstruction, the WA-PLS is used, taking into consideration the individual temperature range of each species.

The taxa used in the figure for cold water are: *Thalassiosira antarctica* var. *borealis* resting spore, *Bacterosira bathyomphala*, *Fragilariopsis cylindrus, Rhizosolenia hebata* f. *hebata, Thalassiosira trifulta*, *Thalassiossira anguste-lineata*, *Nitzschia angularis* and *Thalassiosira hyalina*.

For warm water, the diatom taxa used are: *Thalassiosira gravida, Nitzschia bicapitata, Nitzschia marina, Coscinodiscus radiatus, Thalassionema nitzschioides, Thalassiosira oestrupii, Thalassiosira angulata, Thalassiosira lineata* and *Thalassionema nitzschioides* var. *parva*.

The temperate species are: *Nitzschia atlantica, Thalassiosira nordenskioeldii, Thalassiotrix longissima, Rhizosolenia hebata* f. *semispina, Thalassiosira ferelineata, Thalassiosira nodulolineata, Thalassiosira pacifica* and *Asteromphalus robustus.*

Finally, sea-ice diatoms include: *Fragilaropsis oceanica*, *Porosira glacialis, Actinocyclus curvatulus* and *Coscinodiscus occulus-iridis*.

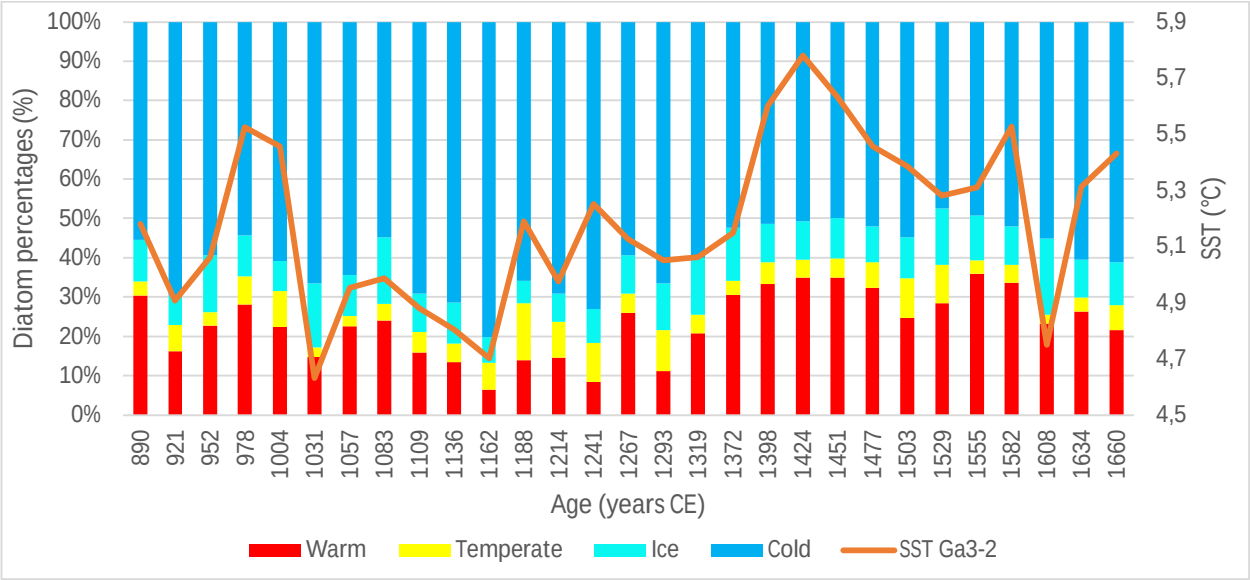

Figure 19 Warm diatoms (red), temperate diatoms (yellow), ice related diatoms (turcoise) and cold temperatures (blue). Sea surface temperature reconstruction for Ga3-2 is plotted as an orange line.

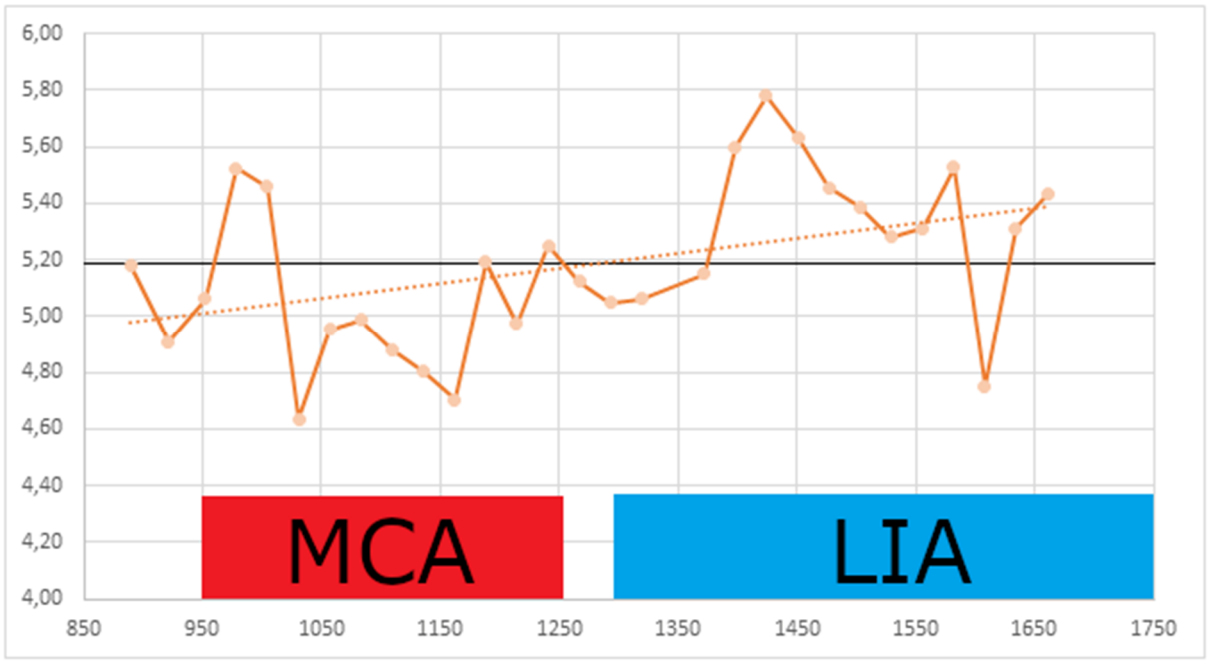

Figure 20 Temperatures for Ga3-2. The black horizontal line shows mean and the dotted line shows the trend. The red rectangle shows the time period for the MCA while the blue rectangle shows the time period for the LIA

The periods known as Medieval Climate Anomaly (MCA) and Little Ice Age (LIA) can be detected in the record, although with opposite temperature trends than otherwise recorded

(Lamb, 1965). During the medieval climate anomaly, which is set between 950 and 1250 (Hughes and Diaz, 1994; Lamb, 1965; Mann et al., 2009), the temperatures in Narsaq Fjørd where high at first, but rapidly decreased and the rest of that period had low temperatures. Per contra, during the Little Ice Age, defined between 1300 and 1850 (Lamb, 1965; Matthes, 1939), the record starts with slightly low temperatures that quickly increase leading to a period with temperatures warmer than the mean for the rest of the record (Figure 20).

The high temperature period at the end of the 10th century coincides with the settlement of the Norse population in south Greenland in 985 CE (McGhee, 2001; Mikkelsen et al., 2008), although it does not explain why they would abandon Greenland in a period of high temperatures around the 1450 CE (Fitzhugh, 2000). The decolonization of Greenland at that time could be explained if the winter conditions were very severe even when summer temperatures were high. It could also indicate that although summer SST was high, atmospheric temperatures at that time were colder.

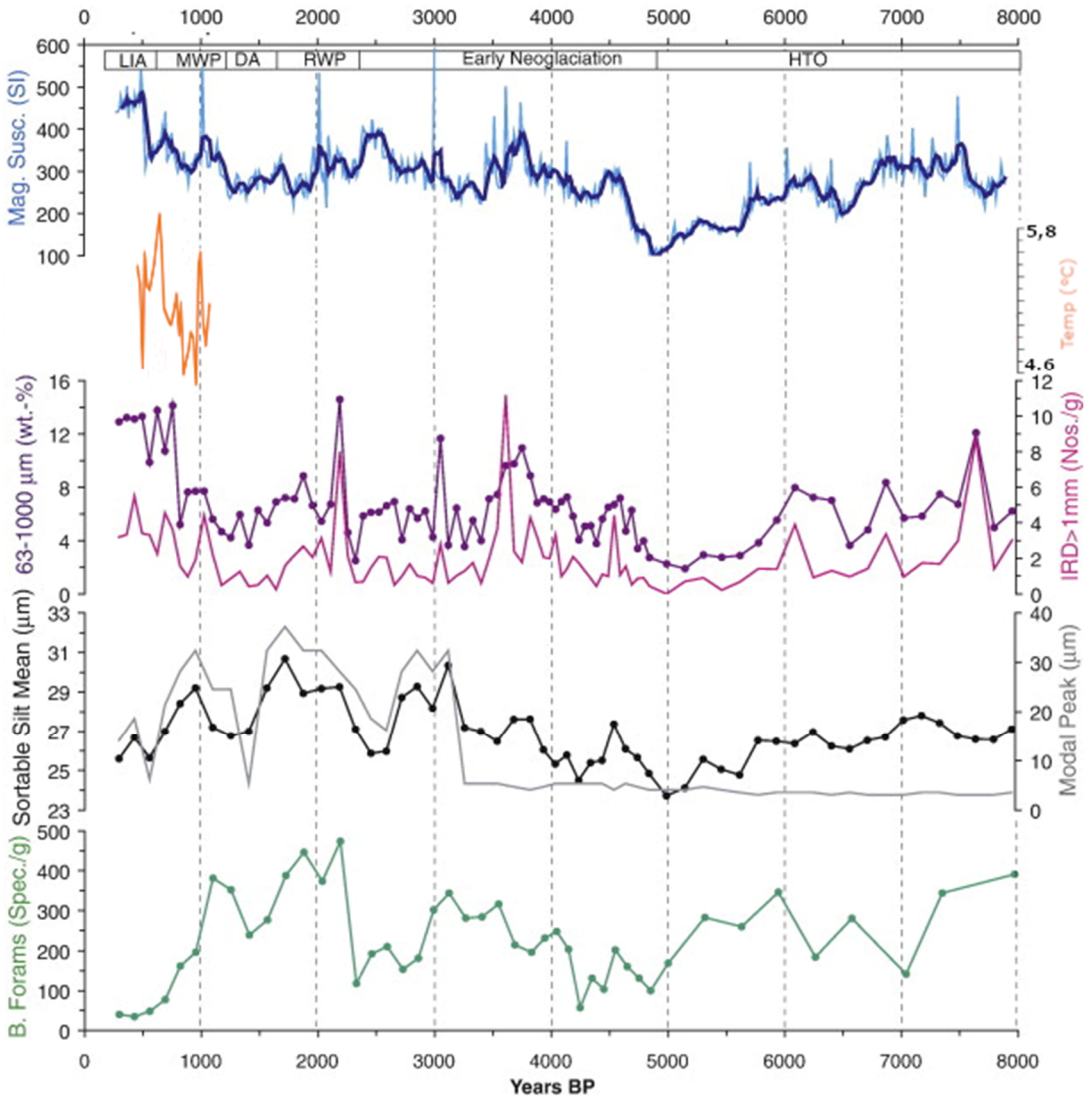

Figure 21 Basic data of core Ga3-2 and temperature record plotted versus age: Magnetic susceptibility (MS) with a 5 pt. running average overlay, 63–1000 µm (wt.%), nos. of IRD grains > 1000 µm/g, sortable silt weighted mean, modal grain size distribution peak values, and nos. of calcareous benthic foraminifera (> 125 µm)/g. LIA: 'Little Ice Age', MWP: 'Medieval Warm Period' (aka. Medieval Climate Anomaly (MCA), DA: 'Dark Ages', RWP: 'Roman Warm Period' HTO: 'Holocene Thermal Optimum'. The orange line indicates the timespan analysed in this study (Modified from Nørgaard-Pedersen and Mikkelsen, 2009) (Same as Figure 14)

Magnetic succeptibility in Figure 21 presents high values during the LIA, back until 1450 CE (or 500 BP), then it lowers but it has a relative peak at 950 CE (1000 BP). If we compare the results to the temperature, we see that the temperature peak at around 970 CE coincides with the high values, and that can indicate that it was a period of ice melting and that ice rafted detritus were deposited at that time.

Description of sediment cores MD-2322 and Rapid 21-COM

The original description of the sediment core MD99-2322 can be found in Jennings et al. (2011); and for the composite sediment core Rapid 21-COM extensive information has been published in Miettinen et al. (2012).

Description of MD99-2322

MD99-2322 is a sediment core collected from 668 m water depth east of Greenland and south of the Greenland-Iceland Ridge campaign (Labeyrie, 1999; Stoner et al., 2007).

The dating of MD99-2322 was obtained through AMS radiocarbon, and a reservoir of 400 years is assumed (Jennings et al., 2011).

The MD99-2322 record shows a colder period from 890 to 990 followed by a warm period until 1100 and then from 1140 to 1200 with a period of temperatures near the mean temperature in between. After 1200 a little cool period follows up to 1270 when a new variable and still cool, but more temperate period starts. That period lasts until 1600, when the temperature rises. Figure 22 and Figure 23 show the temperature records for MD99-2322 with and without smoothing.

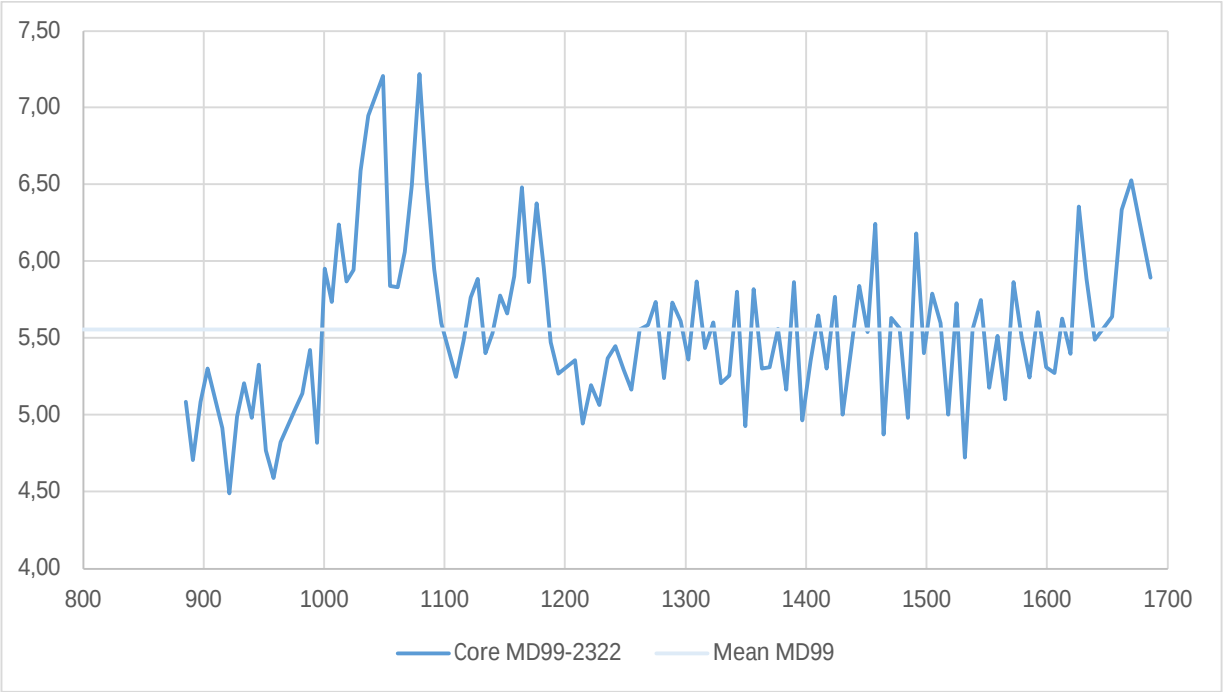

Figure 22 Temperature record for core MD99-2322. Without smoothing. Data from Miettinen (2015).

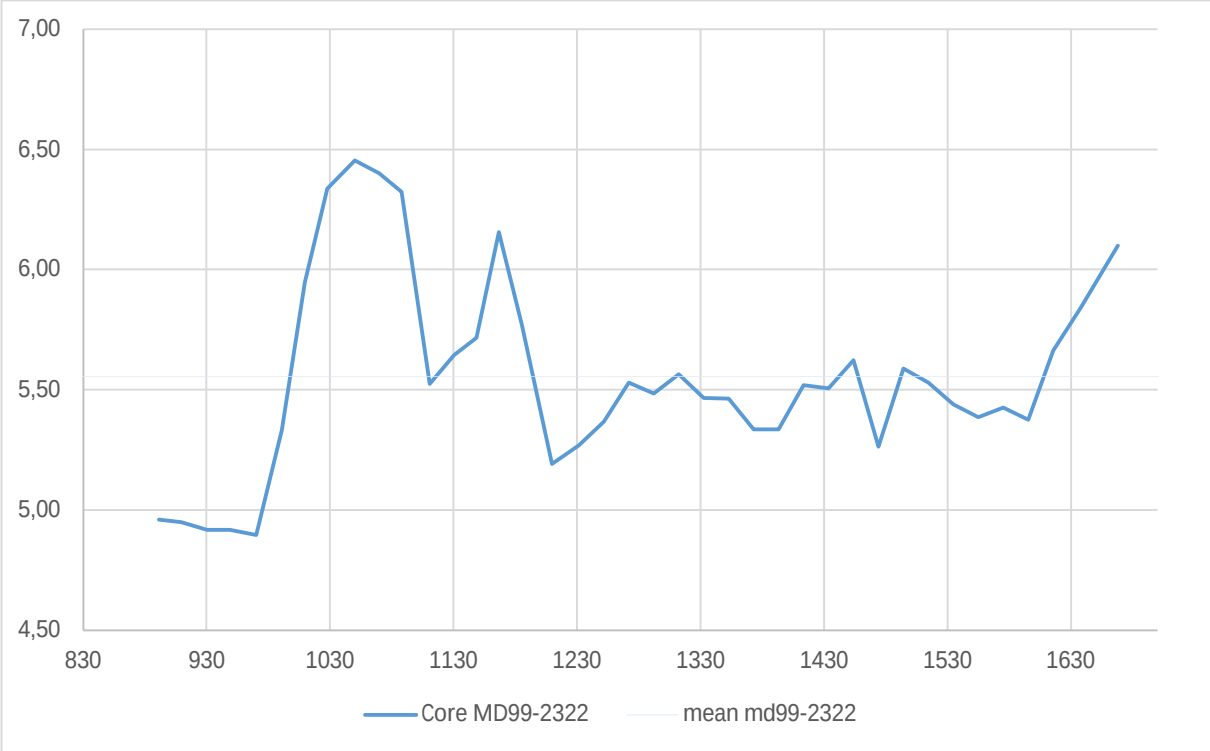

Figure 23 Temperature record for MD99-2322 with a running average to smooth lower scale variabilities and make it more comparable to Ga3-2. Data from Miettinen (2015).

Description of Rapid21-COM

Rapid 21-COM is a composite core consisting of two cores, a box core and a Kasten core. They were retrieved at the southern limb of the Gardar Drift on the eastern flank of Reykjanes Ridge at 2630 m water depth during the RRS Charles Darwin cruise 159 in 2004 (Miettinen et al., 2012).

Dating for this core was obtained through 210Pb dating for the box core and AMS-14C datings for the Kasten core. Further information on these cores are published in Boessenkool et al. (2007); Miettinen et al. (2012); Miettinen et al. (2011); Schmidt et al. (2012).

The beginning of the record from Rapid 21-COM, between 890 and 1000 CE is cold, followed by a short period until 1080 of colder temperatures before they drop until 1200. There is then another short and warm period until 1260 and then a more temperate, almost cool period until 1400, where the temperature gets warmer. Figure 24 and Figure 25 show the temperature record of Rapid 21-COM with and without smoothing.

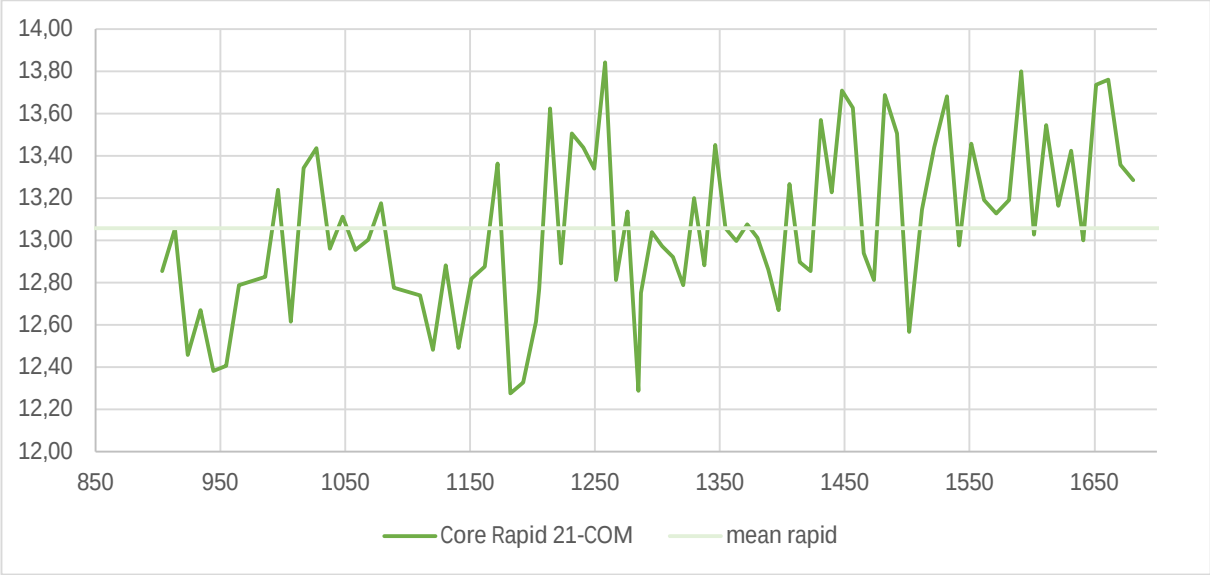

Figure 24 Rapid 21-COM temperature record. Data from Miettinen (2014b).

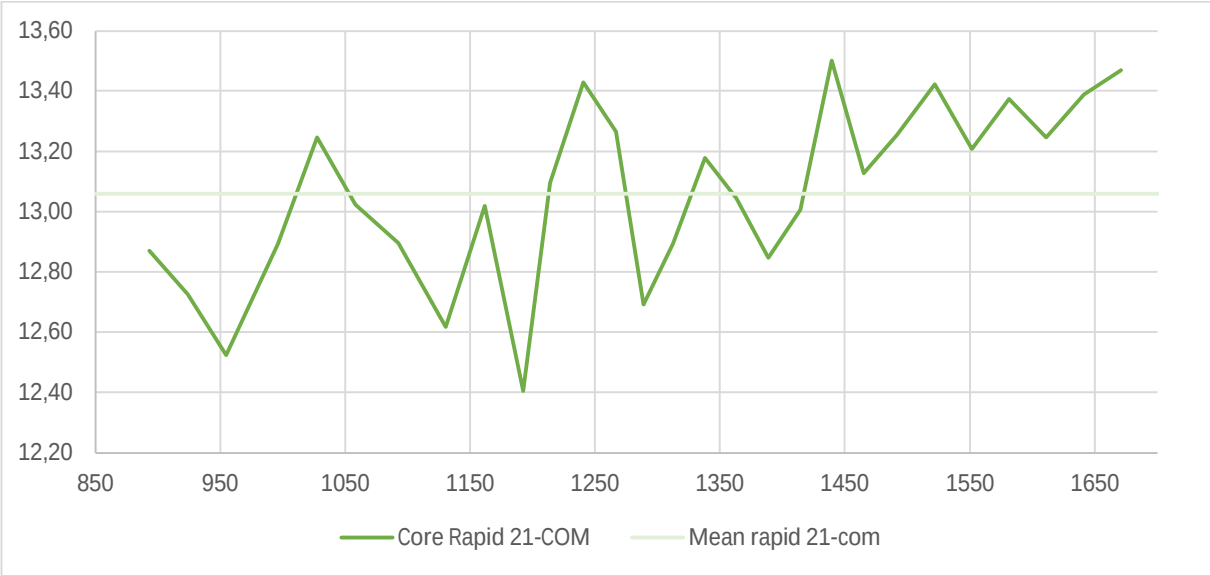

Figure 25 Running average Rapid 21-COM temperature record. Running average with the purpose of smoothing short scale variability. Data from Miettinen (2014b).

Comparison between Ga3-2 and the other sediment cores

The mean SST of cores Ga 3-2 is comparable to that of MD99-2322, with values of 5.2ºC and 5.5ºC respectively. The mean temperature of the Rapid 21-COM record is around 8ºC higher, at 13.1ºC. Figure 26 and Figure 27 plot the temperature of these three cores.

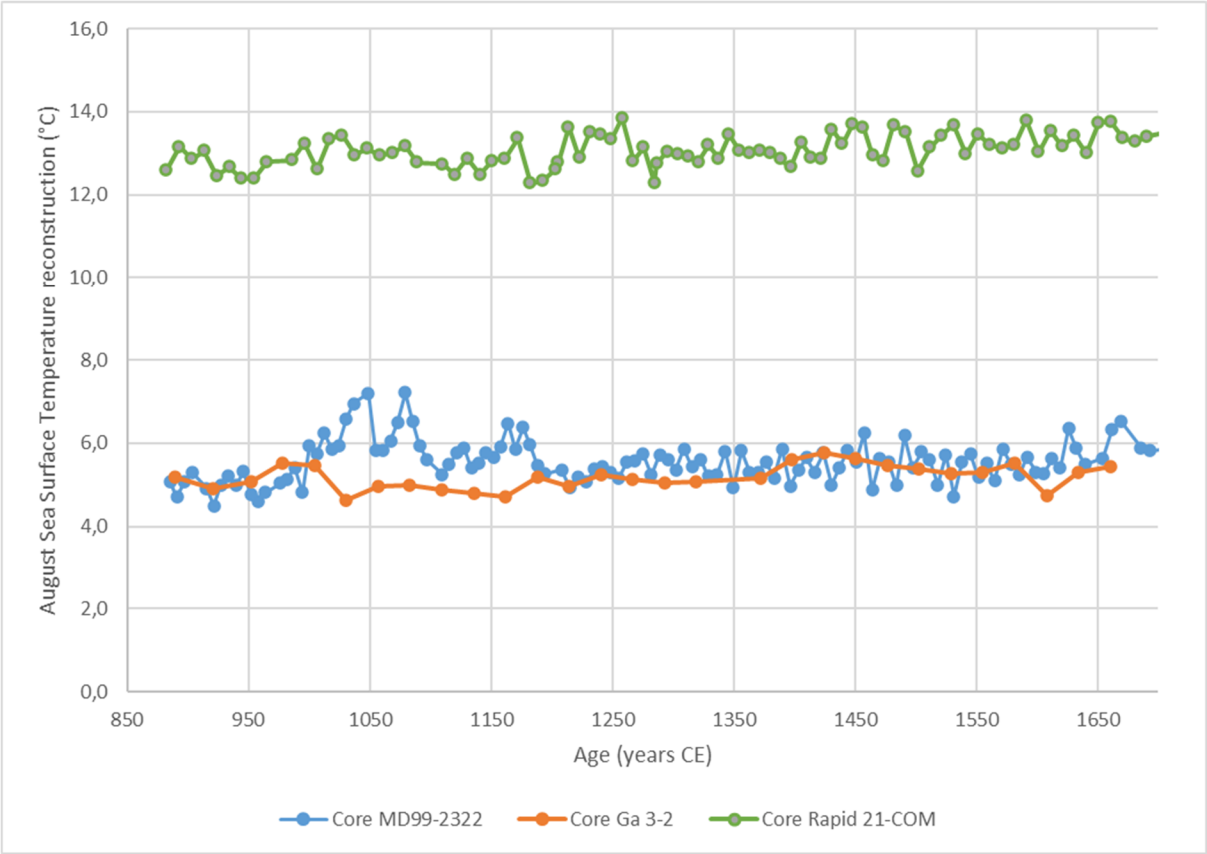

Figure 26 Core temperatures. Comparation between Rapid 21-COM (green), Ga 3-2 (orange) and MD95-2322 (blue). The dots show the datapoints, the line shows the running average in order to better compare all three cores together.

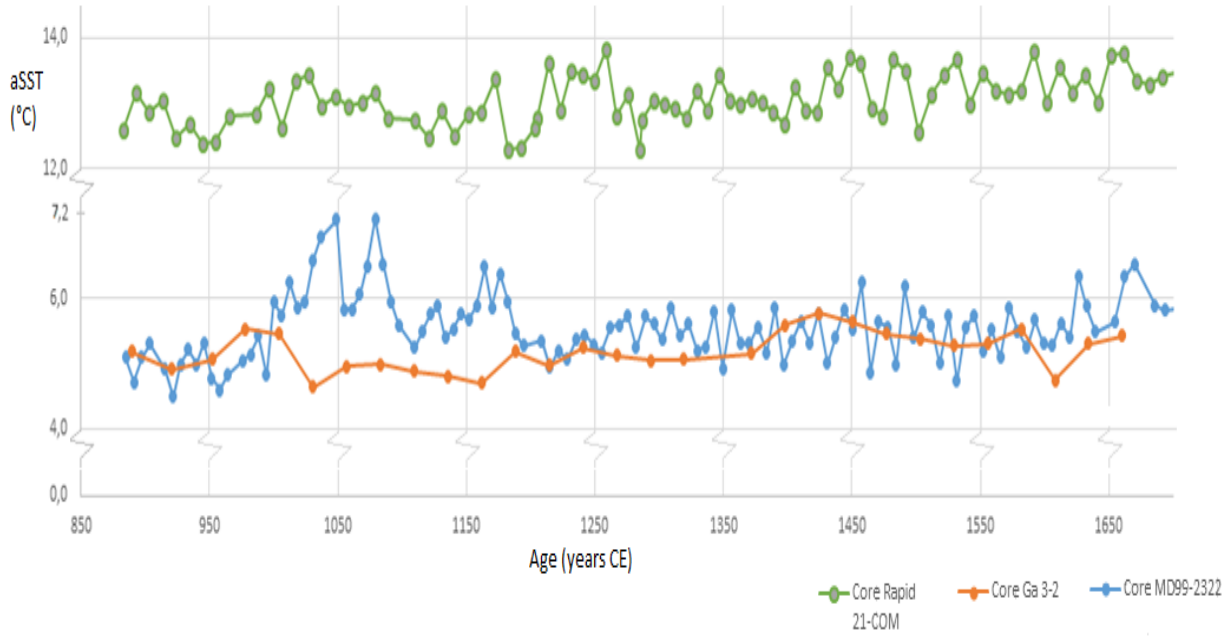

Figure 27 Core temperatures. Note that the y-axis is cut to help visualization. Cores shown are Ga3-2 in orange, MD99-2322 in blue and Rapid 21-COM in green.

The temperature trends in all three cores are not very accentuated and therefore, they can more easily be compared with their deviation to their mean. Figure 28 shows the result.

The oldest part of the record, between 890 and 960-970 CE shows colder than average temperatures for the three cores that are being compared, with the lowermost point being approximately at the same time, around 920 CE. That is followed by an increase of temperature in all three cores, with Ga 3-2 warming up first, almost simultaneously with Rapid 21-COM, while MD99-2322 keeps the cold temperatures for a longer period, warming up from 950 CE. The increase in temperatures is however more dramatic for MD99-2322, and rapidly continues to increase into a period of high temperatures that reaches almost 1ºC above the mean temperature, a peak that occurs from 1030 CE until 1080 CE. Ga3-2 has also a peak with temperatures warmer than average (+0.3ºC) and then the temperature decreases again into a colder period that lasts for 180 years, between 1010 and 1190 CE. As to Rapid 21-COM, it has the same trend with a peak in temperatures that is much more modest, at almost average values, and slightly later, about 20 to 30 years later. The period of colder temperatures shown by Ga3-2 is similar to that of Rapid 21-COM, and both of them show a good inverse correlation against MD99-2322. There is however a minor peak in Ga 3-2, while still cool, are closer to the mean temperature of the record at around 1083 CE, and not long after, at 1100 CE MD99-2322 has a low that is as well around the mean, both to go back to colder (Ga3-2) and warmer (MD99-2322) temperatures until the end of this period, that is around 1190 CE. Rapid 21-COM does not show this peak.

Rapid 21-COM has a period of 50 years between 1200 and 1250 CE where temperatures reach around 0.3ºC higher than their mean. At the same time, MD99-2322 shows the opposite trend (-0.4ºC) and Ga3-2 has an increase of temperature but does not go over the mean and rather remains at cooler temperatures. This is followed by a 100-150 year long period of temperatures

that are around the mean in all three cores, between 1250 and 1370 for Ga 3-2, and between 1250 until 1400 for Rapid 21-COM. Both show thereafter an increase of temperatures that will last the rest of the record until 1660 CE. MD99-2322 continues at an average temperature, with rather cooler than warmer temperatures until 1600 CE, when temperatures increase.

The temperature record of Ga3-2 correlates well with the temperature record of Rapid 21-COM, and Rapid 21-COM seems to have less than 10 years of delay with respect to Ga3-2. In general, Rapid 21-COM and Ga3-2 have a good direct visual correlation, while there apparently is an inverse correlation between Ga3-2 and MD99-3233.

The data for Ga 3-2 show that at the beginning of the time of the MCA the temperature rises slightly (950-1000 CE) to rapidly descent to cold temperatures until the end of the MCA, and it has a high temperature during the Little Ice Age dating from 1300 to 1830, although the record for Ga3-2 ends at 1650.

The temperature during the MCA for Rapid 21-COM is low, the temperature raises between 950 and 1050 CE and then it goes down until around 1200 CE.

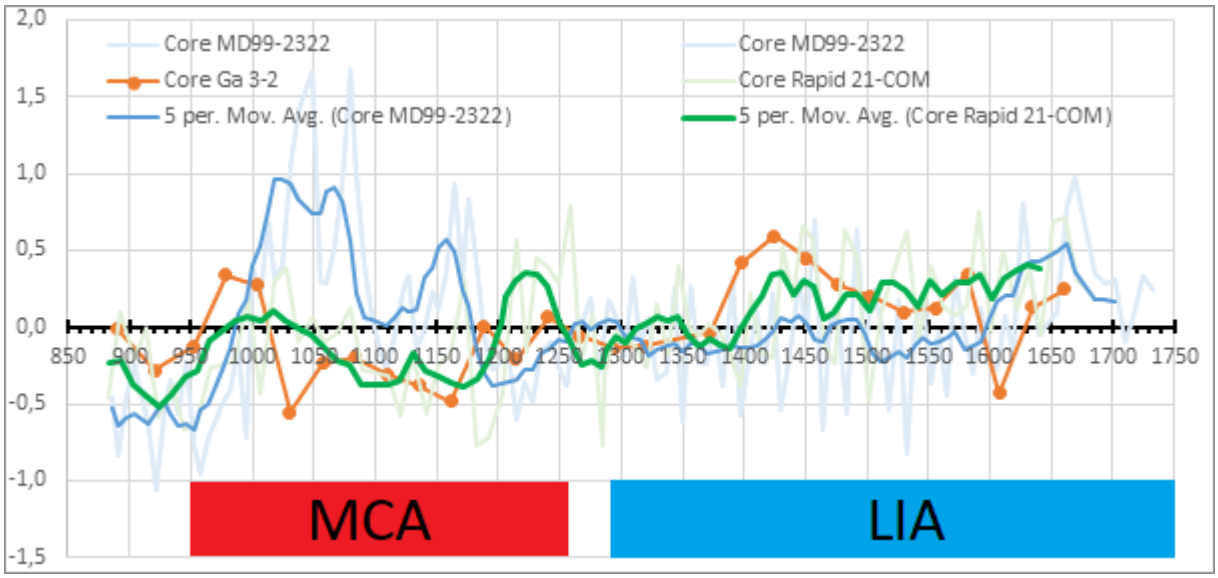

Figure 28 Sediment cores compared using the variability to the mean. x-axis shows age in years CE and y-axis shows the deviation from the mean in °C.

Description of the ice cores GISP 2, DYE-3 and Renland

The Greenland ice core records chosen for comparison with atmospheric climate data are Dye3, Renland and GISP 2. The first is located in southern Greenland and is closest to the core site, Renland is at the eastern coast and under marine influence, and GISP 2 is located to the north at the centre of the inland ice and record regional climate signals (Figure 1). The temperature proxy for the ice cores is $\delta^{18}O$.

Description of DYE-3

Dye 3 was drilled between 1979 and 1981, retrieving 2037.63 m of ice core at 65.18N, 43.82W in the ice sheet in South Greenland (Gundestrup and Hansen, 1984) (Figure 1).

Dye 3 starts with high temperatures that last from 880 to 1080 CE, when it transitions to a period of cooler temperatures that continues until 1200, and is followed by the highest point from the record at the next sample point in a period that seems more or less temperate, a trend that continues until 1370, when another low followed by a period of higher temperatures as shown in Figure 29 below.

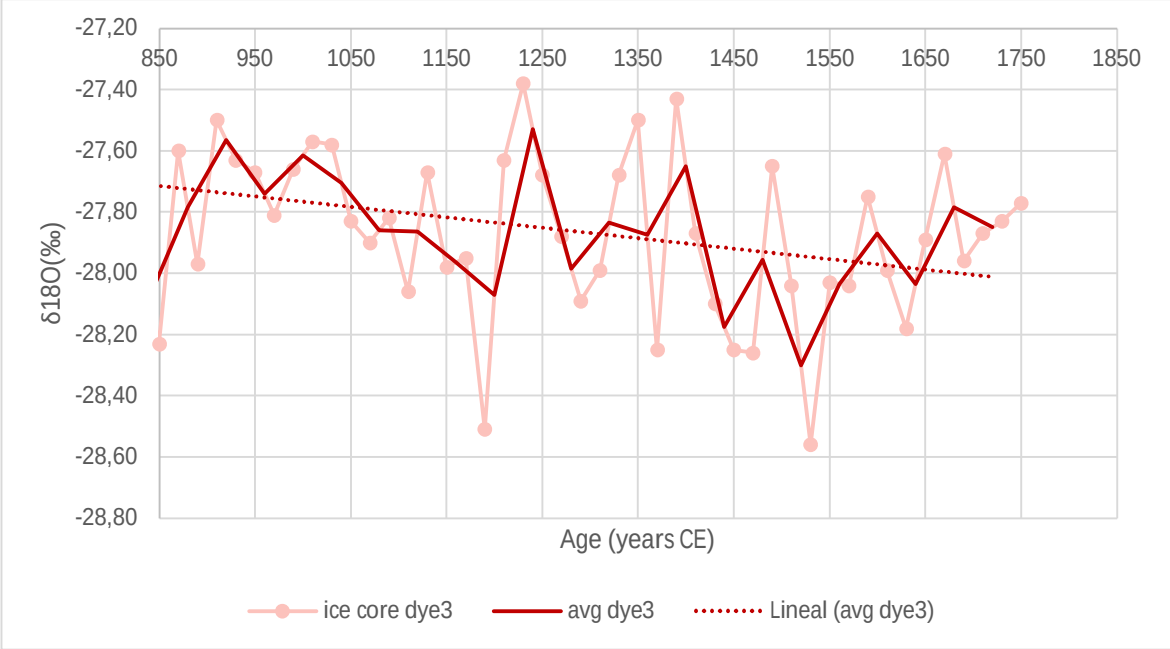

Figure 29 $\delta^{18}O$ for ice core Dye3. Data from Kaufman et al. (2009)

Description of GISP 2

GISP 2 is an ice core drilled between 1988 and 1993, at 72°36'N, 38°30'W. The core consists of 3053m of ice and penetrated all the way into bedrock. The record includes data for the last 4000 years (Grootes et al., 1993).

The record between 890 and 1660 CE shows a decreasing trend, with high variability. The data has been smoothed to 30 years average per point.

At the beginning of the record analysed here, the temperature is higher than the mean until 990 CE. The temperature is under the mean for around 50 years after that and then proceeds to be at higher temperatures until approximately 1190 CE. Then a period of temperatures like the mean continues until 1290 CE. This is followed for cold temperatures for 100 years and warmer from 1380 until 1500 CE. Then the temperature goes down the rest of the record until 1690. In general, GISP 2 seems opposite from Ga3-2 until the end, where Ga3-2 shows a maintained warm period from 1400 until 1600 CE with a low point in 1608 CE to then be warm again, while GISP 2 begins to cool at around 1500 CE and stays cold until the end of the plotted record at 1680 CE.

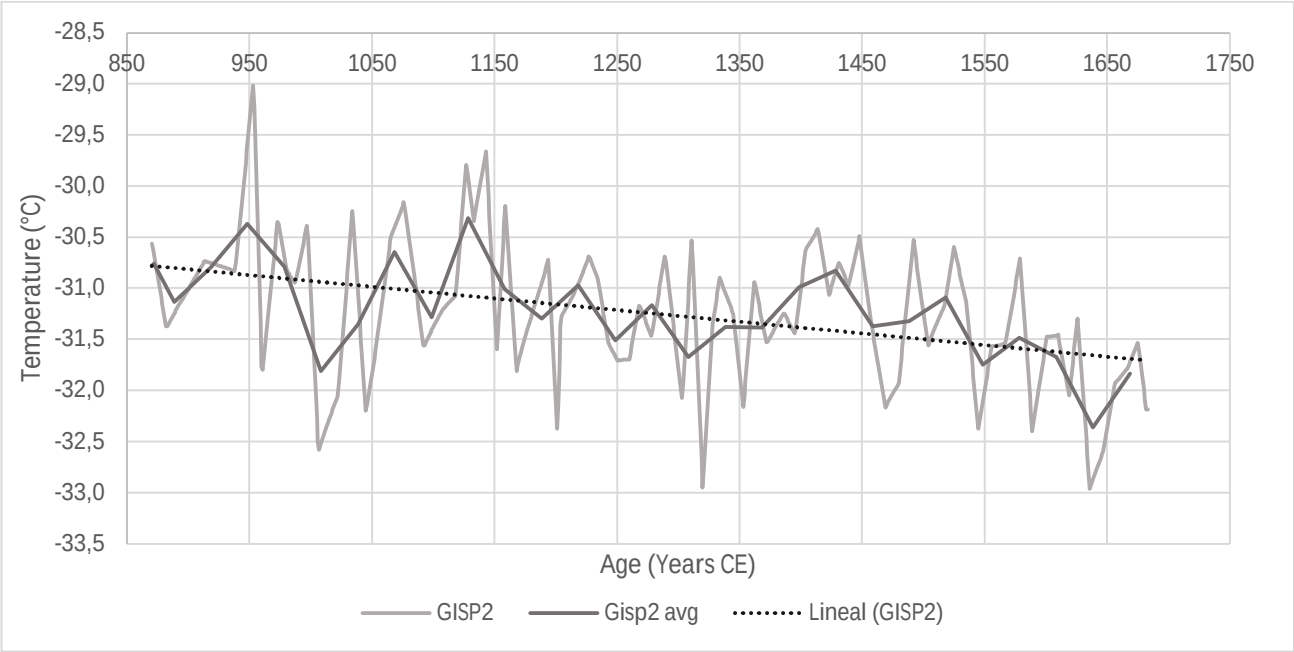

Figure 30 Temperature data for core GISP 2. Data from Kaufman et al. (2009)

Description of Renland

Renland is an ice core drilled at 71°16'N and 26°44'W, in the eastern coast of Greenland, and has a length of 325 m. It was drilled in 1988. The information this core provides is therefore atmospheric temperatures in the coastal area.

The record of this core shows a slight decrease of temperature over time. The record starts at higher moderate temperatures until 950 CE, then there is a zig-zag with 100 year intervals, with a warm peak at 970 and 1160, and cold at 1070. After that, there is a longer cold period that lasts until the datapoint at 1360 CE. This is followed by the warmest plotted in this study for this core, in 1390, which is part of a warm period that continues until 1550. After that, there is a period of lower temperatures. The end of the record shows the temperatures were on an increasing trend.

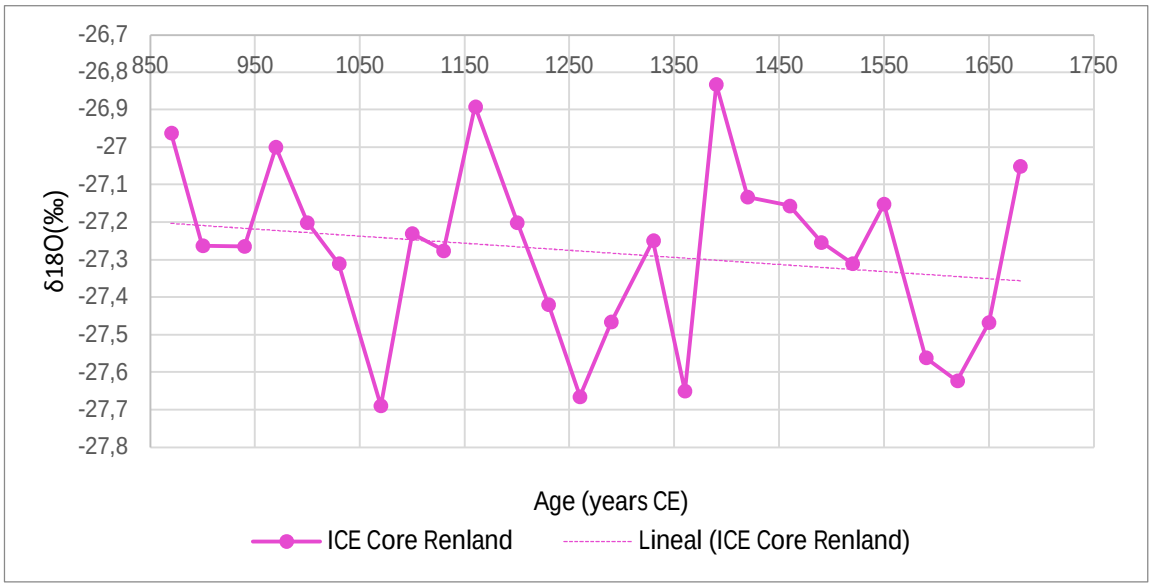

Figure 31 $\delta^{18}O$ for ice core Renland. Data from Kaufman et al. (2009)

Comparison between Ga3-2 and ice cores

Figure 32 plots the deviation from the mean temperature for the different ice cores and sediment core Ga3-2. Plotted in orange, Ga3-2 shows a good correlation to Renland (pink) and GISP 2 (gray). While Ga3-2 and Renland show a good correlation along the whole record, Dye3 does not follow the same trend between 1400 and 1550 but rather stays cold, opposite to the two other ice cores and Ga3-2.

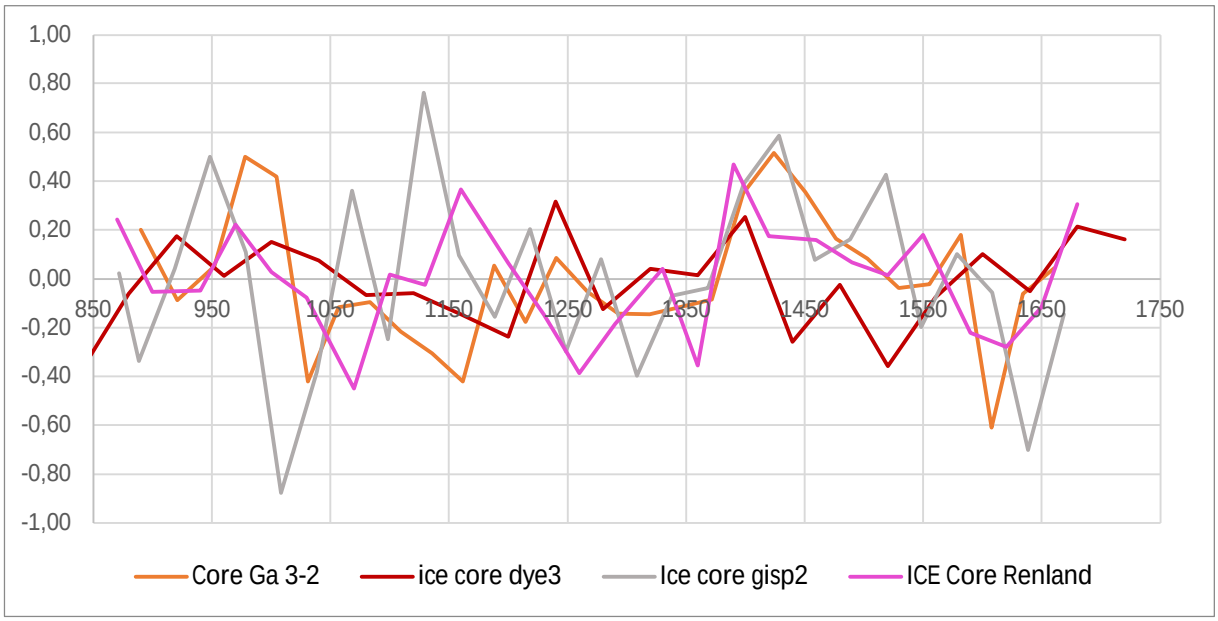

Figure 32 Comparison between sediment core Ga3-2 (orange) and ice cores Dye3 (red), GISP 2 (gray) and Renland (pink). The y-axis shows the deviation from their means, both from temperature (for Ga3-2 and GISP 2) or d18O (Renland and dye3)

Cores Ga3-2 and Renland show very good correlation during LIA (between 1300 CE and the end of the record in 1650 CE). The correlation is in fact good for almost the entire record, except for the second half of the MCA, between 1100 and 1250 CE, when Ga3-2 still shows low SST temperatures, while Renland records a higher temperature period.

GISP 2 shows a similar trend to Ga3-2 from 1200 CE and onwards. GISP 2 also shows the highest discrepancies at the second half of MCA. In this case, GISP 2 has a temperature peak in 1130 CE.

As of core Dye3, the biggest discrepancies are during the LIA. While Ga3-2, Renland and GISP 2 registers high temperatures, Dye3 records show lower temperatures after 1420 CE.

The good correlation between SST in Narsaq sound and the data obtained from the ice cores could indicate that the conditions in the sound are driven by atmospheric factors. This is likely due to the core site being inside the fjord and surrounded by glaciers.

Comparison to other records

If we continue to compare to other records in the region, Figure 33, some work gathered by Moffa-Sánchez et al. (2019) is presented together with the Narsaq core Ga3-2 (in yellow-orange in *m*).

The temperature trend for Ga3-2, inside the fjord, is opposite to the temperature indicated by foraminifera *Neogloboquadrina pachyderma* in Figure 33 *m* (a higher the percentage of this species indicates a colder water temperature), particularly after around 1400 CE. In case of haematite-stained grains (Figure 33 *g*), a higher percentage indicates a larger influence from drift ice. When comparing the two records, Ga3-2 displays lower temperatures with low drift ice and higher temperatures when there is an increase in drift ice. Both records (Rapid 35-COM and GS06-144-03) are from the shelf in southern Greenland (Figure 34).

The fact that Ga3-2 does not show correlation with the work from Moffa-Sánchez et al. (2019) can be related to the different characteristics in the proxy used. Diatoms need light and therefore live in the uppermost part of the water column, so they reflect changes in the surface water (Justwan et al., 2008) while coccoliths and planktic foraminifera usually are found deeper in the water column and therefore reflect temperatures from a different water mass. Similarly, as presented in the introduction, diatoms represent best the Sea Surface Temperature in august, whereas other proxies like foraminifera are more species-dependent and might represent other seasons or have no seasonal specific response (Kawahata et al., 2002; Moffa-Sánchez et al., 2019). The Ga3-2 diatom assemblage probably reveals the qualities of the EGC and the melt waters from the ice in the area.

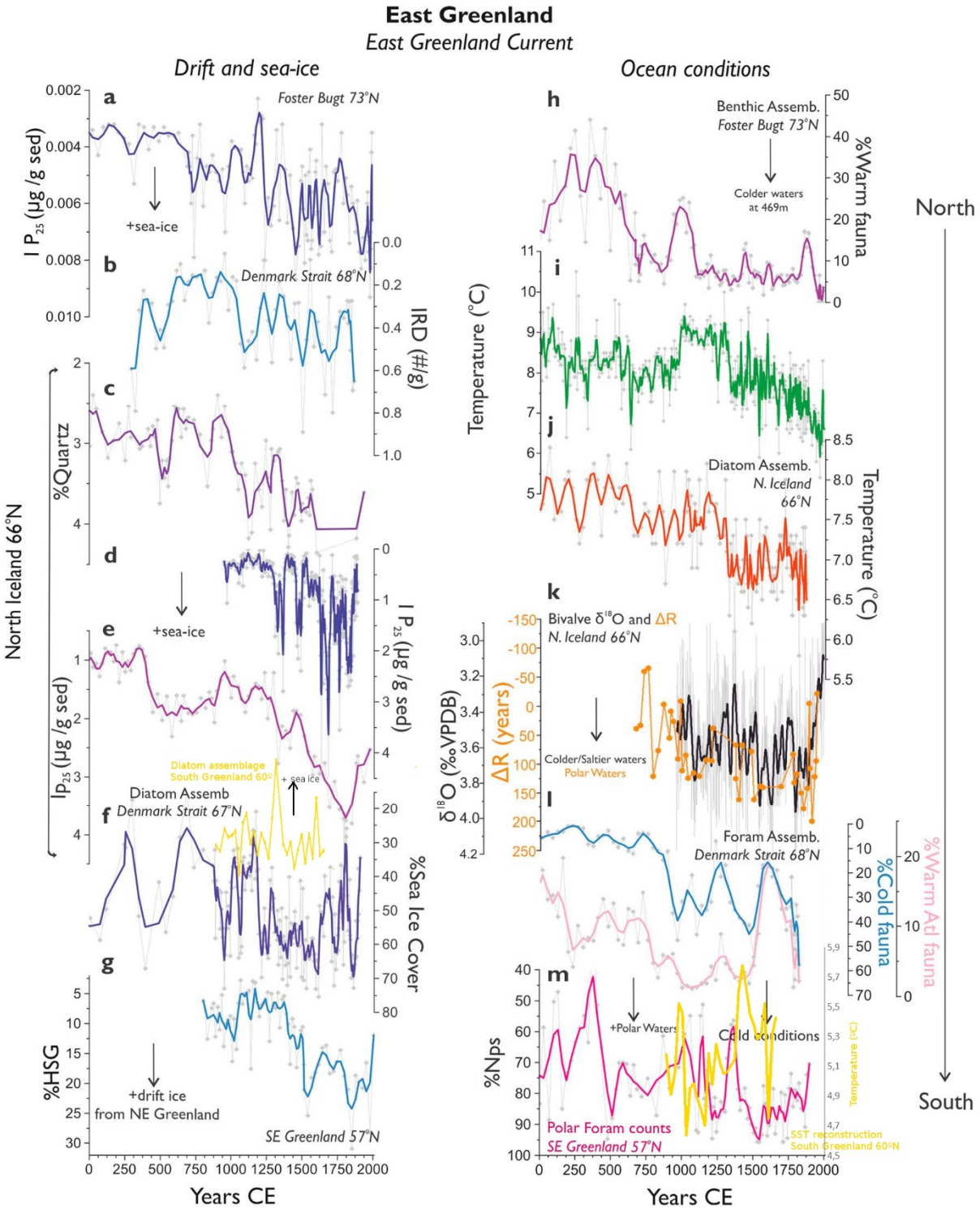

Figure 33 Ice and oceanographic conditions along Eastern Greenland and North Iceland. Left panel shows sea/drift ice conditions (a) sea ice conditions in PS2641 BC/GC at Foster Bugt (Kolling et al., 2017); (b) drift ice recorded in the Denmark Strait JM96-1206/2GC (Perner et al., 2016)North Iceland; (c) %Quartz from MD99-2269 (Moros et al., 2006); sea ice biomarker (d) MD99-2275 (Massé et al., 2008) and (e) MD99-2269 (Cabedo-Sanz et al., 2016); (f) April sea ice cover from diatom assemblages in the West Denmark Strait, MD99-2322 (Miettinen et al., 2015);and (g) Haematite Stained Grains (HSG) transported from northwest Greenland to South Greenland (GS06-144-03;Alonso-Garcia et al. (2017)). Right panel shows oceanographic conditions (h) benthic foraminiferal assemblages at ~430 m, which are indicator of Atlantic Intermediate Waters (PS2641 BC/GC; Perner et al. (2015)), North Iceland upper water column conditions; (i) sea surface temperatures from alkenones (MD99–2275; (Sicre et al., 2008; Sicre et al., 2011)); (j) summer sea surface temperatures from diatom assemblages in MD99–2275(Jiang et al., 2015); (k) δ18Oshell (black) (Reynolds et al., 2016) and ΔR (orange) (Wanamaker et al., 2012) from Arctica islandica from the North Iceland shelf; (l) benthic assemblage from ~400-mdeep in the Northern

Denmark Strait JM96-1206/2GC (Perner et al., 2016); (m)Pink and gray: % planktonic foraminifera species N. pachyderma from the Eastern Labrador Sea, South Greenland; RAPiD-35-COM (Moffa-Sánchez and Hall, 2017). Bold lines on raw data are weighted three-point smoothing. Yellow-orange (m): Sea surface temperature reconstruction from diatoms in Narsaq sound (sediment core Ga3-2). Yellow-orange (e): Sea ice reconstruction from diatoms in Narsaq sound (sediment core Ga3-2) Modified from Moffa-Sánchez, 2019.

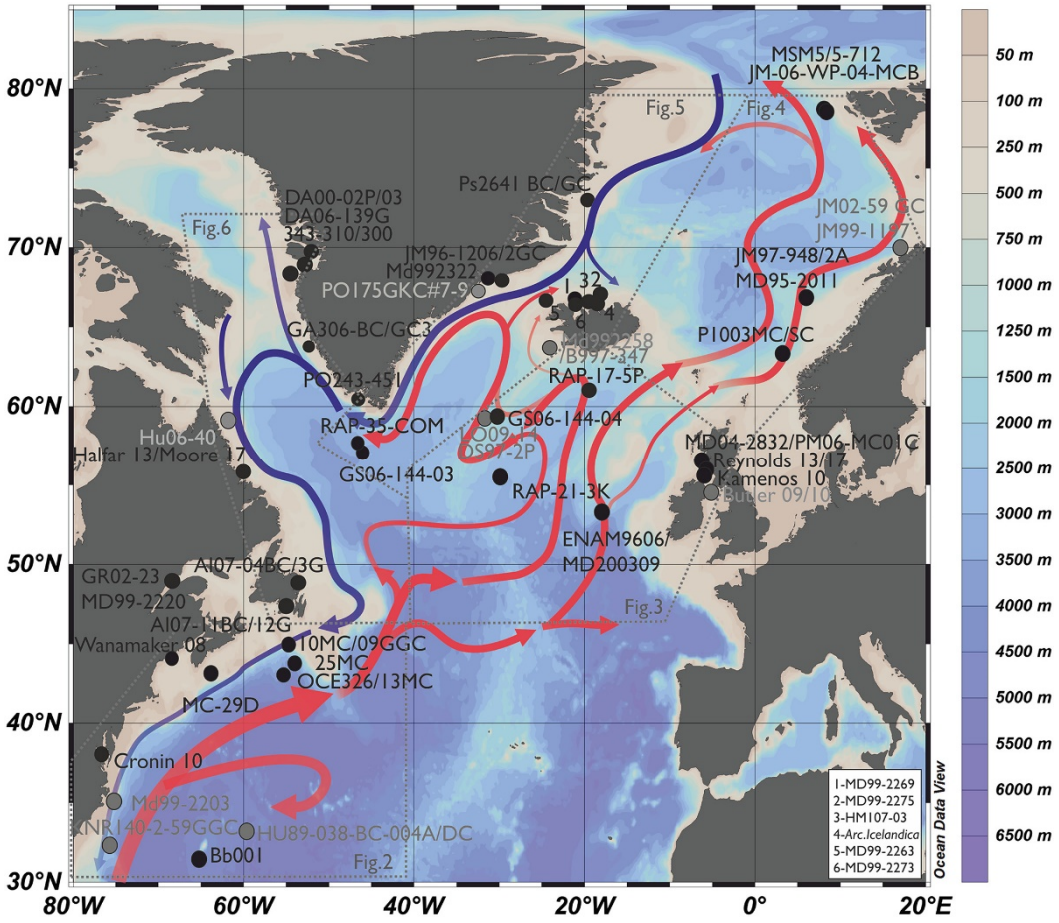

Figure 34 Map with the proxy records used in Figure 33. Based on Orvik and Niiler (2002), Daniault et al. (2016), and Bosse et al. (2018). Red arrows indicate the pathway of relatively warm and saline waters and blue arrows the pathway of cold southward polar waters.(Moffa-Sánchez et al., 2019)

The diatom assemblage from the north of Iceland (MD99-2275) show a general opposing trend to that of Ga3-2. That, together with the similar trend of Ga3-2 to Rapid 21-COM (Reykjanes Ridge) support the idea by Seidenkrantz et al. (2007) of an opposing climate of south Greenland and north Europe, with ocean currents playing a major role (Figure 35).

In this scenario, cold periods in southern Greenland might be linked with a weaker Irminger Current with most of the NAC continuing northeastwards along the eastern Atlantic, while warm periods are caused by a stronger western deviation of the NAC, with warmer waters reaching the southern part of Greenland, while western Europe receives little heat transport from the NwAC (Miettinen et al., 2012; Seidenkrantz et al., 2007).

This opposite trend between Greenland and the eastern Atlantic and eastern Nordic seas could be due to NAO variations, and the consequent variation in air pressure of the air system. This hypothesis has already been proposed e.g. Lasher and Axford (2019); Trouet et al. (2009).

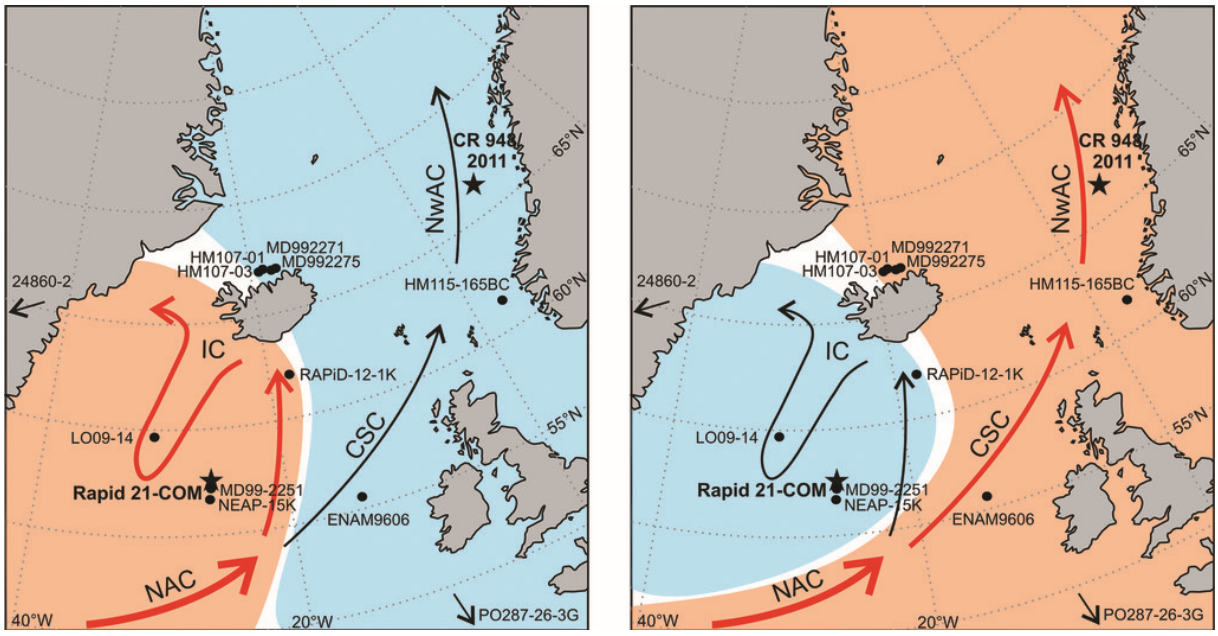

Figure 35 Schematic map for aSST during cold periods (left) and warm periods (right). Red arrows show the currents transporting the most heat. The shading indicates surface water temperatures (red for warm and blue for cold) abbreviations: NAC=North Atlantic Current CSC=Continental Slope Current NwAC=North-west Atlantic Current IC=Irminger Current (Miettinen et al., 2012)

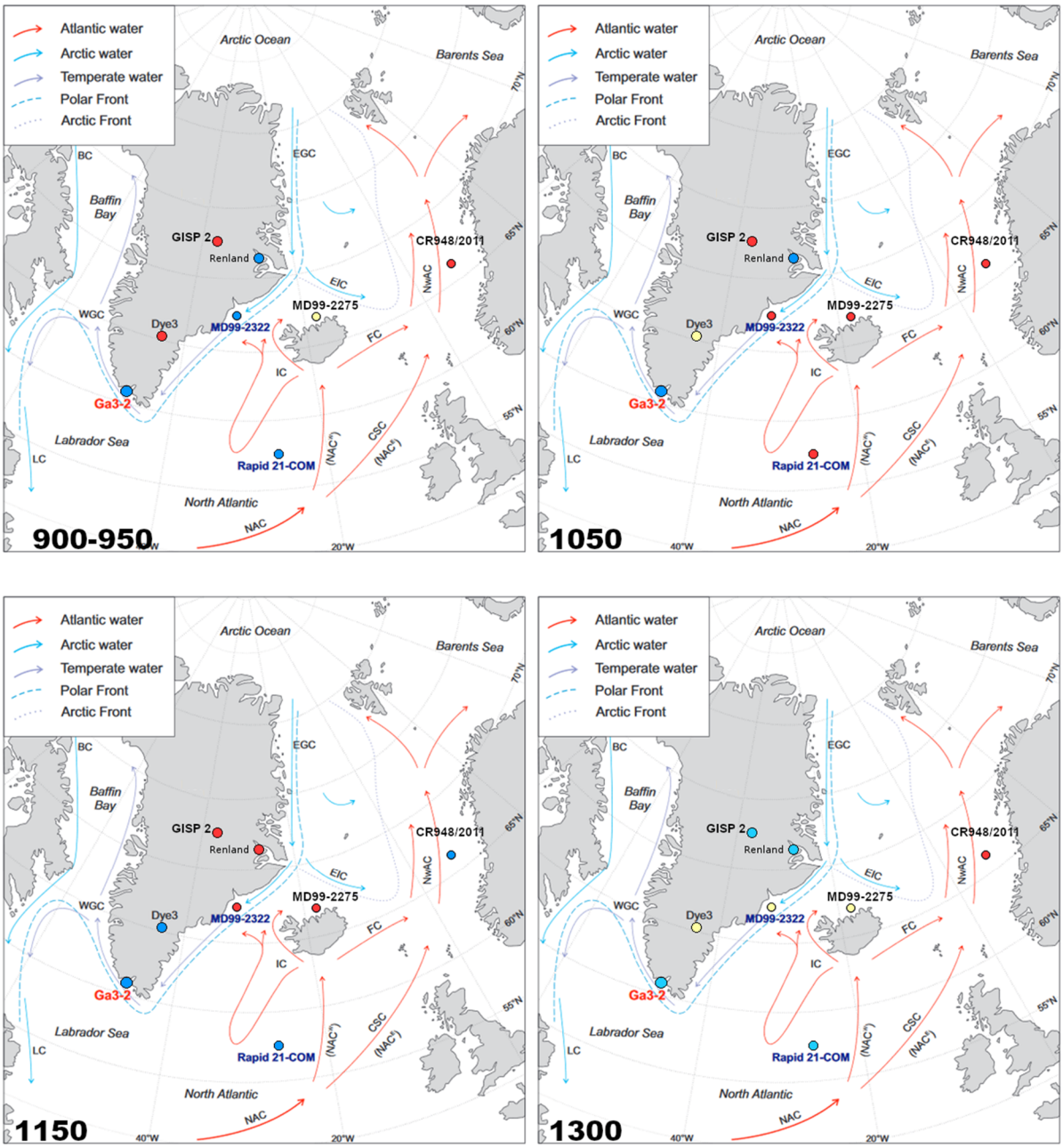
Atlantic water
Arctic water
Temperate water
Polar Front
Arctic Front
Arctic Ocean
Barents Sea
BC
Baffin Bay
EGC
GISP 2
Renland
CR948/2011
EIC
NwAC
WGC
Dye3
MD99-2322
MD99-2275
FC
IC
Ga3-2
Labrador Sea
LC
Rapid 21-COM
(NAC*)
CSC
(NAC*)
North Atlantic
NAC
70°N
65°N
60°N
55°N
40°W
20°W
900-950
1050
1150
1300

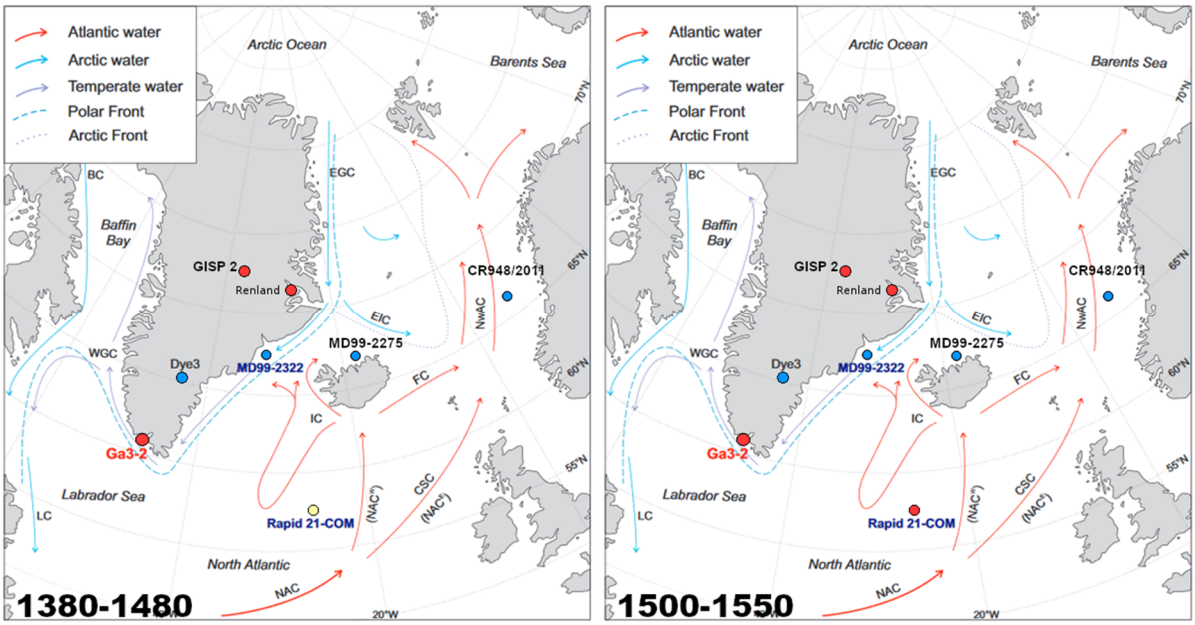

Figure 36 Temperature of the records plotted (red for warm, blue for cold and yellow for temperate) showing the relation of different periods in some of the records used for comparison. The numbers on the left down corner indicate the approximate time period the maps represent in years CE. Modified from Miettinen et al. (2012).

In Figure 36 the relative Sea surface Temperature of Ga3-2 is presented together with some of the sedimentary records and ice records. In this set of maps, it is noticeable how the relation between Ga3-2 and CR948/2011 from the Vøring Plateau in the eastern Nordic Seas is opposite. Rapid 21-COM is most similar with Ga3-2, GISP 2 and Renland, and they have the same trends, although this is not always the case (like shown in the first two plots between 900-950 and 1050).

A newly published study by Torricella et al. (2022) from the Svalbard coast identifies the Medieval Climate Anomaly with warm temperatures and the Little ice age with cold temperatures. This result, opposite to the trends spotted in the Narsaq fjord, fit to the model in Figure 35 and the CR948/2011 record (Miettinen et al., 2012).

Conlusions

It is important to note that the records focussed on in this study represents the time between the 9th and the 17th century, and the diatom samples used in Ga3-2 have well preserved frustules that show little to no signs of erosion.

The analysis of the samples has provided new information about the august Sea Surface Temperatures in high resolution (c. 30 years per sample) for the Narsaq Sound in South Greenland between 890 and 1660 CE, including the periods of the Medieval Climate Annomaly and the Little Ice Age.

The similarities between core Ga3-2 (South Greenland) and core Rapid 21-COM (Reykjanes ridge in the central north Atlantic) indicate that summer climate conditions of south Greenland are dependent on the water coming from the warm Irminger Current. It does not show many similarities to MD99-2322, which is located on the Eastern shelf of Greenland, in the Denmark strait, indicating that the influence of the East Greenland current might not be as strong at the Ga3-2 core site in summer.

While the sea surface temperature data obtained from the south Greenland record of Ga3-2 shows opposing trends than that of the East shelf of Greenland (MD99-2322; south of the Greenland-Scotland Ridge), it fits well with the atmospheric temperature north of the ridge (Renland ice core). This indicates that the august Sea Surface Temperature in Narsaq Sound could have been significantly affected by atmospheric processes, probably due to the meltwater input from land-glaciers.

The lower temperatures during the Medieval Climate Anomaly possibly indicate a lower inflow of warm Atlantic waters and therefore indicates a weaker Irminger Current during that period. Contrastingly, the high summer temperatures in Narsaq Sound during the Little Ice age fit to an increased entry of warm water in the area, probably the Irminger Current.

This study gives some insight in the summer climate of south Greenland and compares to other diatom studies. But comparison to other proxies is still challenging. Further studies to match the different proxies are necessary to better understand the overall development of past climate. The study presents a likely explanation for the obtained results, although other explanations are still viable.

The data available for reconstructions of climate and ocean circulation are still scarce. An increase of temporal and areal coverage with more high-resolution studies will help reveal the likely causes of the temperature variability and will be an advantage when modelling possible future changes of the climate, as clearly the factors involved are complex.

References

Aldaz, L., and Deutsch, S., 1967, On a relationship between air temperature and oxygen isotope ratio of snow and firn in the South Pole region: Earth and Planetary Science Letters, v. 3, p. 267-274.

Alonso-Garcia, M., Kleiven, H. K. F., McManus, J. F., Moffa-Sanchez, P., Broecker, W. S., and Flower, B. P., 2017, Freshening of the Labrador Sea as a trigger for Little Ice Age development: Climate of the Past, v. 13, no. 4, p. 317-331.

Andersen, C., Koc, N., and Moros, M., 2004, A highly unstable Holocene climate in the subpolar North Atlantic: evidence from diatoms: Quaternary Science Reviews, v. 23, no. 20-22, p. 2155-2166.

Backman, J., Jakobsson, M., Løvlie, R., Polyak, L., and Febo, L. A., 2004, Is the central Arctic Ocean a sediment starved basin?: Quaternary Science Reviews, v. 23, no. 11-13, p. 1435-1454.

Bellucci, A., Gualdi, S., Scoccimarro, E., and Navarra, A., 2008, NAO–ocean circulation interactions in a coupled general circulation model: Climate dynamics, v. 31, no. 7, p. 759-777.

Berner, K., Koç, N., Divine, D., Godtliebsen, F., and Moros, M., 2008, A decadal-scale Holocene sea surface temperature record from the subpolar North Atlantic constructed using diatoms and statistics and its relation to other climate parameters: Paleoceanography, v. 23, no. 2.

Bidgood, M., Mitlehner, A., Jones, G., and Jutson, D., 1999, Towards a stable and agreed nomenclature for North Sea Tertiary diatom floras—the 'Coscinodiscus' problem: Geological Society, London, Special Publications, v. 152, no. 1, p. 139-153.

Bjerknes, J., 1964, Atlantic air-sea interaction, Advances in geophysics, Volume 10, Elsevier, p. 1-82.

Boessenkool, K. P., Hall, I. R., Elderfield, H., and Yashayaev, I., 2007, North Atlantic climate and deep-ocean flow speed changes during the last 230 years: Geophysical Research Letters, v. 34, no. 13.

Cabedo-Sanz, P., Belt, S. T., Jennings, A. E., Andrews, J. T., and Geirsdóttir, Á., 2016, Variability in drift ice export from the Arctic Ocean to the North Icelandic Shelf over the last 8000 years: a multi-proxy evaluation: Quaternary Science Reviews, v. 146, p. 99-115.

Chen, C.-T. A., Lui, H.-K., Hsieh, C.-H., Yanagi, T., Kosugi, N., Ishii, M., and Gong, G.-C., 2017, Deep oceans may acidify faster than anticipated due to global warming: Nature Climate Change, v. 7, no. 12, p. 890.

Czervionke, L., Daniels, D., Wehrli, F., Mark, L., Hendrix, L., Strandt, J., Williams, A., and Haughton, V., 1988, Magnetic susceptibility artifacts in gradient-recalled echo MR imaging: American journal of neuroradiology, v. 9, no. 6, p. 1149-1155.

Dansgaard, W., Johnsen, S., Reeh, N., Gundestrup, N., Clausen, H., and Hammer, C., 1975, Climatic changes, Norsemen and modern man: Nature, v. 255, no. 5503, p. 24-28.

Duperon, T., 1974, Core catcher for core samplers, Google Patents.

Fitzhugh, W. W., 2000, Vikings: The North Atlantic Saga: AnthroNotes.

Flesche Kleiven, H., Jansen, E., Fronval, T., and Smith, T. M., 2002, Intensification of Northern Hemisphere glaciations in the circum Atlantic region (3.5-2.4 Ma) - ice-rafted detritus evidence: Palaeogeography, palaeoclimatology, palaeoecology, v. Vol.184(3–4), p. 213-223.

Gildor, H., and Tziperman, E., 2000, Sea ice as the glacial cycles' climate switch: Role of seasonal and orbital forcing: Paleoceanography, v. 15, no. 6, p. 605-615.

Goh, K., 1991, Carbon dating: Carbon Isotope Techniques, v. 1, p. 125.

Goosse, H., Guiot, J., Mann, M. E., Dubinkina, S., and Sallaz-Damaz, Y., 2012, The medieval climate anomaly in Europe: Comparison of the summer and annual mean signals in two reconstructions and in simulations with data assimilation: Global and Planetary Change, v. 84, p. 35-47.

Grootes, P. M., Stuiver, M., White, J., Johnsen, S., and Jouzel, J., 1993, Comparison of oxygen isotope records from the GISP2 and GRIP Greenland ice cores: nature, v. 366, no. 6455, p. 552-554.

Grove, J. M., 2012, The little ice age, Routledge.

Guiot, J., Corona, C., and members, E., 2010, Growing season temperatures in Europe and climate forcings over the past 1400 years: PloS one, v. 5, no. 4, p. e9972.

Gundestrup, N., and Hansen, B. L., 1984, Bore-hole survey at Dye 3, south Greenland: Journal of Glaciology, v. 30, no. 106, p. 282-288.

Hasle, G. R., Syvertsen, E. E., Steidinger, K. A., Tangen, K., and Tomas, C. R., 1996, Identifying marine diatoms and dinoflagellates, Elsevier.

Heiden, H., and Kolbe, R., 1928, Die tarinen Diatomeen der Deutsche Sicipolar Erpedition 1901–1903: Deutsche Sicipolar-Expedition i, v. 90.

Hopkinson, B. M., Dupont, C. L., Allen, A. E., and Morel, F. M., 2011, Efficiency of the CO2-concentrating mechanism of diatoms: Proceedings of the National Academy of Sciences, v. 108, no. 10, p. 3830-3837.

Hughes, M. K., and Diaz, H. F., 1994, Was there a 'Medieval Warm Period', and if so, where and when?: Climatic change, v. 26, no. 2, p. 109-142.

Hughes, T. P., Kerry, J. T., Baird, A. H., Connolly, S. R., Chase, T. J., Dietzel, A., Hill, T., Hoey, A. S., Hoogenboom, M. O., and Jacobson, M., 2019, Global warming impairs stock–recruitment dynamics of corals: Nature, v. 568, no. 7752, p. 387.

Hurrel, J. W., Kushnir, Y., Ottersen, G., and Visbeck, M., 2003, The North Atlantic Oscillation: climatic significance and environmental impact: American Geophysical Union, v. 279, p. 279.

Jahn, R., and Kusber, W.-H., 2009, A key to diatom nomenclature: Diatom Research, v. 24, no. 1, p. 101-111.

Jennings, A., Andrews, J., and Wilson, L., 2011, Holocene environmental evolution of the SE Greenland Shelf North and South of the Denmark Strait: Irminger and East Greenland current interactions: Quaternary Science Reviews, v. 30, no. 7-8, p. 980-998.

Jiang, H., Muscheler, R., Björck, S., Seidenkrantz, M.-S., Olsen, J., Sha, L., Sjolte, J., Eiríksson, J., Ran, L., and Knudsen, K.-L., 2015, Solar forcing of Holocene summer sea-surface temperatures in the northern North Atlantic: Geology, v. 43, no. 3, p. 203-206.

Johnsen, S., Clausen, H., Dansgaard, W., Fuhrer, K., Gundestrup, N., Hammer, C., Iversen, P., Jouzel, J., and Stauffer, B., 1992, Irregular glacial interstadials recorded in a new Greenland ice core: Nature, v. 359, no. 6393, p. 311-313.

Justwan, A., Koç, N., and Jennings, A. E., 2008, Evolution of the Irminger and East Icelandic Current systems through the Holocene, revealed by diatom-based sea surface temperature reconstructions: Quaternary Science Reviews, v. 27, no. 15-16, p. 1571-1582.

Katz, M. E., Finkel, Z. V., Grzebyk, D., Knoll, A. H., and Falkowski, P. G., 2004, Evolutionary trajectories and biogeochemical impacts of marine eukaryotic phytoplankton: Annual Review of Ecology, Evolution, and Systematics, p. 523-556.

Kaufman, D. S., Schneider, D. P., McKay, N. P., Ammann, C. M., Bradley, R. S., Briffa, K. R., Miller, G. H., Otto-Bliesner, B. L., Overpeck, J. T., and Vinther, B. M., 2009, Recent warming reverses long-term Arctic cooling: Science, v. 325, no. 5945, p. 1236-1239.

Kawahata, H., Nishimura, A., and Gagan, M. K., 2002, Seasonal change in foraminiferal production in the western equatorial Pacific warm pool: evidence from sediment trap experiments: Deep Sea Research Part II: Topical Studies in Oceanography, v. 49, no. 13-14, p. 2783-2800.
Kent, D. V., 1982, Apparent correlation of palaeomagnetic intensity and climatic records in deep-sea sediments: Nature, v. 299, no. 5883, p. 538-539.
Knight, J. R., Allan, R. J., Folland, C. K., Vellinga, M., and Mann, M. E., 2005, A signature of persistent natural thermohaline circulation cycles in observed climate: Geophysical Research Letters, v. 32, no. 20.
Knutz, P. C., Sicre, M. A., Ebbesen, H., Christiansen, S., and Kuijpers, A., 2011, Multiple-stage deglacial retreat of the southern Greenland Ice Sheet linked with Irminger Current warm water transport: Paleoceanography, v. 26, no. 3.
Koc Karpuz, N., and Schrader, H., 1990, Surface sediment diatom distribution and Holocene paleotemperature variations in the Greenland, Iceland and Norwegian Sea: Paleoceanography, v. 5, no. 4, p. 557-580.
Koç, N., Jansen, E., and Haflidason, H., 1993, Paleoceanographic reconstructions of surface ocean conditions in the Greenland, Iceland and Norwegian seas through the last 14 ka based on diatoms: Quaternary Science Reviews, v. 12, no. 2, p. 115-140.
Kolling, H. M., Stein, R., Fahl, K., Perner, K., and Moros, M., 2017, Short-term variability in late Holocene sea ice cover on the East Greenland Shelf and its driving mechanisms: Palaeogeography, Palaeoclimatology, Palaeoecology, v. 485, p. 336-350.
Labeyrie, L. D., 1999, CAMPAGNE INTERPOLE MD99-114/IMAGES V.
Lamb, H. H., 1965, The early medieval warm epoch and its sequel: Palaeogeography, Palaeoclimatology, Palaeoecology, v. 1, p. 13-37.
Landerer, F. W., Wiese, D. N., Bentel, K., Boening, C., and Watkins, M. M., 2015, North Atlantic meridional overturning circulation variations from GRACE ocean bottom pressure anomalies: Geophysical Research Letters, v. 42, no. 19, p. 8114-8121.
Lasher, G. E., and Axford, Y., 2019, Medieval warmth confirmed at the Norse Eastern Settlement in Greenland: Geology, v. 47, no. 3, p. 267-270.
Mann, M. E., Zhang, Z., Rutherford, S., Bradley, R. S., Hughes, M. K., Shindell, D., Ammann, C., Faluvegi, G., and Ni, F., 2009, Global signatures and dynamical origins of the Little Ice Age and Medieval Climate Anomaly: science, v. 326, no. 5957, p. 1256-1260.
Marshall, J., Kushnir, Y., Battisti, D., Chang, P., Czaja, A., Dickson, R., Hurrell, J., McCartney, M., Saravanan, R., and Visbeck, M., 2001, North Atlantic climate variability: phenomena, impacts and mechanisms: International Journal of Climatology: A Journal of the Royal Meteorological Society, v. 21, no. 15, p. 1863-1898.
Massé, G., Rowland, S. J., Sicre, M.-A., Jacob, J., Jansen, E., and Belt, S. T., 2008, Abrupt climate changes for Iceland during the last millennium: Evidence from high resolution sea ice reconstructions: Earth and Planetary Science Letters, v. 269, no. 3-4, p. 565-569.
Matthes, F. E., 1939, Report of committee on glaciers, April 1939: Eos, Transactions American Geophysical Union, v. 20, no. 4, p. 518-523.
Matthews, J. A., and Briffa, K. R., 2005, The 'Little Ice Age': re-evaluation of an evolving concept: Geografiska Annaler: Series A, Physical Geography, v. 87, no. 1, p. 17-36.
McGhee, R., 2001, Ancient people of the Arctic, UBC Press.
Miettinen, A., 2014a, Diatoms: Encyclopedia of Marine Geosciences, p. 1-7.
-, 2018, Diatoms in arctic regions: potential tools to decipher environmental changes: Polar Science, v. 18, p. 220-226.

Miettinen, A., Divine, D., Koç, N., Godtliebsen, F., and Hall, I. R., 2012, Multicentennial variability of the sea surface temperature gradient across the subpolar North Atlantic over the last 2.8 kyr: Journal of climate, v. 25, no. 12, p. 4205-4219.
Miettinen, A., Divine, D. V., Husum, K., Koç, N., and Jennings, A., 2015, Exceptional ocean surface conditions on the SE Greenland shelf during the Medieval Climate Anomaly: Paleoceanography, v. 30, no. 12, p. 1657-1674.
Miettinen, A., Koç, N., Hall, I. R., Godtliebsen, F., and Divine, D., 2011, North Atlantic sea surface temperatures and their relation to the North Atlantic Oscillation during the last 230 years: Climate dynamics, v. 36, no. 3-4, p. 533-543.
Miettinen, A. a. D., D. and Husum, Katrine and Koc, Nalan and Jennings, Anne, 2015, SE Greenland shelf 2900 Year Diatom August SST reconstruction.
Miettinen, A. a. D., D. and Koc, Nalan and Godtliebsen, Fred and Hall, Ian, 2014b, Subpolar North Atlantic 2000 Year Diatom August SST Reconstruction.
Mikkelsen, N., Kuijpers, A., and Arneborg, J., 2008, The Norse in Greenland and late Holocene sea-level change: Polar Record, v. 44, no. 1, p. 45-50.
Moffa-Sánchez, P., and Hall, I. R., 2017, North Atlantic variability and its links to European climate over the last 3000 years: Nature Communications, v. 8, no. 1, p. 1-9.
Moffa-Sánchez, P., Moreno-Chamarro, E., Reynolds, D., Ortega, P., Cunningham, L., Swingedouw, D., Amrhein, D. E., Halfar, J., Jonkers, L., and Jungclaus, J. H., 2019, Variability in the northern North Atlantic and Arctic oceans across the last two millennia: A review: Paleoceanography and Paleoclimatology.
Moros, M., Andrews, J. T., Eberl, D. D., and Jansen, E., 2006, Holocene history of drift ice in the northern North Atlantic: Evidence for different spatial and temporal modes: Paleoceanography, v. 21, no. 2.
Nørgaard-Pedersen, N., and Mikkelsen, N., 2009, 8000 year marine record of climate variability and fjord dynamics from Southern Greenland: Marine Geology, v. 264, no. 3-4, p. 177-189.
Oksman, M., Juggins, S., Miettinen, A., Witkowski, A., and Weckstr?m, K., 2019, The biogeography and ecology of common diatom species in the northern North Atlantic, and their implications for paleoceanographic reconstructions: Marine Micropaleontology, v. 148, p. 1-28.
PAGES 2k Consortium, Continental-scale temperature variability during the past two millennia, *in* Proceedings Nature geoscience2013, Volume 6, p. 339-346.
PAGES, P. I. W. G. o., 2016, Interglacials of the last 800,000 years: Reviews of Geophysics, v. 54, no. 1, p. 162-219.
Park, W., and Latif, M., 2019, Ensemble global warming simulations with idealized Antarctic meltwater input: Climate Dynamics, v. 52, no. 5-6, p. 3223-3239.
Perner, K., Jennings, A. E., Moros, M., Andrews, J. T., and Wacker, L., 2016, Interaction between warm Atlantic-sourced waters and the East Greenland Current in northern Denmark Strait (68 N) during the last 10 600 cal a BP: Journal of Quaternary Science, v. 31, no. 5, p. 472-483.
Perner, K., Moros, M., Lloyd, J. M., Jansen, E., and Stein, R., 2015, Mid to late Holocene strengthening of the East Greenland Current linked to warm subsurface Atlantic water: Quaternary Science Reviews, v. 129, p. 296-307.
Plass, G. N., 1959, Carbon dioxide and climate: Scientific American, v. 201, no. 1, p. 41-47.
Reynolds, D., Scourse, J., Halloran, P., Nederbragt, A., Wanamaker, A. D., Butler, P., Richardson, C., Heinemeier, J., Eiriksson, J., and Knudsen, K., 2016, Annually resolved North Atlantic marine climate over the last millennium: Nature communications, v. 7, no. 1, p. 1-11.
Robinson, S. G., Maslin, M. A., and McCave, I. N., 1995, Magnetic susceptibility variations in Upper Pleistocene deep-sea sediments of the NE Atlantic:

Implications for ice rafting and paleocirculation at the Last Glacial Maximum: Paleoceanography, v. 10, no. 2, p. 221-250.
Rothpletz, A., 1896, Ueber die Flysch-Fucoiden und einige andere fossile Algen, sowie über liasische, Diatomeen führende Hornschwämme: Zeitschrift der Deutschen Geologischen Gesellschaft, p. 854-914.
-, 1900, Ueber einen neuen jurassischen Hornschwamm und die darin eingeschlossenen Diatomeen: Zeitschrift der Deutschen Geologischen Gesellschaft, p. 154-160.
Sager, W. W., and Hall, S. A., 1990, 26. MAGNETIC PROPERTIES OF BLACK MUD TURBIDITES FROM ODP LEG 116, DISTAL BENGAL FAN, INDIAN OCEAN1.
Sancetta, C., 1981, Oceanographic and ecologic significance of diatoms in surface sediments of the Bering and Okhotsk seas: Deep Sea Research Part A. Oceanographic Research Papers, v. 28, no. 8, p. 789-817.
Schleussner, C.-F., Divine, D., Donges, J. F., Miettinen, A., and Donner, R. V., 2015, Indications for a North Atlantic ocean circulation regime shift at the onset of the Little Ice Age: Climate dynamics, v. 45, no. 11, p. 3623-3633.
Schmidt, G., Jungclaus, J. H., Ammann, C., Bard, E., Braconnot, P., Crowley, T., Delaygue, G., Joos, F., Krivova, N., and Muscheler, R., 2012, Climate forcing reconstructions for use in PMIP simulations of the Last Millennium (v1. 1): Geoscientific Model Development, no. 1, p. 185-191.
Seidenkrantz, M.-S., Aagaard-Sørensen, S., Sulsbrück, H., Kuijpers, A., Jensen, K. G., and Kunzendorf, H., 2007, Hydrography and climate of the last 4400 years in a SW Greenland fjord: implications for Labrador Sea palaeoceanography: The Holocene, v. 17, no. 3, p. 387-401.
Sicre, M.-A., Jacob, J., Ezat, U., Rousse, S., Kissel, C., Yiou, P., Eiríksson, J., Knudsen, K. L., Jansen, E., and Turon, J.-L., 2008, Decadal variability of sea surface temperatures off North Iceland over the last 2000 years: Earth and Planetary Science Letters, v. 268, no. 1-2, p. 137-142.
Sicre, M. A., Hall, I. R., Mignot, J., Khodri, M., Ezat, U., Truong, M. X., Eiríksson, J., and Knudsen, K. L., 2011, Sea surface temperature variability in the subpolar Atlantic over the last two millennia: Paleoceanography, v. 26, no. 4.
Sieminska, J., 2000, The discoveries of diatoms older than the Cretaceous: The origin and early evolution of diatoms: fossil, molecular and biogeographical approaches, p. 55-74.
Sieminska, J., and Kwiecinska, B., 2000, The Proterozoic diatoms from the Przeworno marbles: The Origin and Early Evolution of the Diatoms: Fossil, Molecular and Biogeographical Approaches. Cracow: Szafer Institute of Botany, Polish Academy of Sciences, p. 117-121.
Sorhannus, U., 2007, A nuclear-encoded small-subunit ribosomal RNA timescale for diatom evolution: Marine Micropaleontology, v. 65, no. 1-2, p. 1-12.
Spielhagen, R. F., Werner, K., Sørensen, S. A., Zamelczyk, K., Kandiano, E., Budeus, G., Husum, K., Marchitto, T. M., and Hald, M., 2011, Enhanced modern heat transfer to the Arctic by warm Atlantic water: Science, v. 331, no. 6016, p. 450-453.
Stoner, J. S., Jennings, A., Kristjánsdóttir, G. B., Dunhill, G., Andrews, J. T., and Hardardóttir, J., 2007, A paleomagnetic approach toward refining Holocene radiocarbon-based chronologies: Paleoceanographic records from the north Iceland (MD99-2269) and east Greenland (MD99-2322) margins: Paleoceanography, v. 22, no. 1.
ter Braak, C. J., and Juggins, S., Weighted averaging partial least squares regression (WA-PLS): an improved method for reconstructing environmental variables from species assemblages, *in* Proceedings Twelfth International Diatom Symposium1993, Springer, p. 485-502.
Tomas, C. R., 1997, Identifying marine phytoplankton, Elsevier.

Torricella, F., Gamboa Sojo, V. M., Gariboldi, K., Douss, N., Musco, M. E., Caricchi, C., Lucchi, R. G., Carbonara, K., and Morigi, C., 2022, Multiproxy investigation of the last 2,000 years BP marine paleoenvironmental record along the western Spitsbergen margin: Arctic, Antarctic, and Alpine Research, v. 54, no. 1, p. 562-583.

Trouet, V., Esper, J., Graham, N. E., Baker, A., Scourse, J. D., and Frank, D. C., 2009, Persistent positive North Atlantic Oscillation mode dominated the medieval climate anomaly: science, v. 324, no. 5923, p. 78-80.

Trouet, V., Scourse, J., and Raible, C., 2012, North Atlantic storminess and Atlantic Meridional Overturning Circulation during the last Millennium: Reconciling contradictory proxy records of NAO variability: Global and Planetary Change, v. 84, p. 48-55.

Trumbore, S., 2000, Age of soil organic matter and soil respiration: radiocarbon constraints on belowground C dynamics: Ecological applications, v. 10, no. 2, p. 399-411.

Vellinga, M., and Wood, R. A., 2002, Global climatic impacts of a collapse of the Atlantic thermohaline circulation: Climatic change, v. 54, no. 3, p. 251-267.

Vermassen, F., O'Regan, M., West, G., Cronin, T. M., and Coxall, H. K., 2021, Testing the stratigraphic consistency of Pleistocene microfossil bioevents identified on the Alpha and Lomonosov Ridges, Arctic Ocean: Arctic, Antarctic, and Alpine Research, v. 53, no. 1, p. 309-323.

Wanamaker, A. D., Butler, P. G., Scourse, J. D., Heinemeier, J., Eiríksson, J., Knudsen, K. L., and Richardson, C. A., 2012, Surface changes in the North Atlantic meridional overturning circulation during the last millennium: Nature Communications, v. 3, no. 1, p. 1-7.

Wanner, H., Brönnimann, S., Casty, C., Gyalistras, D., Luterbacher, J., Schmutz, C., Stephenson, D. B., and Xoplaki, E., 2001, North Atlantic Oscillation–concepts and studies: Surveys in geophysics, v. 22, no. 4, p. 321-381.

Weckström, K., Roche, B. R., Miettinen, A., Krawczyk, D., Limoges, A., Juggins, S., Ribeiro, S., and Heikkilä, M., 2020, Improving the paleoceanographic proxy tool kit–On the biogeography and ecology of the sea ice-associated species Fragilariopsis oceanica, Fragilariopsis reginae-jahniae and Fossula arctica in the northern North Atlantic: Marine Micropaleontology, v. 157, p. 101860.

Zamelczyk, K., Rasmussen, T. L., Raitzsch, M., and Chierici, M., 2020, The last two millennia: climate, ocean circulation and paleoproductivity inferred from planktic foraminifera, south-western Svalbard margin.

Figures

Figure 1 Map with marine core Ga3-2 and other cores referred to in this study. The main ocean currents in the area are also represented: Baffin Current (BC), Continental Slope Current (CSC), East Greenland Current (EGC), East Irminger Current (EIC), Faroe Current (FC), Irminger Current (IC), Labrador Current (LC), North Atlantic current (NAC) with both east and west ramifications (NAC^{E} and NAC^{W} respectively), Northwestern Atlantic Current (NwAC) and West Greenland Current (WGC). Modified from Miettinen et al. (2012).....9

Figure 2 a) Map for the core site Ga3-2. Left upper corner shows the zoomed out map of the area corresponding to the south of Greenland. The black dashed arrow represents the East Greenland current (EGC) and the red dashed arrow represents the Irminger current (IC). b) Multibeam bathymetric map of Narsaq Sound, with the black dot to mark the Ga3-2 core site. The CTD (see Figure 4) points are also plotted as St. 0, St. 2 and St.3 (Nørgaard-Pedersen and Mikkelsen, 2009).....12

Figure 3 Picture from the Narsaq sound during the Galathea 3 cruise (picture from Niels Nørgaard-Pedersen).....13

Figure 4 Hydrographic profiles of temperature, salinity, and density from the shelf area (St. 0, outside the Ikersuaq Fjord Sill, the outer Ikersuaq Fjord (St. 2), and mid fjord area near Narsaq Sound (St. 3). Data recorded by the Danish Meteorological 14

Figure 5 Diatom images of specimens from this study taken with Axiocam 105 color and processed with ZEN (blue edition). A: Fragilariopsis reginae-jahniae; B: Nitzschia bicapitata; C: Thalassiotrix ikipedia; D: Nitzschia angularis; E: Fragilariopsis cylindrus; F: Odontella aurita; G: Rhizosolenia hebata f. hebata; H: T. ikipedia on the top, Thalassiosira antarctica var. borealis in the middle and Fragilariopsis oceanica down; I: Thalassiosira gravida; J: Thalassiosira nordenskioldii; K: Actinocyclus curvatulus; L: Bacterosira bathyomphala; M:

Thalassiosira trifulta; N: Thalassiosira hyalina; O: Porosira glacialis; P: Coscinodiscus asteromphalus; Q: detail of the centre of a C. asteromphalus.....18
Figure 6 Life cycle of diatoms (Tomas, 1997).....18
Figure 7 Images of the different types of corers used for the sediment cores. Upper left: Sketch of a Gravity Corer penetrating the sediment (https://commons.wikimedia.org/wiki/File:Gravity-corer_hg.png) Hannes Grobe/AWI 2009. Upper middle: Kasten Corer (https://commons.wikimedia.org/wiki/File:Gravity_corer-ps_hg.jpg) Hannes Grobe/ AWI 2006. Upper right: Piston corer (https://commons.wikimedia.org/wiki/File:Piston-corer_model_hg.jpg) Hannes Grobe, AWI 2008. Down: Box corer (https://commons.wikimedia.org/wiki/File:Giant-box-corer_hg.jpg) Hannes Grobe 2006. 22
Figure 8 Sketch of a section of a corer with a catcher (left) and view of a catcher from top (right). Modified from (Duperon, 1974).....23
Figure 9 Sketch of the sample preparation. 26
Figure 10 Sketch of slide preparation. A line of Mountex fluid (orange) was extended over the slide. Then the slide cover (right) was placed with the sample side facing down on the slide.27
Figure 11 Core Ga3-2 open in half. Above from 1 to 57 cm, bellow from 57 to 157cm. Figures from Nørgaard-Pedersen and Mikkelsen (2009).....31
Figure 12 Lithological log, AMS- ^{14}C, coarse fraction content (63-1000 µm (%), >1000µm (%)) and age model of Ga 3-2 modified from (Nørgaard-Pedersen and Mikkelsen, 2009).....32
Figure 13 Sedimentation rate of the first 214 cm for the core Ga 3-2 33
Figure 14 Basic data of core Ga3-2 and temperature record plotted versus age: Magnetic susceptibility (MS) with a 5 pt. running average overlay, 63–1000 µm (wt.%), nos. of IRD grains > 1000 µm/g, sortable silt weighted mean, modal grain size distribution peak values, and nos. of calcareous benthic foraminifera (> 125 µm)/g. LIA: ‘Little Ice Age’, MWP: ‘Medieval

Warm Period' (aka. Medieval Climate Anomaly (MCA), DA: 'Dark Ages', RWP : 'Roman Warm Period' HTO: 'Holocene Thermal Optimum'. The orange line indicates the timespan analysed in this study (Modified from Nørgaard-Pedersen and Mikkelsen, 2009) (Same as Figure 21).....34

Figure 15 Relative abundances of main diatom species present in the record from Ga3-2. Species with <1% abundance in all samples were omitted. See the enlarged figure in Appendix 2.....35

Figure 16 August Sea Surface Temperature reconstruction for Ga3-2 (yellow). The dark horizontal line represents the mean temperature for the record and the dashed line represents the linear trend. Colder periods are presented with a blue background, a temperate period has a beige color and warm periods have a red background. The green arrow presents the current temperature.....38

Figure 17 Qualitative Sea ice cover reconstruction from ice diatom assemblage for Ga3-2 ...39

Figure 18 Relation between sea ice (blue) and SST (red) in core Ga3-2 40

Figure 19 Warm diatoms (red), temperate diatoms (yellow), ice related diatoms (turcoise) and cold temperatures (blue). Sea surface temperature reconstruction for Ga3-2 is plotted as an orange line.....44

Figure 20 Temperatures for Ga3-2. The black horizontal line shows mean and the dotted line shows the trend. The red rectangle shows the time period for the MCA while the blue rectangle shows the time period for the LIA.....44

Figure 21 Basic data of core Ga3-2 and temperature record plotted versus age: Magnetic susceptibility (MS) with a 5 pt. running average overlay, 63–1000 µm (wt.%), nos. of IRD grains > 1000 µm/g, sortable silt weighted mean, modal grain size distribution peak values, and nos. of calcareous benthic foraminifera (> 125 µm)/g. LIA: 'Little Ice Age', MWP: 'Medieval Warm Period' (aka. Medieval Climate Anomaly (MCA), DA: 'Dark Ages', RWP: 'Roman

Warm Period' HTO: 'Holocene Thermal Optimum'. The orange line indicates the timespan analysed in this study (Modified from Nørgaard-Pedersen and Mikkelsen, 2009) (Same as Figure 14).....46
Figure 22 Temperature record for core MD99-2322. Without smoothing. Data from Miettinen (2015).....48
Figure 23 Temperature record for MD99-2322 with a running average to smooth lower scale variabilities and make it more comparable to Ga3-2. Data from Miettinen (2015).....48
Figure 24 Rapid 21-COM temperature record. Data from Miettinen (2014b). 49
Figure 25 Running average Rapid 21-COM temperature record. Running average with the purpose of smoothing short scale variability. Data from Miettinen (2014b).....50
Figure 26 Core temperatures. Comparation between Rapid 21-COM (green), Ga 3-2 (orange) and MD95-2322 (blue). The dots show the datapoints, the line shows the running average in order to better compare all three cores together.....51
Figure 27 Core temperatures. Note that the y-axis is cut to help visualization. Cores shown are Ga3-2 in orange, MD99-2322 in blue and Rapid 21-COM in green. 51
Figure 28 Sediment cores compared using the variability to the mean. x-axis shows age in years CE and y-axis shows the deviation from the mean in °C. 53
Figure 29 $\delta^{18}O$ for ice core Dye3. Data from Kaufman et al. (2009).....54
Figure 30 Temperature data for core GISP 2. Data from Kaufman et al. (2009) 56
Figure 31 $\delta^{18}O$ for ice core Renland. Data from Kaufman et al. (2009) 57
Figure 32 Comparison between sediment core Ga3-2 (orange) and ice cores Dye3 (red), GISP 2 (gray) and Renland (pink). The y-axis shows the deviation from their means, both from temperature (for Ga3-2 and GISP 2) or d18O (Renland and dye3) 58
Figure 33 Map with the proxy records used in Figure 34. Based on Orvik and Niiler (2002), Daniault et al. (2016), and Bosse et al. (2018). Red arrows indicate the pathway of relatively

warm and saline waters and blue arrows the pathway of cold southward polar waters.(Moffa-Sánchez et al., 2019).....61
Figure 34 Ice and oceanographic conditions along Eastern Greenland and North Iceland. Left panel shows sea/drift ice conditions (a) sea ice conditions in PS2641 BC/GC at Foster Bugt (Kolling et al., 2017); (b) drift ice recorded in the Denmark Strait JM96-1206/2GC (Perner et al., 2016)North Iceland; (c) %Quartz from MD99-2269 (Moros et al., 2006); sea ice biomarker (d) MD99-2275 (Massé et al., 2008) and (e) MD99-2269 (Cabedo-Sanz et al., 2016); (f) April sea ice cover from diatom assemblages in the West Denmark Strait, MD99-2322 (Miettinen et al., 2015);and (g) Haematite Stained Grains (HSG) transported from northwest Greenland to South Greenland (GS06-144-03;Alonso-Garcia et al. (2017)). Right panel shows oceanographic conditions (h) benthic foraminiferal assemblages at ~430 m, which are indicator of Atlantic Intermediate Waters (PS2641 BC/GC; Perner et al. (2015)), North Iceland upper water column conditions; (i) sea surface temperatures from alkenones (MD99–2275; (Sicre et al., 2008; Sicre et al., 2011)); (j) summer sea surface temperatures from diatom assemblages in MD99–2275(Jiang et al., 2015); (k) δ18Oshell (black) (Reynolds et al., 2016) and ΔR (orange) (Wanamaker et al., 2012) from Arctica islandica from the North Iceland shelf; (l) benthic assemblage from ~400-mdeep in the Northern Denmark Strait JM96-1206/2GC (Perner et al., 2016); (m)Pink and gray: % planktonic foraminifera species N. pachyderma from the Eastern Labrador Sea, South Greenland; RAPiD-35-COM (Moffa-Sánchez and Hall, 2017). Bold lines on raw data are weighted three-point smoothing. Orange: Sea surface temperature reconstruction from diatoms in Narsaq sund (sediment core Ga3-2). Modified from Moffa-Sánchez, 2019. 60
Figure 35 Schematic map for aSST during cold periods (left) and warm periods (right). Red arrows show the currents transporting the most heat. The shading indicates surface water temperatures (red for warm and blue for cold) abbreviations: NAC=North Atlantic Current

CSC=Continental Slope Current NwAC=North-west Atlantic Current IC=Irminger Current (Miettinen et al., 2012) 62
Figure 36 Temperature of the records plotted (red for warm, blue for cold and yellow for temperate) showing the relation of different periods in some of the records used for comparison. The numbers on the left down corner indicate the approximate time period the maps represent in years CE. Modified from Miettinen et al. (2012).....64

Tables

Table 1 Information of the sediment cores compared in this study. 20
Table 2 AMS-14C dates on benthic foraminifera in core Ga3-2. Modified from Nørgaard-Pedersen and Mikkelsen (2009) 24
Table 3 Temperature record for Ga 3-2. Blue represents colder than the mean temperature and Red represents warmer than the mean temperature. In light yellow the temperatures that are similar to the mean. The coldest and warmest temperatures are marked with bold letters. 37
Table 4 Sea diatom taxa and their ecological response to temperature and ice. (SST= August sea surface temperature, SIC=April sea ice cover). The models (I) no relationship (II) through monotone sigmoid, (III) monotone sigmoid with plateau, (IV) unimodal symmetric, (V) unimodal skewed, (VI) bimodal with equal peaks and (VII) bimodal with unequal peaks to aSST (°C) and April sea ice for the 21 studied diatom taxa. (Oksman et al., 2019).....42

Appendix 1: Diatom taxa from Ga3-2 samples from

Actinocyclus curvatulus Janisch (in A. Schmidt, 1878)[1]

Asteromphalus robustus Castracane[2]

Bacterosira bathyomphala (Cleve) Syvertsen & Hasle = *Bacteriosira fragilis* Gran[1]

Bacteriastrum hyalinum Lauder[4]

Coscinodiscus asteromphalus Ehrenberg[1]

Coscinodiscus marginatus Ehrenberg[1]

Coscinodiscus oculus-iridis Ehrenberg[2]

Coscinodiscus radiatus Ehrenberg[1]

Fragilariopsis cylindrus (Grunow) Krieger[1]

Fragilariopsis oceanica Grunow[1]

Nitzschia angularis W. Smith[5]

Nitzschia atlantica (Cleve) Cleve accepted as *Nitzschia pungens var. atlantica* Cleve[6]

Nitzschia atlantica (Paasche) Hasle accepted as *Fragilariopsis atlantica* Paasche[7]

Nitzschia bicapitata Cleve[8]

Nitzschia marina Grunow[9]

Porosira glacialis (Grunow) Jørgensen[2]

Rhizosolenia alata Brightwell[1]

Rhizosolenia borealis Sundström[1]

Rhizosolenia hebetata Bailey f. *hebetata*[2]

Rhizosolenia hebetata (Hensen) Gran f. *semispina*[1]

Thalassionema nitzschioides (Grunow) ex Mereschkowsky[2]

Thalassiosira angulate (Gregory) Hasle[1]

Thalassiosira anguste-lineata (A. Schmidt) G. Fryxell & Hasle[1]

Thalassiosira antarctica Comber var. *borealis* resting spore[2]

Thalassiosira ferelineata Hasle & Fryxell[1]

Thalassiosira gravida Cleve[1]

Thalassiosira hyalina (Grunow) Gran[2]

Thalassiosira lineata Jousé[1]

Thalassionema nitzschioides var. parva (Heiden & Kolbe)[3]

Thalassiosira nodulolineata accepted as *Coscinodiscus nodulolineatus* Hendey[10]

Thalassiosira nordenskioldii Cleve[2]

Thalassiosira oestrupii = *Shionodiscus oestrupii* (Ostenfeld) Alverson[1]

Thalassiosira pacifica Gran & Angst[1]

Thalassiosira trifulta = *Shionodiscus trifultus* (G. Fryxell) Alverson[2]

Thalassiotrix longissima (Cleve) Cleve & Grunow[2]

1: Hasle et al. (1996)

2: Sancetta (1981)

3: Heiden and Kolbe (1928)

4: Kociolek, J.P.; Blanco, S.; Coste, M.; Ector, L.; Liu, Y.; Karthick, B.; Kulikovskiy, M.; Lundholm, N.; Ludwig, T.; Potapova, M.; Rimet, F.; Sabbe, K.; Sala, S.; Sar, E.; Taylor, J.; Van de Vijver, B.; Wetzel, C.E.; Williams, D.M.; Witkowski, A.; Witkowski, J. (2022). DiatomBase. Bacteriastrum hyalinum Lauder, 1864. Accessed through: World Register of Marine Species at: https://www.marinespecies.org/aphia.php?p=taxdetails&id=149119 on 2022-11-18

5: Kociolek, J.P.; Blanco, S.; Coste, M.; Ector, L.; Liu, Y.; Karthick, B.; Kulikovskiy, M.; Lundholm, N.; Ludwig, T.; Potapova, M.; Rimet, F.; Sabbe, K.; Sala, S.; Sar, E.; Taylor, J.; Van de Vijver, B.; Wetzel, C.E.; Williams, D.M.; Witkowski, A.; Witkowski, J. (2022). DiatomBase. Nitzschia angularis W.Smith, 1853. Accessed through: World Register of Marine Species at: https://www.marinespecies.org/aphia.php?p=taxdetails&id=149591 on 2022-11-18

6: Kociolek, J.P.; Blanco, S.; Coste, M.; Ector, L.; Liu, Y.; Karthick, B.; Kulikovskiy, M.; Lundholm, N.; Ludwig, T.; Potapova, M.; Rimet, F.; Sabbe, K.; Sala, S.; Sar, E.; Taylor, J.; Van de Vijver, B.; Wetzel, C.E.; Williams, D.M.; Witkowski, A.; Witkowski, J. (2022). DiatomBase. Nitzschia pungens var. atlantica Cleve, 1897. Accessed through: World Register of Marine Species at: https://www.marinespecies.org/aphia.php?p=taxdetails&id=593887 on 2022-11-18

7: Kociolek, J.P.; Blanco, S.; Coste, M.; Ector, L.; Liu, Y.; Karthick, B.; Kulikovskiy, M.; Lundholm, N.; Ludwig, T.; Potapova, M.; Rimet, F.; Sabbe, K.; Sala, S.; Sar, E.; Taylor, J.; Van de Vijver, B.; Wetzel, C.E.; Williams, D.M.; Witkowski, A.; Witkowski, J. (2022). DiatomBase. Fragilariopsis atlantica Paasche, 1961. Accessed through: World Register of Marine Species at: https://www.marinespecies.org/aphia.php?p=taxdetails&id=549203 on 2022-11-18

8: Kociolek, J.P.; Blanco, S.; Coste, M.; Ector, L.; Liu, Y.; Karthick, B.; Kulikovskiy, M.; Lundholm, N.; Ludwig, T.; Potapova, M.; Rimet, F.; Sabbe, K.; Sala, S.; Sar, E.; Taylor, J.; Van de Vijver, B.; Wetzel, C.E.; Williams, D.M.; Witkowski, A.; Witkowski, J. (2022). DiatomBase. Nitzschia bicapitata Cleve, 1901. Accessed through: World Register of Marine Species at: https://www.marinespecies.org/aphia.php?p=taxdetails&id=341566 on 2022-11-18

9: Kociolek, J.P.; Blanco, S.; Coste, M.; Ector, L.; Liu, Y.; Karthick, B.; Kulikovskiy, M.; Lundholm, N.; Ludwig, T.; Potapova, M.; Rimet, F.; Sabbe, K.; Sala, S.; Sar, E.; Taylor, J.; Van de Vijver, B.; Wetzel, C.E.; Williams, D.M.; Witkowski, A.; Witkowski, J. (2022). DiatomBase. *Nitzschia marina* Grunow, 1880. Accessed through: World Register of Marine Species at: https://www.marinespecies.org/aphia.php?p=taxdetails&id=418205 on 2022-11-18

10: Kociolek, J.P.; Blanco, S.; Coste, M.; Ector, L.; Liu, Y.; Karthick, B.; Kulikovskiy, M.; Lundholm, N.; Ludwig, T.; Potapova, M.; Rimet, F.; Sabbe, K.; Sala, S.; Sar, E.; Taylor, J.; Van de Vijver, B.; Wetzel, C.E.; Williams, D.M.; Witkowski, A.; Witkowski, J. (2022). DiatomBase. Thalassiosira nodulolineata (Hendey) Hasle & Fryxell, 1977. Accessed through: World Register of Marine Species at: https://www.marinespecies.org/aphia.php?p=taxdetails&id=148929 on 2022-11-18

Appendix 2 Diatom abundances in Ga 3-2 (%)

Cal. Age (yrs BP)	TL.LONG.	TN.NITZ.	RH.HEB.H.	RH.HEB.S.	RH.BOR.	PR.ALATA	RH.BERG.	BACT.FR.	R.TESS.	P.GLAC.	A.CURV.	A.ROBUST.	H.CUNE.	TS.GR.SP.	TS.GR.VG.
290	2,4	0,3	0,2	0,5	0,0	0,0	0,0	3,1	0,0	1,0	0,3	0,0	0,0	37,0	20,4
316	0,9	0,0	0,0	0,4	0,0	0,0	0,0	2,2	0,0	1,3	0,4	0,0	0,0	44,0	23,4
342	0,7	0,0	0,0	0,4	0,0	0,0	0,0	6,9	0,0	2,2	0,4	0,0	0,0	43,3	23,6
368	0,7	0,0	0,0	0,2	0,0	0,0	0,0	3,3	0,0	0,0	0,5	0,0	0,0	35,2	32,9
395	0,6	0,0	0,8	0,0	0,0	0,0	0,0	5,3	0,0	0,8	0,0	0,0	0,0	36,6	36,6
421	0,4	0,0	0,4	0,8	0,0	0,0	0,0	2,5	0,0	0,4	0,4	0,0	0,0	36,6	27,4
447	1,3	0,0	0,0	0,8	0,0	0,0	0,0	5,1	0,0	0,8	0,0	0,4	0,0	44,2	24,2
473	1,4	0,0	0,0	0,7	0,0	0,0	0,0	3,2	0,0	1,1	0,4	0,0	0,0	41,4	31,9
499	2,1	0,0	1,9	0,5	0,0	0,0	0,0	1,4	0,0	0,5	0,9	0,0	0,0	29,2	32,1
526	2,0	0,0	0,4	1,8	0,4	0,0	0,0	3,1	0,0	1,8	0,4	0,4	0,0	35,0	32,8
552	1,1	0,0	0,5	0,9	0,0	0,0	0,0	2,3	0,0	0,5	1,4	0,0	0,0	35,9	31,3
578	1,7	0,0	0,0	0,0	0,0	0,0	0,0	3,4	0,0	0,8	0,8	0,0	0,0	41,2	29,0
631	2,0	2,3	0,0	0,0	0,0	0,0	0,0	5,0	0,0	3,0	3,0	0,0	0,0	44,3	14,0
657	3,0	0,2	0,3	0,6	0,0	0,0	0,0	3,1	0,0	3,5	0,9	0,0	0,0	46,5	10,4
683	1,2	0,0	0,0	0,0	0,0	0,0	0,0	2,4	0,0	1,0	0,5	0,0	0,0	47,6	23,8
709	2,3	0,0	0,6	2,1	0,0	0,0	0,0	3,4	0,0	1,2	0,3	0,0	0,0	44,9	5,5
736	1,7	0,3	0,8	0,6	0,0	0,0	0,0	4,2	0,0	1,7	0,3	0,0	0,0	57,6	11,4
762	1,8	0,0	0,5	0,5	0,0	0,0	0,0	2,7	0,0	1,4	0,0	0,3	0,0	56,1	12,9
788	2,9	0,0	1,2	0,8	0,0	0,0	0,0	2,7	0,0	1,9	1,5	0,4	0,0	65,6	3,5
814	1,8	0,0	0,6	0,9	0,0	0,0	0,0	1,5	0,0	3,0	0,6	0,0	0,0	50,8	13,3
841	1,7	0,0	0,5	1,0	0,0	0,0	0,0	3,7	0,0	3,5	0,5	0,0	0,0	55,1	15,4
867	0,7	0,0	0,0	0,5	0,0	0,0	0,0	4,2	0,0	2,4	0,5	0,5	0,0	39,6	24,1
893	0,2	0,0	0,0	0,2	0,0	0,0	0,0	1,3	0,0	0,9	0,0	0,4	0,0	49,8	20,6
919	0,2	0,0	0,5	0,0	0,0	0,0	0,0	4,1	0,0	2,3	0,0	0,5	0,0	48,9	13,6
946	2,3	0,8	1,3	1,3	0,0	0,4	0,0	3,8	0,0	1,7	0,4	1,3	0,0	45,5	20,2
972	1,6	1,2	0,0	1,2	0,0	0,0	0,0	3,7	0,0	2,1	0,0	0,0	0,0	37,8	26,3
998	1,5	0,0	0,0	0,2	0,0	0,0	0,0	4,6	0,0	1,9	0,0	0,0	0,0	42,1	22,9
1029	2,9	0,9	0,2	1,3	0,0	0,0	0,0	1,8	0,0	2,2	0,4	0,0	0,0	56,4	15,1
1060	0,6	0,0	0,0	0,2	0,0	0,0	0,0	2,9	0,0	1,2	0,8	0,0	0,0	43,9	31,1

Cal. Age (yrs BP)	TS.ANG.LIN.	TS.ECC.	TS.TRIF.	TS.LINE.	TS.NORD.	TS.OEST.	TS.HYAL.	TS.ANG.	TS.PACIF.	TS.FEREL.	COS.RAD.	COS.MAR.	COS.NOD.
290	0,0	0,0	0,0	0,0	2,4	0,0	3,8	1,0	0,0	0,3	0,0	0,0	0,0
316	0,0	0,0	0,0	0,4	1,3	0,0	4,0	1,8	0,0	0,4	0,0	0,0	0,0
342	0,0	0,0	0,4	0,4	0,7	0,0	1,1	0,7	0,0	0,0	0,0	0,0	0,0
368	0,0	0,0	0,0	0,0	1,9	0,0	2,4	1,9	1,0	0,5	0,0	0,0	0,0
395	0,4	0,0	0,8	0,4	1,1	0,0	1,1	0,8	0,0	0,0	0,0	0,0	0,0
421	0,8	0,0	0,0	1,7	5,0	0,0	0,4	0,0	0,0	0,0	0,0	0,0	0,0
447	0,0	0,0	0,0	1,3	5,1	0,0	0,4	0,4	0,4	0,0	0,0	0,0	0,0
473	0,0	0,0	0,0	0,4	4,2	0,0	1,8	1,1	0,0	0,0	0,0	0,0	0,0
499	0,0	0,0	0,0	0,9	2,4	0,0	2,8	2,4	0,0	0,0	0,0	0,0	0,0
526	0,4	0,0	0,0	0,4	0,4	0,0	1,8	0,9	0,0	0,0	0,0	0,0	0,0
552	0,0	0,0	0,0	1,8	1,8	0,0	2,8	0,9	0,0	0,5	0,0	0,0	0,0
578	0,0	0,0	0,0	1,3	0,0	0,0	2,1	1,3	0,0	0,0	0,0	0,0	0,0
631	0,3	0,0	1,7	0,0	1,0	0,3	5,7	3,0	1,0	0,0	1,0	2,0	0,0
657	0,3	0,0	0,9	0,0	4,1	0,0	4,4	0,3	1,6	0,0	0,0	0,0	0,0
683	1,0	0,0	0,5	2,4	1,4	0,0	2,9	0,5	1,0	0,0	0,0	0,0	0,0
709	0,3	0,0	0,9	0,0	2,7	0,3	3,4	1,8	1,8	0,0	0,9	0,3	0,0
736	0,6	0,0	0,0	0,6	3,6	0,0	1,7	3,0	2,5	0,0	0,0	0,0	0,0
762	0,3	0,0	0,0	0,3	6,0	0,0	1,4	0,8	4,9	0,0	0,0	0,0	0,0
788	0,0	0,0	0,0	1,2	1,9	0,0	0,8	1,9	0,8	0,0	0,0	0,0	0,0
814	0,3	0,0	0,6	0,0	1,8	0,0	3,0	0,3	0,0	0,0	0,0	0,0	0,0
841	0,2	0,0	0,2	0,2	2,2	0,0	1,2	0,7	0,0	0,0	0,0	0,2	0,0
867	0,0	0,0	0,0	0,5	1,9	0,0	0,9	0,5	0,0	0,0	0,0	0,0	0,0
893	0,0	0,0	0,4	0,9	0,9	0,9	3,6	0,4	0,0	0,0	0,0	0,0	0,0
919	0,0	0,0	1,4	1,4	1,4	0,5	0,9	0,0	0,0	0,0	0,0	0,0	0,0
946	0,4	0,0	0,4	0,0	2,9	0,0	3,4	0,0	0,0	0,0	0,4	0,0	0,0
972	0,4	0,0	0,4	0,0	2,1	0,0	2,1	0,8	0,0	0,8	0,4	0,0	0,0
998	0,0	0,0	0,4	0,4	1,5	0,0	0,4	0,4	0,4	0,0	0,0	0,0	0,0
1029	0,0	0,0	0,9	0,0	1,8	0,0	1,8	0,4	0,0	0,0	0,0	0,0	0,0
1060	0,0	0,0	0,0	0,0	1,7	0,0	2,1	0,0	0,0	0,0	0,0	0,0	0,0

Cal. Age (yrs BP)	COS.OC.IRID.	COS.ASTER.	NITZ.MAR.	NITZ.BICAP.	FRAG.CYL.	NITZ.ANG.	FRAG.OCE.	BACT.HYAL.	SYNEDRA.	NITZ.ATL.	NITZ.UZUN	NITZ.SP2.
290	0,3	0,3	0,3	0,0	18,3	0,3	6,6	0,0	0,0	0,5	0,0	0,0
316	0,0	0,0	0,0	1,3	10,6	0,9	5,8	0,0	0,0	0,0	0,0	0,0
342	0,0	0,0	0,0	0,0	6,9	0,4	11,3	0,0	0,0	0,0	0,0	0,0
368	0,0	0,0	0,0	0,0	11,9	1,0	6,2	0,0	0,0	0,0	0,0	0,0
395	0,0	0,0	0,0	0,0	6,0	0,9	6,0	0,0	0,0	0,8	0,0	0,0
421	0,0	0,0	0,0	0,0	7,9	0,0	11,4	0,0	0,0	0,0	0,0	0,0
447	0,0	0,0	0,0	0,0	7,4	0,4	5,1	0,0	0,0	0,0	0,0	0,0
473	0,0	0,0	0,0	0,0	6,9	0,4	5,0	0,0	0,0	0,0	0,0	0,0
499	0,0	0,0	0,0	0,0	13,7	1,7	7,5	0,0	0,0	0,0	0,0	0,0
526	0,0	0,0	1,3	0,4	10,9	0,4	4,8	0,0	0,0	0,0	0,0	0,0
552	0,0	0,0	0,0	0,0	10,6	0,7	5,7	0,0	0,0	0,0	0,0	0,0
578	0,0	0,0	0,0	0,0	7,1	0,4	8,8	0,0	0,0	0,0	0,0	0,0
631	0,0	0,0	0,0	0,7	3,8	1,0	3,8	0,0	0,0	0,0	0,0	0,0
657	0,0	0,0	0,0	0,6	11,5	1,6	4,7	0,0	0,0	0,0	0,0	0,0
683	0,0	0,0	0,0	0,0	6,0	0,5	6,2	0,0	0,0	0,0	0,0	0,0
709	0,0	0,0	0,0	0,0	21,2	0,5	4,0	0,3	0,0	0,9	0,0	0,0
736	0,0	0,0	0,0	0,0	6,4	0,8	1,4	0,0	0,0	0,0	0,0	0,0
762	0,3	0,0	0,0	0,3	6,0	0,5	1,6	0,0	0,0	0,0	0,0	0,0
788	0,0	0,0	0,0	0,0	12,0	0,2	0,4	0,0	0,0	0,0	0,0	0,0
814	0,0	0,0	0,0	0,0	14,2	1,5	5,4	0,0	0,0	0,0	0,0	0,0
841	0,0	0,0	0,0	0,0	10,4	0,0	2,5	0,0	0,0	0,0	0,0	0,0
867	0,0	0,0	0,0	0,0	11,8	0,5	10,6	0,0	0,0	0,0	0,0	0,0
893	0,0	0,0	0,0	0,0	9,9	0,2	8,3	0,0	0,0	0,0	0,0	0,0
919	0,0	0,0	0,0	0,0	12,7	0,9	10,6	0,0	0,0	0,0	0,0	0,0
946	0,0	0,0	0,0	0,8	7,8	0,4	1,9	0,0	0,0	1,3	0,0	0,0
972	0,0	0,0	0,0	0,0	11,1	0,8	5,1	0,0	0,0	1,2	0,0	0,0
998	0,0	0,0	0,0	0,0	14,1	0,6	8,6	0,0	0,0	0,0	0,0	0,0
1029	0,0	0,0	0,0	0,0	9,6	0,2	3,1	0,0	0,0	0,9	0,0	0,0
1060	0,0	0,0	0,2	0,0	7,7	0,6	5,8	0,0	0,0	0,0	0,0	0,0

Cal. Age (yrs BP)	NITZ.CAPUL.	NITZ.KOLACZ.	PSEUD.DOLIOL.	ACT.EHREN	TS.NODULINE.	SP.Y.	COS.LINEAT.	COS.CRENUL.
290	0,0	0,0	0,0	0,0	0,3	0,0	0,0	0,0
316	0,0	0,0	0,0	0,0	0,4	0,0	0,0	0,0
342	0,0	0,0	0,0	0,0	0,7	0,0	0,0	0,0
368	0,0	0,0	0,0	0,0	0,5	0,0	0,0	0,0
395	0,0	0,0	0,0	0,0	1,1	0,0	0,0	0,0
421	0,0	0,0	0,0	0,0	3,7	0,0	0,0	0,0
447	0,0	0,0	0,0	0,0	2,5	0,0	0,0	0,0
473	0,0	0,0	0,0	0,0	0,4	0,0	0,0	0,0
499	0,0	0,0	0,0	0,0	0,0	0,0	0,0	0,0
526	0,0	0,0	0,0	0,0	0,0	0,0	0,0	0,0
552	0,0	0,0	0,0	0,0	1,4	0,0	0,0	0,0
578	0,0	0,0	0,0	0,0	2,1	0,0	0,0	0,0
631	0,0	0,0	0,0	0,0	1,0	0,0	0,0	0,0
657	0,0	0,0	0,0	0,0	1,6	0,0	0,0	0,0
683	0,0	0,0	0,0	0,0	1,4	0,0	0,0	0,0
709	0,0	0,0	0,0	0,0	0,3	0,0	0,0	0,0
736	0,0	0,0	0,0	0,0	1,1	0,0	0,0	0,0
762	0,0	0,0	0,0	0,0	1,4	0,0	0,0	0,0
788	0,0	0,0	0,0	0,0	0,4	0,0	0,0	0,0
814	0,0	0,0	0,0	0,0	0,3	0,0	0,0	0,0
841	0,0	0,0	0,0	0,0	0,5	0,0	0,0	0,0
867	0,0	0,0	0,0	0,0	0,9	0,0	0,0	0,0
893	0,0	0,0	0,0	0,0	0,9	0,0	0,0	0,0
919	0,0	0,0	0,0	0,0	0,5	0,0	0,0	0,0
946	0,0	0,0	0,0	0,0	0,4	0,0	0,0	0,0
972	0,0	0,0	0,0	0,0	0,4	0,0	0,0	0,0
998	0,0	0,0	0,0	0,0	0,0	0,0	0,0	0,0
1029	0,0	0,0	0,0	0,0	0,0	0,0	0,0	0,0
1060	0,0	0,0	0,0	0,0	1,2	0,0	0,0	0,0

Cal. Age (yrs BP)	COS.KUTZING.	COS.STELLER.	COS.AFRICAN.	TN.NITZ.PARV.
290	0,0	0,0	0,0	0,0
316	0,0	0,0	0,0	0,0
342	0,0	0,0	0,0	0,0
368	0,0	0,0	0,0	0,0
395	0,0	0,0	0,0	0,0
421	0,0	0,0	0,0	0,0
447	0,0	0,0	0,0	0,0
473	0,0	0,0	0,0	0,0
499	0,0	0,0	0,0	0,0
526	0,0	0,0	0,0	0,0
552	0,0	0,0	0,0	0,0
578	0,0	0,0	0,0	0,0
631	0,0	0,0	0,0	0,0
657	0,0	0,0	0,0	0,0
683	0,0	0,0	0,0	0,0
709	0,0	0,0	0,0	0,0
736	0,0	0,0	0,0	0,0
762	0,0	0,0	0,0	0,0
788	0,0	0,0	0,0	0,0
814	0,0	0,0	0,0	0,0
841	0,0	0,0	0,0	0,0
867	0,0	0,0	0,0	0,0
893	0,0	0,0	0,0	0,0
919	0,0	0,0	0,0	0,0
946	0,0	0,0	0,0	0,8
972	0,0	0,0	0,0	0,4
998	0,0	0,0	0,0	0,0
1029	0,0	0,0	0,0	0,0
1060	0,0	0,0	0,0	0,0

Appendix 3: Main diatom abundances. Figure 15 – page 3